

EDITORIAL BOARD

Editor-in-Chief

B.E. Paton*Scientists of PWI, Kiev***S.I. Kuchuk-Yatsenko** (*vice-chief ed.*),**V.N. Lipodaev** (*vice-chief ed.*),**Yu.S. Borisov, G.M. Grigorenko,****A.T. Zelnichenko, V.V. Knysh,****I.V. Krivtsun, Yu.N. Lankin,****L.M. Lobanov, V.D. Poznyakov,****I.A. Ryabtsev, V.F. Khorunov,****K.A. Yushchenko***Scientists of Ukrainian Universities***M.N. Brykov**, ZNTSU, Zaporozhie**V.V. Dmitrik**, NTU «KhPI», Kharkov**V.V. Kvasnitsky**, NSU, Nikolaev**V.D. Kuznetsov**, NTUU «KPI», Kiev*Foreign Scientists***N.P. Alyoshin**

N.E. Bauman MSTU, Moscow, Russia

Guan Qiao

Beijing Aeronautical Institute, China

A.S. Zubchenko

DB «Gidropress», Podolsk, Russia

M. Zinigrad

College of Judea & Samaria, Ariel, Israel

V.I. Lysak

Volgograd STU, Russia

Ya. Pilarczyk

Welding Institute, Gliwice, Poland

U. Reisgen

Welding and Joining Institute, Aachen, Germany

O.I. Steklov

Welding Society, Moscow, Russia

G.A. Turichin

St. Petersburg SPU, Russia

Founders

E.O. Paton Electric Welding Institute, NASU

International Association «Welding»

Publisher

International Association «Welding»

Translators

A.A. Fomin, O.S. Kurochko, I.N. Kutianova

Editor

N.A. Dmitrieva

Electron galley

D.I. Sereda, T.Yu. Snegiryova

Address

E.O. Paton Electric Welding Institute,

International Association «Welding»

11 Kazimir Malevich Str. (former Bozhenko Str.),

03680, Kiev, Ukraine

Tel.: (38044) 200 60 16, 200 82 77

Fax: (38044) 200 82 77, 200 81 45

E-mail: journal@paton.kiev.ua

www.patonpublishinghouse.com

State Registration Certificate

KV 4790 of 09.01.2001

ISSN 0957-798X

Subscriptions

\$348, 12 issues per year,

air postage and packaging included.

Back issues available.

All rights reserved.

This publication and each of the articles contained
herein are protected by copyright.Permission to reproduce material contained in this
journal must be obtained in writing from the Publisher.**CONTENTS****SCIENTIFIC AND TECHNICAL**

- Egerland S., Zimmer J., Brunmaier R., Nussbaumer R.,
Posch G. and Rutzinger B.* Advanced gas tungsten arc welding
(surfacing) current status and application 2
- Knysh V.V., Solovej S.A., Nyrkova L.I., Shitova L.G. and
Rybakov A.A.* Improvement of cyclic fatigue life of tee welded
joints by high-frequency mechanical peening under the
conditions of higher humidity and temperature 12
- Lebedev V.A., Lendel I.V., Yarovitsyn A.V., Los E.I. and
Dragan S.V.* Peculiarities of formation of structure of welded
joints in arc surfacing with pulse feed of electrode wire 18
- Lukashevich A.A.* Calculation-experimental method for
determination of spectrum components of non-stationary
loading of carbon steel welded joint 24

INDUSTRIAL

- Tsaryuk A.K., Skulsky V.Yu., Nimko M.A., Gubsky A.N.,
Vavilov A.V. and Kantor A.G.* Improvement of the technology of
welding high-temperature diaphragms in steam turbine flow
section 28
- Kulik V.M., Osadchuk S.A., Nyrkova L.I., Elagin V.P. and
Melnichuk S.L.* Extension of service life of welded tanks of
stainless steel by increasing pitting resistance 37
- Olejnik O.I., Maksimov S.Yu., Paltsevich A.P. and
Goncharenko E.I.* Development of technology of mechanized
arc welding in repair of pressurized main gas pipeline 42
- Vasilev Yu.S., Olejnik N.I. and Parshutina L.S.* Development of
adhesion and adhesion-welding technology for repair of bearing
seats for extension of service life of casing parts of power
equipment 49

INFORMATION

- On the 100th anniversary of Boris I. Medovar 54

ADVANCED GAS TUNGSTEN ARC WELDING (SURFACING) CURRENT STATUS AND APPLICATION

S. EGERLAND, J. ZIMMER, R. BRUNMAIER, R. NUSSBAUMER, G. POSCH and B. RUTZINGER

Fronius International GmbH, Wels, Austria. E-mail: egerland.stephan@fronius.com

Gas Shielded Tungsten Arc Welding (GTAW) — a process well-known providing highest quality weld results joined though by lower performance. Gas metal arc welding is frequently chosen to increase productivity along with broadly accepted quality. Those industry segments, especially required to produce high quality corrosion-resistant surfacing, e.g. applying nickel-based filler materials, are regularly in consistent demand to comply with «zero defect» criteria. In this conjunction weld performance limitations are overcome employing advanced «hot-wire» GTAW systems. This paper, from a welding automation perspective, describes the technology of such devices and deals with the current status in this field, namely the application of dual-cathode hot-wire electrode GTAW cladding, considerably broadening achievable limits. 27 Ref., 2 Tables, 14 Figures.

Keywords: GTAW (cladding), single-cathode GTAW, hot-wire welding, dual-cathode GTAW

Arc welding, to the widest extent, is suggested utilised for fusion welding. The major remainder, i.e. weld surfacing, is supposed reasonably split into «hardfacing» and «corrosion-resistant» weld overlay [1, 2]. Economic considerations drive manufacturers to apply high performance surfacing processes, such as submerged-arc welding or resistance electroslag welding. Although producing broadly acceptable quality, these processes are specifically limited respectively due to compulsory use of flux (limited out-of-position capabilities), high dilution, or undesirable aspect ratios.

Controlled gas metal arc welding processes (e.g. CMT method) have been introduced to the industry coping with dilution related issues, e.g. corrosion [3], and thereby partially replacing submerged-arc and resistance electroslag welding. Surfacing applications exist, however, defining «zero defect» criteria paramount to prevent complicated rework, sustainably assure highest surfacing performance and maintaining long-term component durability. Though joined by limited performance in arc efficiency and weld deposition rate, gas shielded tungsten arc welding (GTAW)

is frequently applied in such cases. To overcome lack of performance, systems have been developed modifying the wire feeding process hereby leading to either «cold-wire» or «hot-wire» GTAW. While the former was early revealing process instabilities and noticeably rather difficult deployable [4, 5], the latter appeared capable of tackling inconsistencies, mainly, by preheating the wire.

Manz [6] early described the advantages, e.g. a significant increase in weld deposition rate through beneficially using the resistive wire heating and, compared with cold-wire GTAW, hereby achieving wire feed rates 3 to 10 times faster into the weld pool [4]. Hot-wire GTAW systems continuously advanced are nowadays well-accepted because of providing user benefits [2, 7, 8]. Information on the operational relationship applying hot-wire and cold-wire GTAW is given in [6] and according to this author proper parameter set up would even allow the deposition of wire without any additional arc. This is due to electrical resistive heating of the wire of a specific composition and diameter according to [6]

$$FR = FL\rho/d^2(\pi/4), \quad (1)$$

where ρ is the apparent resistivity of the wire material; L is the effective wire extension length; and d is the wire diameter. The energy required for melting the wire can be expressed as

$$E_{\text{melt}} = HF\delta d^2(\pi/4), \quad (2)$$

where H is the heat content of the liquid wire volume; F is the wire feed rate; and δ is the apparent wire density.

Figure 1 adopted from [6] schematically depicts the hot-wire GTAW principle.

Wire feed rate can be computed as

$$F = FL(ES)/(\pi d^2/4). \quad (3)$$

ES is here referred to as the «extension sensitivity constant» [6] dependent only on the wire material

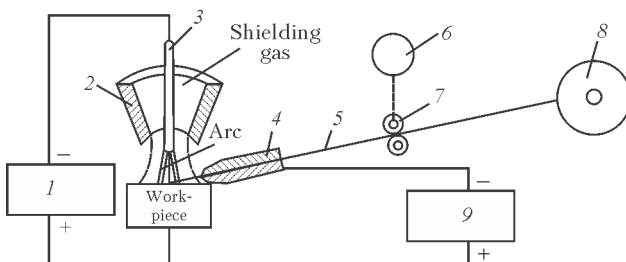


Figure 1. Schematic of hot-wire GTAW system [6]: 1 — GTAW power supply (CC mode); 2 — nozzle; 3 — tungsten electrode; 4 — contact tube; 5 — filler wire; 6 — wire feeder; 7 — feed rolls; 8 — wire reel; 9 — hot wire power supply (CV mode)

composition. Correspondingly, solving for the wire extension length, L leads

$$L = F(\pi d^2/4)^2/P(ES). \quad (4)$$

ES can be derived from equation

$$ES = \rho/H\delta. \quad (5)$$

The apparent resistivity ρ , i.e. the difference between melting and room temperature resistivity, can be approximated as

$$\rho = \rho_{\text{melt}} - \rho_{\text{amb}}/\ln(\rho_{\text{melt}}/\rho_{\text{room}}), \quad (6)$$

while the apparent wire material density δ can be obtained from equation

$$\delta = \delta_{\text{melt}} - \delta_{\text{amb}}/\ln(\delta_{\text{melt}}/\delta_{\text{amb}}). \quad (7)$$

According to [6], ES is proportional to the I^2R deposition rate value; thus, higher resistant wires comparably provide higher deposition rate versus lower resistivity electrodes.

Due to mechanised wire feeding, cold-wire GTAW provides relatively high deposition rates. Frequently joined by instabilities in supplying the wire electrode into the molten pool, however, it may cause irregular wire melting. Chilling phenomena are observed, degrading process stability and weld quality, regardless of whether the wire enters the melt pool either from the leading or trailing edge. The arc is required to melt both the base and the filler material which increases the risk for producing irregular weld beads.

Electrode preheating in hot-wire GTAW makes a considerable part of arc power unneeded to melt the wire. Maintaining an appropriate angle to enter the weld pool ($0 \leq 30 \leq 60^\circ$) [4] the wire can be beneficially located at the trailing edge, close to but not directly interacting with the arc [5].

More recent developments eliminate the second power supply by involving two current control electronic circuits, the first of which provides constant voltage (CV) characteristics for filler wire heating, and the second circuit board provides constant current (CC) characteristics output for controlling the arc current [8]. Although claiming to significantly reduce the amount of equipment regularly needed for hot-wire GTAW, it remains unknown to the authors whether such machines have obtained considerable industrial application, especially for surfacing, that can prove advantageous over cold-wire GTAW because of both reducing penetration depth and dilution as to maintain process stability.

For hot-wire GTAW, Goldsberry [9] presumes that this technology in general has found just limited industrial application since invented in the 1960s. Hence specific studies were mainly conducted to understand phenomena connected to improving productivity, e.g. by involving two wires inductively heated and successfully electromagnetically controlling the weld pool volume in out of position fusion welding [10]. Hori et al. [11] have studied magnetic arc blow phenomena well-known a major issue in employing hot-wire GTAW technology. The authors, who have developed a system to apply high frequency (50–150 Hz) pulsed current

for pre-heating the wire, could overcome instabilities («arcing») caused by electromagnetic fields induced by the gas-shielded tungsten arc and acting on the wire as soon as being detached from the workpiece. Ueguri et al. [12] have tried to assess the optimum relation between welding current and melting rate using parts of the arc heat for wire pre-heating. An increase of travel speed was found mainly permitted by the enlargement of the weld pool width; weld current was found limiting the wire feed rate, following an almost linear relationship with the wire heating current. Also for fusion welding application, Yamamoto et al. [13] have developed «ultra-high-speed» hot-wire GTAW process. To achieve high travel speed and acceptable quality it was found that the wire pre-heating temperature is the most important parameter. Directly related to [13], Shinozaki et al. [14] have thoroughly studied phenomena caused by either the wire temperature and arc thermal input. The authors concluded that filler wire melting is mainly affected by wire pre-heating temperature and base metal melting is mainly caused by the welding arc.

Hot-wire GTAW cladding automation. Welding automation beneficially contributes in raising productivity and efficiency, even when employing single hot-wire GTAW surfacing. Advanced equipment (Figure 2) can be used, e.g. for internal and external GTAW cladding application.

Separately feeding two electrically insulated wires to the weld pool produced by one tungsten electrode, successfully increases productivity. Appropriate welding torches suitable for automated internal or external hot-wire GTAW weld overlay have been developed for industrial application and overcome «single wire» limitations [2]. Applying such equipment allows economically cladding heavy components and simultaneously meet highest quality requirements, i.e. «zero defect» criteria along with providing low dilution ratios.

Multi-cathode GTAW. Increasing GTAW performance or weld deposition rate is regularly joined by increasing welding current, rising arc force or arc pressure, respectively [15, 16]. The latter again is susceptible to cause weld defects, such as undercut or bead humping [17]. To cope with these limitations Yamada in the late 1990s [18] developed and patented [19] a novel high-efficiency GTAW method. Both electrodes, independently operated by two power supplies and electrically insulated to each other, are paired in one welding torch. Feeding hot wire to the weld pool allows increasing the weld performance, i.e. weld deposition rate, in production of large 9 % Ni-steel storage tanks [20]. Electrode geometry and adjustment are stated among the specifics of this method. Multi-cathode GTAW (Figure 3, a) has early been tested to improve both process efficiency and weld quality.

Norrish [21] describes multi-cathode GTAW capable of significantly increasing travel speed and, by



Figure 2. Endless Torch Rotating ETR[®] systems lined up for internal borehole GTAW cladding

elongating the weld pool, preventing weld defects such as undercut. Figure 3, *b* plots welding speed over current in deploying single- and multi-cathode GTAW. Considerable differences become noticeable through beneficially raising the number of cathodes. Undesirable but possible arc deflection between the electrodes is overcome by e.g. employing high-frequency pulsing or magnetic arc stabilisation [21].

Dual-cathode GTAW. Zhang et al. [22] studied the physical phenomena of twin TIG welding, i.e. GTAW employing two electrodes in one welding torch. The authors suggested the Lorentz force to attract both arcs hereby forming a single arc whose pressure gradient is considerably lower versus single-electrode GTAW process.

The attracting force can be calculated as follows [22]:

$$F = k \frac{I_1 I_2}{L}, \quad (8)$$

where k is the constant; I_1 and I_2 , respectively, is the welding current for cathodes 1 and 2; and L is the dis-

tance between both electrodes. F is proposed increasing with rising current I and decreasing with rising distance L . It was attempted to evaluate these relationships and the resulting phenomena effects especially on arc pressure. It was found the latter decreases in dual-cathode GTAW due to a broader area covered by the coupled arc approaching an elliptic cross-section.

Figure 4, *a* [23], for single-cathode welding reveals the arc pressure steeply rising at the arc centre with increasing currents. Figure 4, *b* again for dual-cathode GTAW shows the pressure level flattened and more broadly distributed around the arcs attracted.

Surfacing in general requires low dilution rates to maintain the deposited weld metal properties, e.g. corrosion resistance; weld pool depression again is considered a function of welding current height [16]. Leng et al. [23] connected to [22] have thoroughly studied the relationships between current height and its influence on arc pressure distribution in dual-cath-

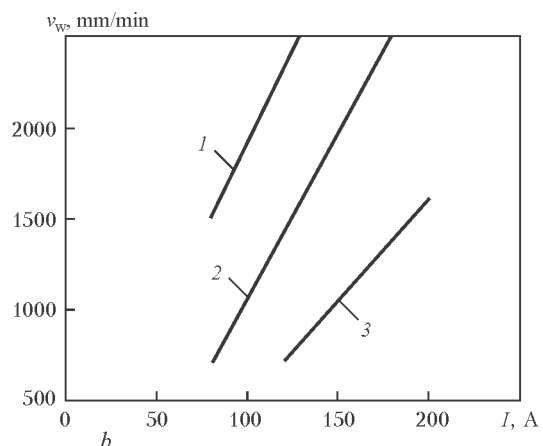
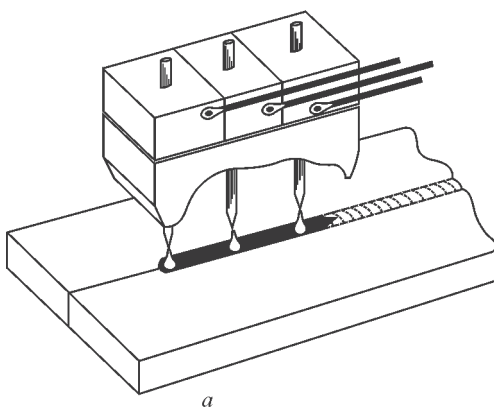


Figure 3. Schematic of multi-cathode GTAW (*a*), and comparison of welding speed (*b*) for complete penetration with AISI 304 stainless steel wire of 1.2 mm diameter: 1 — three-cathode; 2 — two-cathode; 3 — single-electrode GTAW [21]

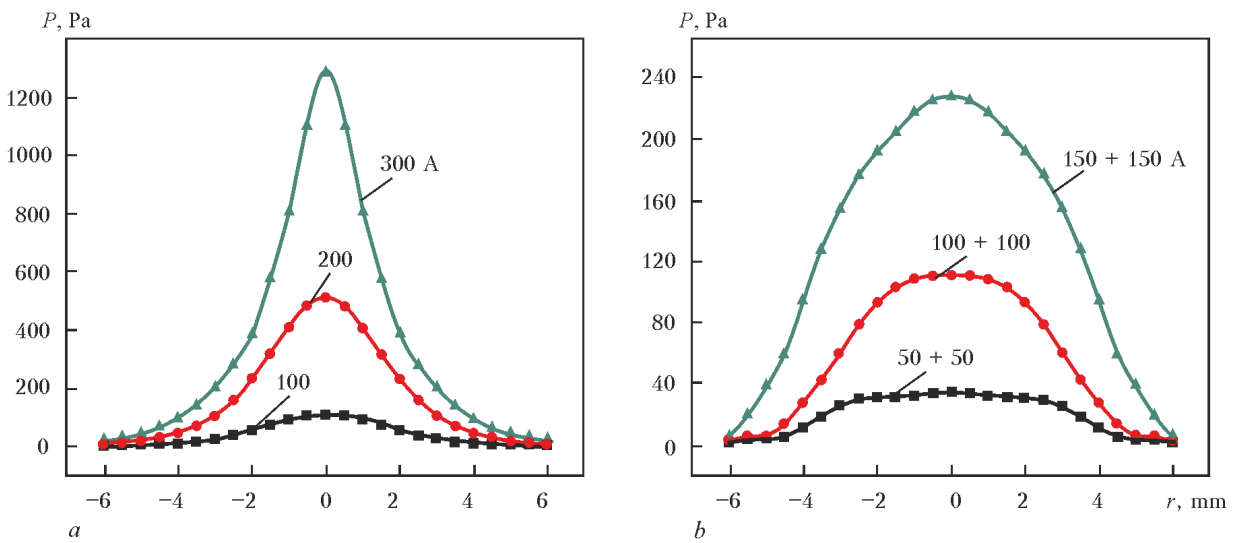


Figure 4. Arc pressure measured for single- (a) and dual-cathode (b) GTAW [23]

ode GTAW. They found the latter decreased versus similar values of current in single-cathode welding.

Assuming the major arc force mainly arising from the plasma jet impinging on the anode surface, according to [23] the arc pressure can be derived from the law of momentum conservation:

$$P = \frac{1}{2} \xi v^2, \tag{9}$$

where P is the arc pressure; ξ is the elemental plasma density; and v is its velocity.

Using Maecker's [24] approach of relating the highest velocity v_c to the maximum current density in the arc centre, and assuming the plasma flow as «incompressible and inviscid»:

$$v_c = \sqrt{\frac{\mu_0 J j}{2\pi \xi}}, \tag{10}$$

where μ_0 is the magnetic permeability of free space, and j denotes the current density, one finally can achieve the relationship between arc pressure P_c and j at the arc centre line [24]:

$$P_c = \frac{\mu_0 J j}{4\pi}, \tag{11}$$

representing the arc pressure as directly proportional to I or j , respectively.

Applying expression (8), indicating the force attracting the arcs towards the centre, one can see the arc pressure increasing in the centre with rising arc currents or decreasing distance between the two cathodes employed. However, due to the split cathodes, both arcs are displaced from the centre, thus, likewise shifting the pressure maxima. According to [23] the force of attraction produces an arc overlapping, however, the resulting peak pressures are located off the centre and, hence, the final «coupling arc» pressure is dropped versus each single or «overlapping arc».

Figure 5, a shows the visible arc appearance of a dual-cathode setup for 200 A total current, and Figure 5, b graphically plots the comparison of the distinct arc pressures produced.

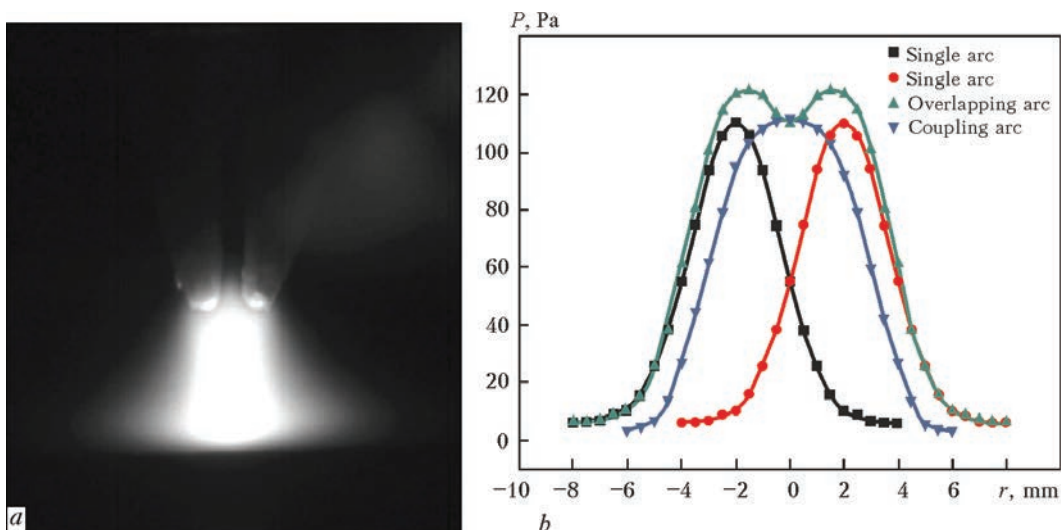


Figure 5. Visible overlapping of 2x100 A arcs (a), and comparison of single, overlapping and coupling arc pressures for 200 total current (b) [23]

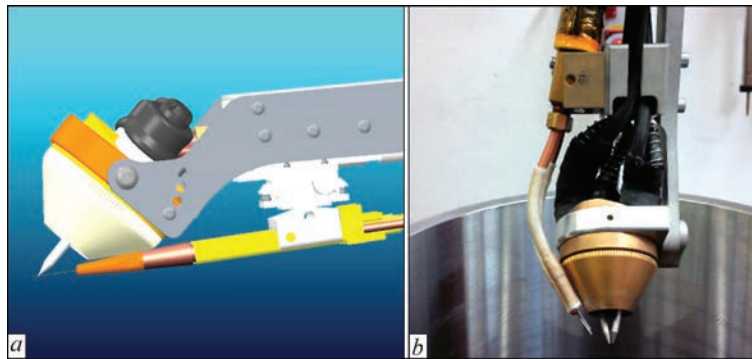


Figure 6. Schematic of single- (a) and real part twin-hot-wire dual-cathode welding torch (b) (FRONIUS SpeedClad®)

In the later work [25] Zhang et al. have applied the Fowler–Milne method to determine temperature distribution profiles in dual-cathode GTAW incorporating the influence of current, arc length and spatial electrode distance. Temperature maxima were found in the centre between both cathodes and current was evaluated increasing the temperature. Arc length was hardly affecting peak temperature but given the experimental setup, it was extending temperature distribution at the anodes. Wider cathode clearance was estimated decreasing the arc centre temperature. Martins [26] developed a dual-cathode welding torch based on commercial components for studying beneficial effects in preventing defects such as bead humping and undercut, while simultaneously increasing process performance.

Motivation. As mentioned above welding current plays a major part in order to increase process efficiency. Knowing dual-cathode GTAW applicable to beneficially preventing from weld defects at higher currents, it was aimed at developing an automation GTAW cladding system upon dual tungsten cathode technology.

Dual-cathode welding torch development. Severe arc interference can occur between both electrodes, capable of finally leading to process abortion due to cathode damage [26]. One of the most substantial technical requirements to meet in dual-cathode GTAW is highly precise and industrially practicable adjustment of both tungsten cathodes in one single welding torch. Arc interaction between both cathodes has to be assured sustainably suppressed, even for long lasting automated application, such as GTAW cladding. Finally, the development of components easily adaptable

to automation hardware already available, such as the ETR® GTAW cladding system, was considered another essential target to achieve.

Figure 6 schematically shows the developed novel type dual-cathode torch head basically employed for fully mechanised single hot-wire or optionally twin hot-wire GTAW application, the latter to further enhance weld deposition rates thus raising travel speed.

System configuration. Adequately assembled the system shall allow for single- and twin-hot-wire cladding. Figure 7, a schematically depicts the configuration for performing the former process, and Figure 7, b — the latter one.

Process mode and stability relevant components are interacting via hardware Local High Speed Bus (LHSB) interface, permitting to employ both pure constant direct current or to superimpose and synchronise current and wire feed motion. Both is of crucial importance in performing smooth start/stop sequences. In its practical configuration, equipped to ETR® column and boom system, the device physically appears (Figure 8). This Figure also shows the superimposed system controller, allowing sophisticated determination of welding paths to follow, according to the design of the part of interest.

Experimental. Given the novel dual-cathode GTAW cladding process and the equipment available, it was attempted to quantify differences and, if possible, to evaluate technological benefits to other weld overlay process variants. It needs mention that a distinct experimental approach was originally taken for achieving preliminary results. That is, single-

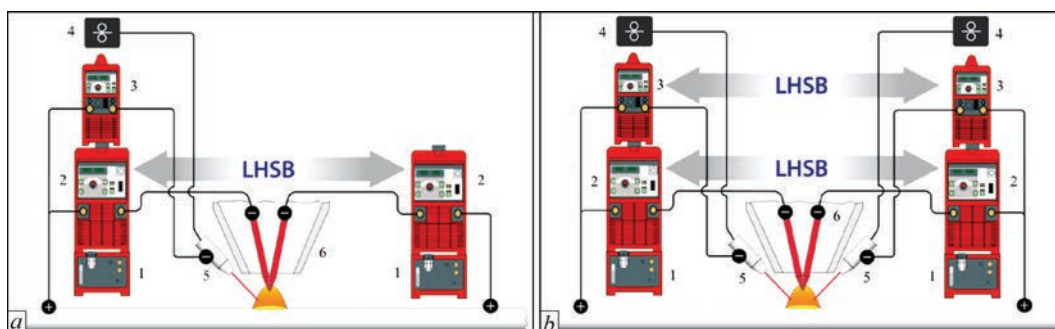


Figure 7. Schematic of dual-cathode single- (a) and twin- (b) hot-wire GTAW cladding system (SpeedClad®): 1 — chiller; 2 — GTAW inverter power supply; 3 — hot wire inverter power supply; 4 — wire feeder; 5 — hot wire contact tube; 6 — dual-cathode torch

and dual-cathode both twin- and single-wire cladding was conducted in the welding position easiest to apply, i.e. PA (AWS — 1F). Subsequently to that the experimental conditions (e.g. welding position) were tangibly aggravated for testing the novel advanced dual-cathode GTAW cladding process. Subsequently the experimental conditions for the application of the dual-cathode GTAW cladding were exacerbated, thereby to prove applicability given the regular industrial environment. Results were compared, and the quantitative differences were summarised.

Single-cathode twin-hot-wire GTAW cladding. Substrate specimens were produced from low carbon base metal S235 JR (according to Euronorm EN 10025) 50 mm thick. Surface was milled and cleaned applying ethyl alcohol prior to welding without preheating. Regular commercial FRONIUS systems and components have been applied, namely Magic Wave 5000 AC/DC GTAW inverter (500 A at 40 % duty cycle), and for hot-wire cladding Transtig 2200 JOB GTAW inverter (220 A at 40 % duty cycle) have been used as power supplies. The 6-axis KUKA articulated robot equipped with 4.5 m hose package + water-cooled TTW 4500 welding torch and superimposed HMI-T10CC system control unit were used for arc motion and process control, respectively. Argon (99.996 % purity) as the shielding gas at flow rate of 12 l/min and 2 % cerium oxide doped 3.2 mm diameter tungsten electrode ground to 60° included angle were applied. Filler wire in both trial series was 1.2 mm nickel-based alloy UNS N06625 (AWS ER NiCrMo-3), «Böhler Nibas 625-IG». Filler metal specific density was 8.44 g/cm³ [27].

All processes, i.e. single-cathode cold- and hot-wire as well as dual-cathode twin-hot-wire cladding, were performed applying two layer and targeting at average layer thickness of about 2.5 mm. According to industrial demands, the metallurgical quality of the second clad layer was evaluated through its iron content related to a specific distance from its surface. That is, ≤55 % Fe at ≤3 mm below the surface had to be consistently proved for meeting the requirements.

Single-cathode twin-hot-wire and dual-cathode single-hot-wire GTAW cladding. Table 1 states the preliminarily conducted welding trials using pulsed and constant straight polarity direct current.

Dual-cathode twin-hot-wire GTAW cladding. Commercial FRONIUS ETR[®] GTAW cladding system (Figure 8) was used comprising FCB 3000-3000/ML 700 Column and Boom paired with FCS

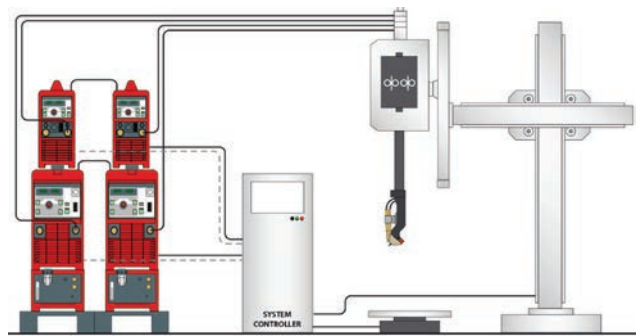


Figure 8. Schematic of dual-cathode GTAW cladding system (SpeedClad[®])

200-1000/ML 375 cross slide and novel TTHW 6000 M SpeedClad[®] GTAW twin-hot-wire torch. The system was completed assembling two DC GTAW power supplies Transtig 5000 JOB (500A at 40 % duty cycle) and two hot-wire power supplies Transtig 2200 JOB, as well as superimposed system control unit FRONIUS FPA 9000.

Tube welded specimens of 155 mm diameter with wall thickness of 20 mm, to simulate internal borehole cladding, were produced from low carbon S 235 JR parent metal. 30 beads were deposited in total applying welding position PC (AWS — 2F). Specimen surfaces were machined and cleaned using ethylene alcohol prior to welding. Consumables were similar to single-cathode hot-wire GTAW cladding, i.e. 1.2 mm UNS N06625 filler wire and argon of 99.996 % purity. Gas flow rate was digitally controlled at 24 l/min, and 2 % cerium oxide doped 4.0 mm tungsten electrodes were used, ground to obtain 56° included angle. Circumferential bead deposition was conducted employing 3.4 mm vertical lateral increment, and electrode gap was maintained constant deploying regular arc voltage control included in the ETR[®] system. Parts were manually preheated to 200 °C using oxyfuel torch (C₃H₈ + O₂). Interpass temperature was chosen 200 °C. For the dual-cathode twin-hot-wire welds Table 2 depicts a WPS excerpt of the essential variables used.

The Table reveals that both wire feed rate to hot-wire current ratio and travel speed have been maintained constant throughout both trial series. In pulsed welding the ratio between pulsed and background cycle defines the height of the output current. Adjusting background and pulsed current time balanced to each other and given the parameters chosen the pulsed process shows slightly higher mean welding current.

Results. *Single-cathode (twin-wire) and dual-cathode (single-wire) cladding.* Figure 9 shows

Table 1. Preliminary experimental data

Process	I_p, A	I_w, A	I_b, A	U_{mean}, V	$v_{w,p}, cm/min$	$v_{h,p}, cm/min$	t_p, ms	t_b, ms	f, Hz	$I_{h,w}, A$
Single-cathode twin-hot-wire	320	—	280	13.5	1.6*	32	200	200	2.5	70
Same	350	—	300	14.2	2.6*	50	150	150	3.3	70
Dual-cathode single-hot-wire	—	450*	—	12.1	7.6	80	—	—	—	190

*Note: these data represent total values, i.e. require division by 2.

Table 2. Experimental data for dual-cathode twin-hot-wire welding (FRONIUS SpeedClad®)

Welding current	I_w, A	I_b, A	U_{mean}, V	$v_{w,p}, m/min$	$v_{h,w}, cm/min$	t_p, ms	t_b, ms	f, Hz	$I_{h,w}, A$
DC constant	370	–	10.4	4.8	120	–	–	–	240
Pulsed current	430	370	11.0	5.0	120	70	70	7.1	250

the macrosections of deposits for single-cathode twin wire and dual-cathode single-wire cladding.

No significant visual variation appears in the penetration profile between pulsed single-cathode twin-wire and constant DCSP dual-cathode single-wire cladding sequence. Iron content was found safely below 5 % for all three welds. Deposition rates achieved were respectively 1.83 (32) and 2.98 kg/h (50 cm/min) for single-cathode twin-wire, and 4.23 kg/h (80 cm/min) for dual-cathode single-wire GTAW cladding.

Dual-cathode (twin-wire) constant and pulsed DCSP cladding. Figure 10, *a* as an overview reveals the compact dual-cathode head processing inside the 155 mm diameter pipe specimen, and Figure 10, *b* shares an idea of high surface layer quality obviously achieved applying this novel method.

According to the parameters in Table 2, Figure 11 represents the macrosections of dual-cathode deposits as subjected to EDX analysis.

For all welding sequences Figure 12 shows the clad quality indicating iron content over the distance of 3 mm below the layer surface (Oxford INCA Energy/

PM 55 system). Deposition rates employing dual-cathode twin-hot-wire were found considerably increased, respectively leading to about 5.6 kg/h for constant DCSP and about 5.7 kg/h for pulsed DCSP. Greater homogeneity is found for higher current–higher travel speed trials. However, the lowest travel speed of 32 cm/min is prone to greater noise in the surface elemental distribution.

Figure 13 represents from EDX analysis the elemental surface layer chemistry focusing on the essential alloying elements particularly in charge of the deposited layer corrosion resistance. Also, for comparison, it involves the analysis of the filler wire employed. Similar elemental distribution can be found in the second layer especially in using the novel dual-cathode twin-hot-wire GTAW cladding method, with minimal differences to the consumable chemistry, exceptionally, of course, the iron content deliberately decreased in the wire.

Based upon theoretical considerations on varying impacts depending maybe on varying orientation angles of two cathodes, i.e. from longitudinal to normal, related to welding direction, additional studies were conducted using the dual-cathode system for both cases.

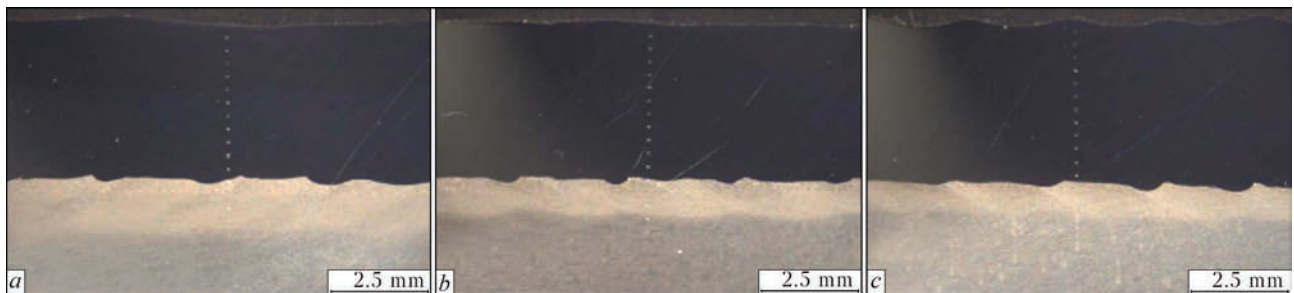


Figure 9. Macrosection of deposits for single-cathode twin-hot-wire cladding at 32 (*a*) and 50 (*b*) cm/min travel speed, and dual-cathode single-hot-wire cladding at 80 cm/min (*c*)

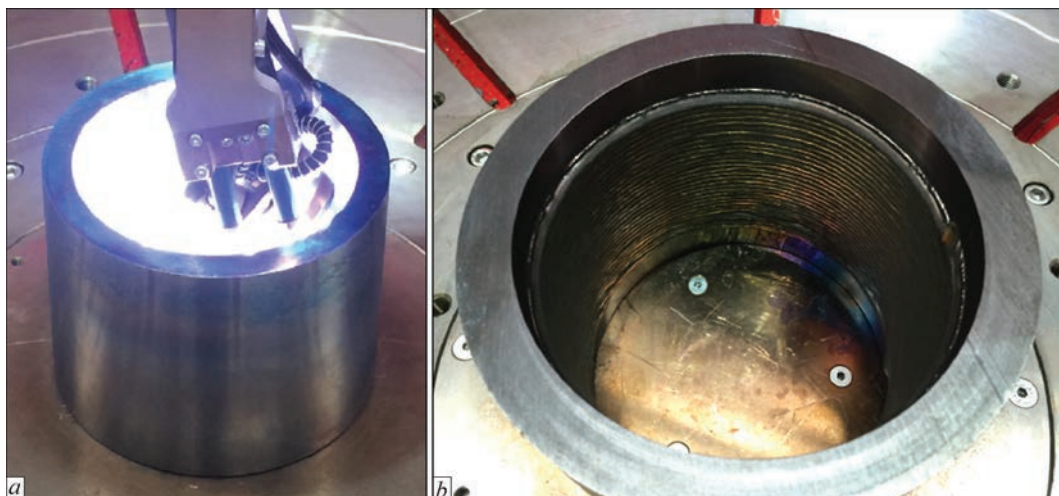


Figure 10. Dual-cathode head (SpeedClad®) during cladding (*a*), and layers deposited using pulsed process (*b*)

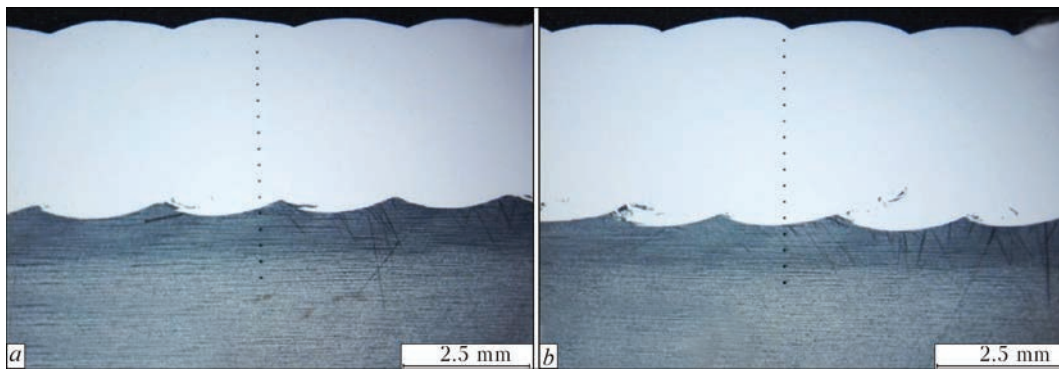


Figure 11. Macrosection of deposits obtained with dual-cathode twin-hot-wire at constantly supplied (a) and pulsed (b) direct current at travel speed of 120 cm/min in welding position PC

As already investigated and numerically modelled by Leng et al. [23] tangible differences could be approved.

Figure 14, a shows the macrosection for the former configuration, i.e. tungsten electrodes arranged longitudinally to welding direction, while Figure 14, b indicates the electrodes twisted by 90° to obtain them arranged normal to welding progression.

The effective influence between both setups can be readily noticed. It is suggested necessary as such to further devote effort in establishing reliable quantitative data on influence of differently twisted electrodes related to weld metal dilution and elemental distribution.

Discussion. The results achieved from the experiments accomplished are suggested valuable due to allowing quantitatively comparing regular high performance GTAW cladding processes, i.e. twin-hot-wire GTAW with a novel approach referred to as dual-cathode GTAW.

The latter can be either used employing a single or two filler wires leading to significantly higher deposition rates. The welding trial matrices chosen, distinguished in a preliminary phase using a dual-cathode

prototype equipment and a final period particularly focusing on industrial application and targeted at achiev-

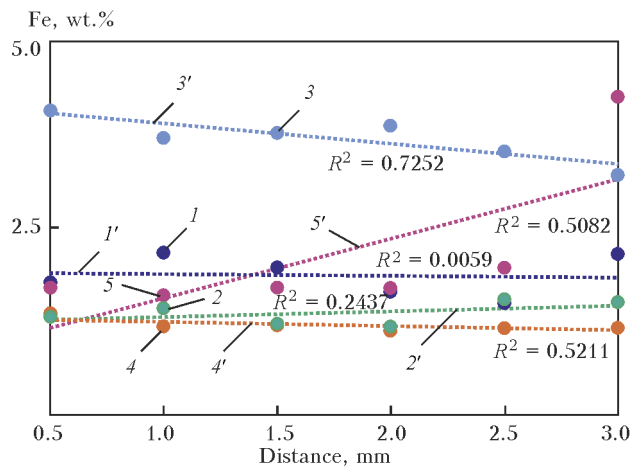


Figure 12. Iron content versus distance below clad layer surface for process applied: 1, 1' — single-cathode, twin-hot-wire, 32 cm/min; 2, 2' — dual-cathode, single-hot-wire, 80 cm/min; 3, 3' — dual-cathode, dual-hot-wire, pulsed DC, 120 cm/min; 4, 4' — single-cathode, twin-hot-wire, 50 cm/min; 5, 5' — dual-cathode, dual-hot-wire, constant DC, 120 cm/min

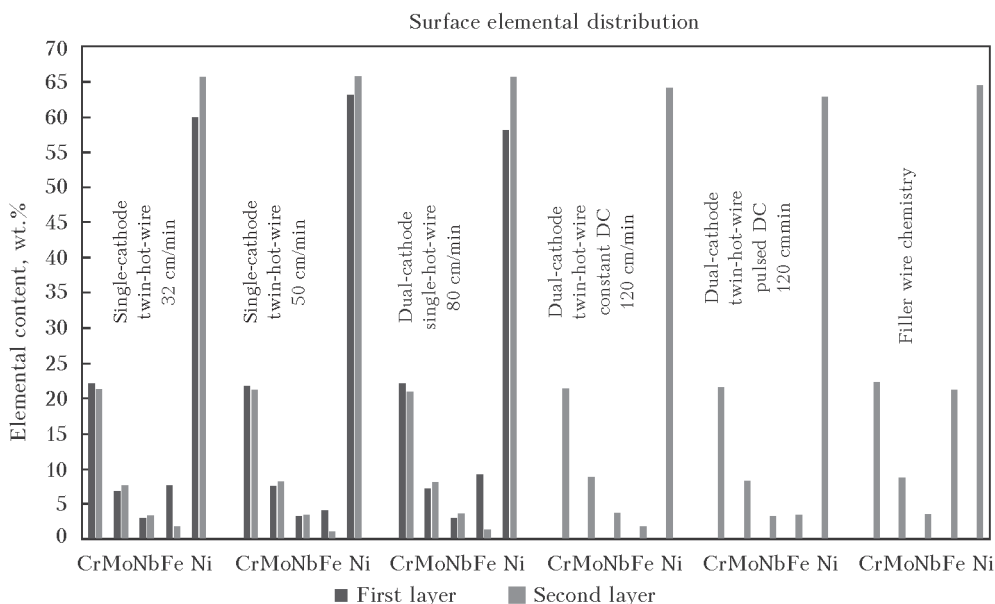


Figure 13. Elemental distribution on clad layer surface compared with filler wire chemistry (analysis for dual-cathode twin-wire deposits was conducted only for the second layer)

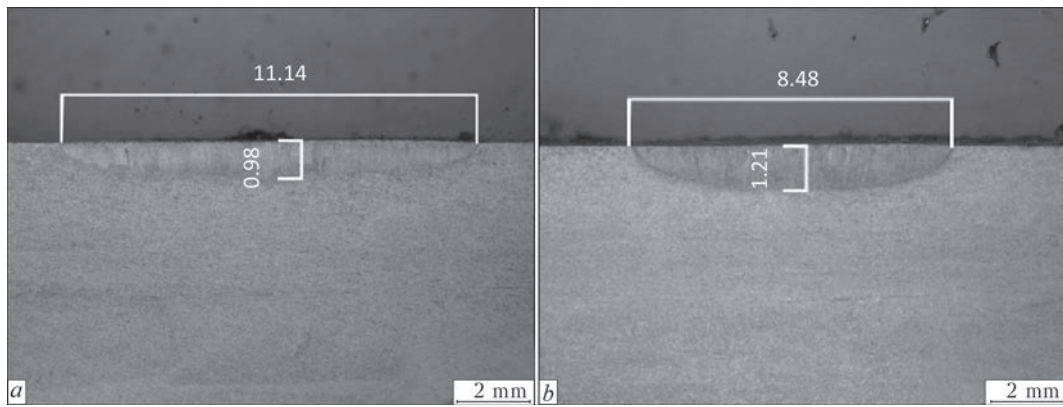


Figure 14. Results of dual-cathode GTAW autogenously employed with electrodes adjusted longitudinal (a) and normal to welding direction (b) (cathode diameter of 4.0 mm; total welding current of 300 A (2×150 A); cathode clearance of about 2.0 mm; electrode-to-workpiece distance of 4.0 mm; and travel speed of 40 cm/min)

ing meaningful assessment on process performance and quality aspects to meet, are supposed showing the investigations of other researchers approved.

Although focusing on fusion welding, multiple cathode GTAW has been investigated by Norrish [21], Yamada [18, 19], Kobayashi [20] et al. However, we could find the novel developed method also capable of increasing welding speed, as to overcome weld defects and rising productivity in GTAW cladding. Yet outstanding in quantitative approval and, hence, only qualitatively suggested at this stage, we suppose that the fundamental mechanism of both low dilution and eliminating weld defects (undercut) arises from a lower arc pressure at the same total current versus single-cathode welding, connected to the specific cathode arrangement in the welding head developed. It needs mention though that the results derived by other researchers considerably differ to each other. That is Kobayashi et al. [20] found respectively arc pressures of about 1500 Pa for a single cathode (200 A welding current + 2 mm «arc length») and about 250 Pa for their dual-cathode arrangement; for the same total current and similar experimental setup Zhang et al. [22] and Leng et al. [23] determined maximum arc pressures of about 500 (single-cathode) and about 95 Pa (dual-cathode).

Apart from these differences we nonetheless suggest the relationship between welding current height and arc pressure, as e.g. postulated by Adonyi et al. [15] and Rokhlin and Guu [16], also applicable to GTAW hot-wire cladding; at least for the experimental conditions described in this paper. This is due to the higher dilution ratios observed when changing the dual-cathode arrangement with pulsed direct current (thereby increasing the mean current) versus constant applied DCSP.

Despite achieving a higher mean current the deposition rate was found relatively little raised with the pulsed sequence, which is suggested explainable by the only slightly increased wire feed rate versus the constant current sequence (5.0 versus 4.8 m/min). Considering further

dilution ratios — found raised for pulsed current GTAW and correspondingly the constant ratio between wire feed rate and hot-wire current one may suggest though the results of Shinozaki et al. [14] as approved; supposing that filler wire melting is mainly influenced by hot-wire current instead of being a function of the arc current. However, we suggest that further work appears required in this conjunction to assess both these assumptions as well as evaluating the relationship between wire feed rate, hot-wire current and arc current.

Given our experiments (see Figure 14), i.e. changing the dual-cathode orientation angle related to welding progression, we suggest the considerations of Leng et al. [23] on varying current density and temperature fields around the cathodes, valuably contributing to future research, especially in connection to dual-cathode twin-hot-wire GTAW cladding. Hence, and although not yet practically proved by the investigations dealt with in this paper, it is supposed that both weld dilution and deposited bead height can be positively affected incorporating the dual-cathode orientation angle, hereby further to improve weld metal elemental distribution and secondary properties, e.g. clad layer corrosion resistance.

Conclusions

From the experiments explained in this paper we can draw the following conclusions:

- single-cathode gas tungsten arc hot-wire cladding employing two wires of 1.2 mm diameter, and typical UNS N06625 chemistry was found reliably leading to welding results safely meeting industrial requirements;
- novel dual-cathode GTAW system was compared with the results obtained in single-cathode GTAW cladding;
- novel system was proved capable of considerably raising welding performance, i.e. deposition rate and travel speed, and nonetheless to safely meet all industrial requirements;
- iron content, as the qualitative indicator for clad layer quality, was quantified reliably remaining below

threshold when employing the dual-cathode GTAW cladding system both single-wire (welding position PA) and twin-wire (welding position PC);

- relationship between welding current height and arc pressure appears approved and applicable also to an experimental setup as used in this investigation;

- although not quantitatively approved in this investigation, the reduced arc pressure is supposed the major factor in dropping the depth of penetration when employing dual-cathode GTAW cladding, hereby considerably reducing the dilution ratio versus single-cathode GTAW cladding at similar welding current;

- hot-wire current is suggested mainly affecting deposition rate versus arc current and as such our results appear to confirm the findings of other researchers;

- experimental results on varying dual-cathode orientation angle related to welding direction (longitudinal or normal) are suggested approving theoretical considerations of other researchers and are considered valuable for future work;

- dual-cathode GTAW is supposed finally to future sustainably and reliably broadening the range of high quality cladding applications required complying with «zero-defect» criteria.

Acknowledgements. *The authors are grateful to Mr. Emre Güneruz, Mr. Franz Bichler and Mr. Andreas Bauer, all with FRONIUS International, who have performed the experimental work, as well as to Mr. Uwe Kroiss of FRONIUS International's R&D department for conducting the dual-cathode orientation trials.*

- Egerland, S. (2010) Controlled GMA welding processes prove applicability for high-quality weld overlay. In: *Welding and Repair Technology for Power Plants: Proc. of 9th Int. EPRI Conf.* (2010 June 23–25, Fort Myers). Palo Alto: Electric Power Research Institute.
- Egerland, S. (2009) Status and perspectives in overlaying under particular consideration of sophisticated welding processes. *Quart. J. JWS*, 27(2), 50–54.
- Egerland, S., Helmholdt, R. (2008) Overlaying (cladding) of high temperature affected components by using the cold metal transfer process. In: *Safety and reliability of welded components in energy and proc. industry*, 327–332. Graz: Verlag der Technischen Universität.
- Freeman, N.D., Manz, A.F., Saenger, J.F.Jr. *Inventors; Union Carbide Corp, assign. Method for depositing metal with a TIG arc.* Pat. US 3483354. Publ. Dec. 9, 1969.
- Manz, A.F., Norman, R., Wroth, R.S. *Inventors; Union Carbide Corp, assign. Electric arc working with hot wire addition.* Pat. US 3163743. Publ. Dec. 29, 1964.
- Manz, A.F. *Inventors; Union Carbide Corp, assign. Consumable electrode arcless electric working.* Pat. US 3122629A. Publ. Feb. 25, 1964.
- Hori, K., Myoga, T., Shinomiya, M. et al. *Inventors; Kaisha BHK assign. Semi-automatic hot wire TIG welding equipment.* Pat. US 4801781. Publ. Jan. 31, 1989.
- Mizuno, T., Shimizu, T. *Inventors; Kaisha MDK assign. Hot wire welding system.* Pat. US 4464558A. Publ. Aug. 7, 1984.
- Goldsberry, C. (2007) Hot-wire TIG: Not new but gaining appeal. <http://weldingdesign.com/archive/hot-wire-tig-not-new-gaining-appeal>
- Manabe, Y., Wada, H., Zenitani, S. (2000) Investigation on TIG welding using 2 filler wires with electromagnetically controlled molten pool process in horizontal position. *Quart. J. JWS*, 8(1), 40–50; <http://dx.doi.org/10.2207/qjw.18.40>
- Hori, K., Watanabe, H., Myoga, T. et al. (2004) Development of hot wire TIG welding methods using pulsed current to heat filler wire: Research on pulse heated hot wire TIG welding processes. *Welding Int.*, 18(6), 456–468; <http://dx.doi.org/10.1533/wint.2004.3281>
- Ueguri, S., Tabata, Y., Shimizu, T. et al. (1986) A study on control of deposition rate in hot-wire TIG welding. *Quart. J. JWS*, 4(4), 678–684; <http://dx.doi.org/10.2207/qjw.4.678>
- Yamamoto, M., Shinozaki, K., Myoga, T. et al. (2008) Development of ultra-high-speed GTA welding process using pulse-heated hot-wire. In: *Pre-Prints of the 82nd Nat. Meeting of JWS*, 228–229.
- Shinozaki, K., Yamamoto, M., Nagamitsu, Y. et al. (2009) Melting phenomenon during ultra-high-speed GTA welding method using pulse-heated hot-wire. *Quart. J. JWS*, 27(2), 22–26; <http://dx.doi.org/10.2207/qjw.27.22s>
- Adonyi, Y., Richardson, R., Baeslack, W. (1992) Investigation of arc force effects in subsurface GTA welding. *Welding J.*, 71(9), 321–330.
- Rokhlin, S., Guu, A. (1993) A study of arc force, pool depression, and weld penetration during gas tungsten arc welding. *Ibid.*, 72(8), 381–390.
- Mendez, P., Eagar, T. (2003) Penetration and defect formation in high-current arc welding. *Ibid.*, 82(10), 296–306.
- Yamada, M. (1998) Development of high efficiency TIG welding method. *1st Rep. of JWS*, 63, 24–25.
- Yamada, M., Tejima, A. *Inventors; Ishikawajima-Harima Heavy Industries Co. assign. TIG welding apparatus and method.* Pat. US 6982397. Publ. Jan. 3, 2006.
- Kobayashi, K., Nishimura, Y., Iijima, T. et al. (2013) Practical application of high efficiency twin-arc TIG welding method (SEDAR-TIG) for PCLNG storage tank. *Welding in the World*, 48(7/8), 35–39.
- Norrish, J. (2006) *Advanced welding processes*. Cambridge: Woodhead Publ.
- Zhang, G., Leng, X., Lin, W. (2006) Physics characteristic of coupling arc of twin-tungsten TIG welding. *Transact. of Non-Ferrous Metals Soc. of China*, 16(4), 813–817.
- Leng, X., Zhang, G., Wu, L. (2006) The characteristic of twin-electrode TIG coupling arc pressure. *J. Phys. D: Appl. Phys.*, 39(6), 1120–1126; <http://dx.doi.org/10.1088/0022-3727/39/6/017>
- Maecker, H. (1955) Plasmaströmungen in Lichtbögen infolge eigenmagnetischer Kompression. *Zeitschrift für Physik*, 141(1), 198–216.
- Zhang, G., Xiong, J., Gao, H. et al. (2012) Effect of process parameters on temperature distribution in twin-electrode TIG coupling arc. *J. Quantitative Spectroscopy & Radiative Transfer*, 113(15), 1938–1945; <http://dx.doi.org/10.1016/j.jqsrt.2012.05.018>
- Martins, É.A. (2010) *Avaliação da soldagem tig autógena duplo cátodo twin Tig [trabalho de graduação]*. Florianópolis: Universidade Federal de Santa Catarina .
- (2006) *Special Metals Corporation. Inconel alloy 625. Special Metals: Material Manufacturer Data Sheet.*

Received 15.01.2016

IMPROVEMENT OF CYCLIC FATIGUE LIFE OF TEE WELDED JOINTS BY HIGH-FREQUENCY MECHANICAL PEENING UNDER THE CONDITIONS OF HIGHER HUMIDITY AND TEMPERATURE

V.V. KNYSH, S.A. SOLOVEJ, L.I. NYRKOVA, L.G. SHITOVA and A.A. RYBAKOV

E.O. Paton Electric Welding Institute, NASU

11 Kazimir Malevich Str., 03680, Kiev, Ukraine. E-mail: office@paton.kiev.ua

The study provides experimental evidence of effectiveness of application of high-frequency mechanical peening (HFMP) to improve the fatigue resistance characteristics of tee welded joints in metal structures, which operate under moderate climatic conditions. Corrosion damage characteristic for such structures after long-term service was achieved by soaking the welded joint in G4 humidity chamber at increased humidity and temperature for 1200 h. Metallographic studies were performed of the weld zone and HAZ in as-welded (unstrengthened) and HFMP-strengthened states before and after corrosive medium impact. It is established that as a result of HFMP strengthening, the joint resistance to the impact of higher humidity and temperature becomes higher. Fatigue tests of welded joints in the initial and strengthened states before and after soaking in the humidity chamber were performed. It is found that strengthening by HFMP technology before the corrosive impact allows increasing the limited endurance limit, based on $2 \cdot 10^6$ cycles, of tee welded joints by 48 % and increasing the cyclic fatigue life 6–8 times. 12 Ref., 1 Table, 7 Figures.

Keywords: tee welded joint, corrosive medium, fatigue, high-frequency mechanical peening, ultrasonic impact treatment, improvement of corrosion fatigue resistance

Engineering metal structures in long-term service can be exposed to simultaneous impact of external alternating loading and corrosive media. The service life of such structures is determined by corrosion fatigue resistance of their most loaded joints and components. In order to improve fatigue resistance characteristics of structural components and elements, various methods of surface plastic deformation (SPD) of metal are widely used in practice. Review of the main SPD methods is given in [1].

Over the recent years, investigations have been actively pursued to establish the effectiveness of SPD application to improve the characteristics of corrosion fatigue and corrosion resistance of metals and their welded joints [2–12]. Some works on these subjects are devoted to effectiveness of application of such SPD method, as high-frequency mechanical peening (HFMP) [3, 7, 9, 11, 12] (known in foreign publications as ultrasonic impact treatment). So, in [9] it was shown that depending on technological parameters of HFMP performance, corrosion resistance of strengthened surface layer of the material, determined by corrosion potential, can both increase, or decrease relative to base material. Experimental studies of corrosion fatigue of low-alloyed steel welded joints in NaCl solution demonstrated that strengthening by HFMP technology allows essentially increasing their

cyclic fatigue life [3, 7, 11]. Study [12] shows the good prospects for application of combined strengthening of welded joints by electrospark alloying and HFMP to improve their fatigue corrosion resistance, compared to strengthening just by HFMP. Note that in these studies the time of specimen soaking in corrosive medium was from 10 up to 200 h during corrosion fatigue testing. At such a time of specimen staying in corrosive medium, no essential corrosion damage of HFMP-strengthened metal layer usually takes place, that may lead to obtaining overestimated characteristics of corrosion fatigue resistance of welded joints, required for design of structures for long-term operation. Corrosion damage, characteristic for metal structures in service, can be produced by pre-soaking the welded joints in corrosive media.

The objective of this work is assessment of effectiveness of HFMP technology application to improve fatigue resistance characteristics of tee welded joints at the stage of manufacturing the metal structures, long-term operation of which will proceed under the conditions of higher humidity and temperature.

Material and investigation procedure. Experimental studies for corrosion fatigue were performed on specimens of tee welded joints of low-alloyed 15KhSND steel ($\sigma_y = 400$ MPa, $\sigma_t = 565$ MPa), which is widely applied for fabrication of elements of met-

al structures in long-term service (for instance, span structures of railway and road bridges), has higher strength, is readily weldable, resistant to atmospheric conditions, and serviceable in the temperature range from -70 up to 45 °C. Chemical composition of 15KhSND steel is as follows, wt.%: 0.142 C; 0.466 Si; 0.63 Mn; 0.02 S; 0.013 P; 0.31 Ni; 0.66 Cr; 0.34 Cu.

Blanks for welded joint specimens were cut out of hot-rolled sheets of 12 mm thickness (category 12). Dimensions of blanks for tee joints were 350×70 mm. Tee welded joints were produced by manual arc welding with UONI 13/55 electrodes of transverse stiffeners (also from 15KhSND steel) from two sides of the plate by fillet welds. The root (first layer) was welded by 3 mm electrodes, the weld (second layer) was formed by 4 mm electrodes. Figure 1 gives the shape and geometrical dimensions of specimens of tee welded joints. Specimen thickness is due to wide application of 12 mm thick rolled stock in engineering welded structures, and the test portion width of 50 mm was selected proceeding from test equipment capacity.

Experimental studies were conducted in servohydraulic machine URS-20 at alternating tension with cycle asymmetry $R_\sigma = 0$ and 5 Hz frequency at regular loading. The criterion of test completion was total fracture of specimens or exceeding the test base of $2 \cdot 10^6$ stress reversal cycles.

Four series of specimens of tee welded joints were tested:

- 1st: specimens in as-welded (unstrengthened) state;
- 2nd: specimens strengthened by HFMP;
- 3rd: specimens in unstrengthened state after soaking in corrosive medium;
- 4th: specimens strengthened by HFMP after soaking in corrosive medium.

Welded joint strengthening by HFMP technology was conducted with USTREAT-1.0 unit, in which the compact impact hand tool with piezoceramic transducer is connected to ultrasonic generator of 500 W output power. At welded joint strengthening by HFMP, surface plastic deformation was applied to a narrow zone of weld metal to HAZ transition (along the fusion line). Single-row four striker head with 3 mm striker diameter was used as strengthening tool. Speed of HFMP performance at tee joint treatment was equal to 1 mm/s. Amplitude of impact hand tool waveguide edge oscillations was set to 25 μm .

To produce prior corrosion damage, welded specimens of third and fourth series were placed into G4 chamber, in which they were soaked for 1200 h at increased humidity (95 %) and temperature (40 °C).

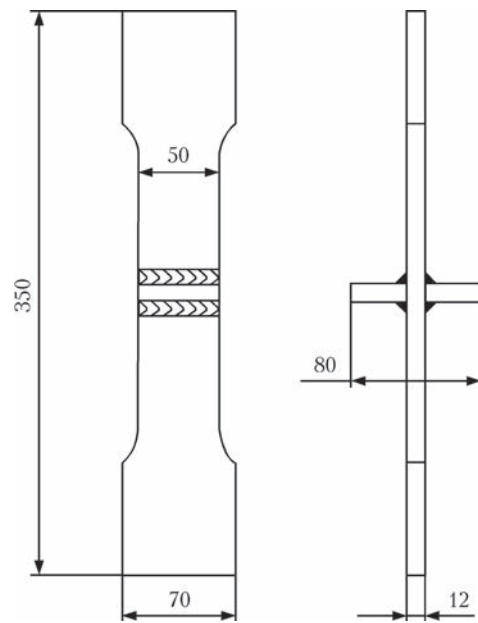


Figure 1. Shape and geometrical dimensions of tee welded joint specimen

Metallographic studies of surface layer of metal of welds and HAZ of tee joints in as-welded (unstrengthened) state and in the state after strengthening by HFMP were performed before and after soaking in the chamber at increased humidity and temperature.

Investigation results. Metallographic studies of base metal and welded joint established the following. Microstructure of base metal of 15KhSND steel rolled stock is ferritic-pearlitic, with about 30–35 % fraction of pearlitic component, striation of 3–4 points from B range to GOST 5640. Grain size corresponds to #7–9 of scale 1 to GOST 5639.

Dimensions of welds and HAZ were determined before microstructural studies of welded joints. Fillet weld width was equal to 12.8–14.3 mm, height was 9.5–12.0 mm. Here, the height of the first weld layer was 4.5 to 6.5 mm, that of the second was 6.8–8.3 mm; that of the HAZ was equal to 1.04–2 mm due to visible changes in metal structure in rolled stock surface layers, and in metal layers farther from the surface it was 3.0–3.8 mm.

Microstructure of the first metal layer was a cellular ferritic-pearlitic structure with grain size #6–8 to GOST 5639 scale 1. Ferrite grains with fine precipitates of MAC-phase of granular type and precipitate-free grains were also detected. Pearlite formations have the form of narrow regions along ferrite grain boundaries. Microstructure of the second layer of weld metal has sufficiently uniform dendritic ferritic-pearlitic structure. Ferrite component contains grains with plate-like MAC-phase precipitates of the type of upper bainite, fine particles of grain type (of lower bainite type), as well as grains of quite large acicular ferrite.

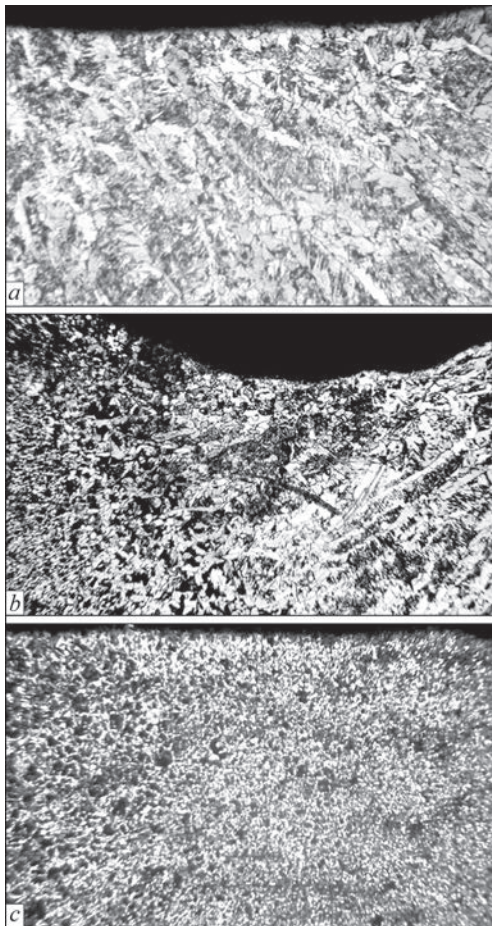


Figure 2. Microstructure ($\times 100$) of surface layer of weld (*a*), CGZ (*b*) and HAZ (*c*) metal of tee welded joint in as-welded state

HAZ metal microstructure is as follows. Immediately at the surface, grain size of coarse-grain zone (CGZ) corresponds to #3–4 to GOST 5639, and its extent is 0.52 mm (2–3 grains). At about 3 mm dis-

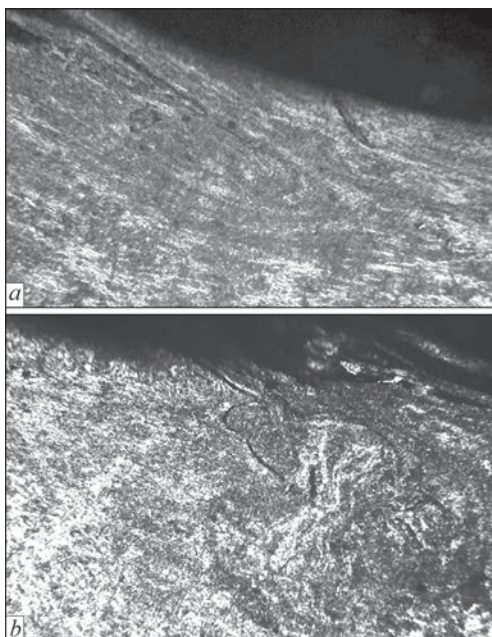


Figure 3. Microstructure ($\times 250$) of weld (*a*) and HAZ (*b*) metal after strengthening by HFMP technology

tance from the surface, CGZ size increases up to 1.04–1.20 mm, but grain size remains on the level of #3–4. Size of pearlite-ferrite grains in fine-grain zone, the size of which is about 1 mm, is equal to #7–10. In CGZ metal of first weld, mainly a mixture of #5–8 ferrite-pearlite grains of up to 0.91 mm length was formed. CGZ structure in the second weld consists of ferrite with densely distributed in its matrix MAC-phase precipitates, with chaotic dispersed particles of grain type, less often — with ordered plate-like particles (of lower or upper bainite type). Grains demonstrate fragmentation – grain division into individual fragments with MAC-phase of different morphology and orientation. Grain boundaries are fringed with ferrite in the form of 1–3 μm wide interlayers and sequences of elongated #8–9 grains. Hardness of first weld metal layer is in the range of $HV0.98-232-241$, that of the second one is $HV0.98-292-325$. Microstructure of surface layer of weld metal, CGZ metal and HAZ metal of tee welded joint in as-welded state is given in Figure 2.

After HFMP, characteristic grooves of practically the same size formed on the line of weld fusion with base metal in the surface layers of the metal of welds and HAZ. Groove width is in the range of 3.0–3.5 mm, their depth being 280–340 μm . Plastically deformed layers of weld metal of 1.70–1.82 mm width and HAZ metal of 1.3–1.7 mm width formed under the groove. Depth of plastically deformed layer of weld and HAZ metal, due to visible changes of metal structure under the groove, was equal to 390–650 μm .

HFMP essentially changed the cast structure of weld metal (Figure 3, *a*). Elongated bainite grains, with grain shape coefficients $K_{sh} = 5-17$ ($K_{sh} = a/b$, where a and b are the length and width of elongated grain, respectively), which are practically parallel to groove bottom, and thread-like ferrite veins formed in the surface layer of metal of up to 130 μm depth. Ferrite grains with $K_{sh} = 4-7$ and individual baintie grains are observed at 260 μm distance from groove bottom.

Changes of grain structure of HAZ metal were also found (Figure 3, *b*). Bainite and ferrite grains elongated at an angle to groove bottom, with $K_{sh} = 7-15$, form in CGZ surface layers of up to 280 μm depth. With further distance from groove bottom, fine ferrite-pearlite grains of #9–11 are observed also in fine-grain zone. Several delaminations of 40 to 300 μm length were found in strengthened metal layer.

Measurements of microhardness were performed in plastically deformed metal layer. Owing to an essential increase of the level of dislocation density as a result of HFMP, microhardness of strengthened metal layer ($HV0.2-344-445$) is by 27 % higher than that of CGZ and by 35 % higher than that of weld metal.

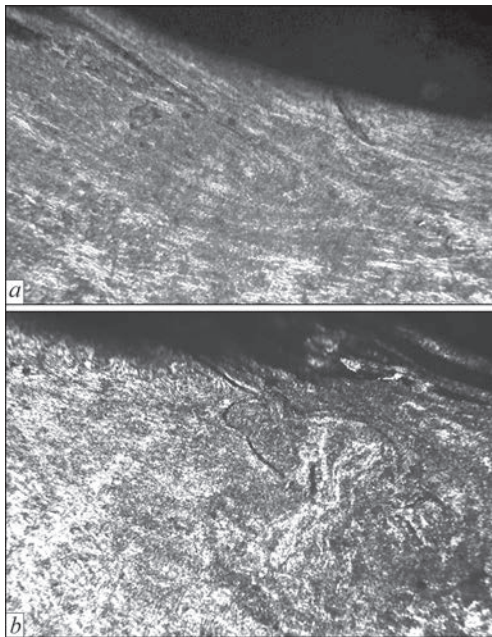


Figure 4. Corrosion damage in HAZ metal of tee welded joint in unstrengthened state after testing at increased humidity and temperature: *a* — $\times 100$; *b* — $\times 250$

In surface layers of metal of weld and HAZ in as-welded (unstrengthened) state quite deep and extended corrosion damage in the form of spots of up to 2.80×0.26 mm size, and sometimes in the form of cavities of up to 1.56×1.17 mm size, is observed after soaking in G4 chamber at higher humidity and temperature (Figure 4). In surface layers of fillet weld metal and HAZ, plastically deformed by HFMP, similar types of corrosion were found (Figure 5, *a, b*) after soaking in G4 chamber, their maximum size not exceeding 1.95×0.16 mm. Moreover, the strengthened layer of weld metal demonstrates corrosion in the form of acicular intercrystalline cracks with corrosion products of 0.65 – 1 mm length and up to 0.65 mm depth (Figure 5, *c*).

The Table gives the results of metallographic investigations with calculated values of the extent of damage and total dimensions of damage area projections, depth of corrosion spot and cavity penetration into the surface layers of metal of fillet welds and HAZ. Depth of cavity penetration into HAZ metal surface layer is not more than 0.39 and 0.26 mm for welded joints in as-welded and HFMP-strengthened states, respectively. Corrosion cavities in surface layers of weld metal both in as-welded state and in HFMP-strengthened state are deeper and reach 1.17 mm. This is, apparently, related to specifics of forming the second weld layer in manual arc welding. On the whole, specimens of tee welded joints, strengthened by HFMP technology, have higher resistance to the impact of higher humidity and temperature (see the Table).

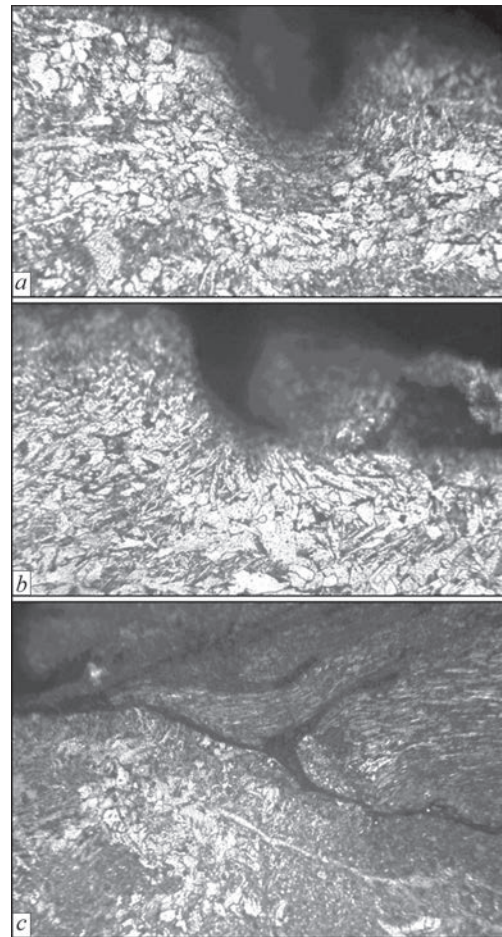


Figure 5. Corrosion damage in the form of spots (*a, b*) and cracks (*c*) in surface layer of metal of tee welded joint strengthened by HFMP, after testing under the conditions of increased humidity and temperature: *a* — $\times 100$; *b, c* — $\times 250$

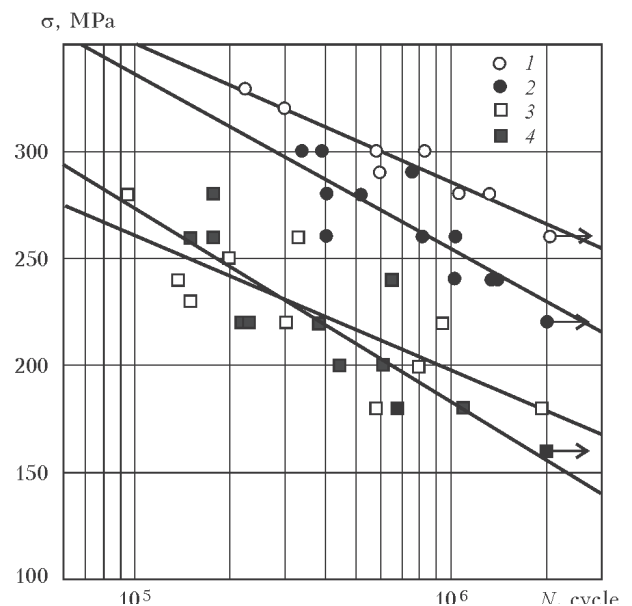


Figure 6. Fatigue curves of tee welded joints of 15KhSND steel: *1, 2* — in HFMP-strengthened state; *3, 4* — in as-welded (unstrengthened) state, before and after soaking in G4 humidity chamber for 1200 h, respectively

Dimensions of corrosion damage in surface layers of metal of welds and HAZ of tee welded joints of 15KhSND steel after soaking for 1200 h at increased humidity and temperature

Specimen state	Spot corrosion of weld surface layers			Spot corrosion of HAZ surface layers		
	Extent of damage, %	Depth of damage, mm	Total projection of damage area, mm	Extent of damage, %	Depth of damage, mm	Total projection of damage area, mm
Unstrengthened	31.2	0.091–1.17	17.615	38.5	0.13–0.39	5.85
HFMP-strengthened	23	0.13–1.17	12.44	29	0.13–0.26	4.42



Figure 7. Appearance of weld zone in as-welded (a) and HFMP-strengthened (b) state after soaking for 1200 h at increased humidity and temperature

Results of fatigue testing of all four series of specimens are given in Figure 6, and the appearance of weld zone in as-welded and HFMP-strengthened states after soaking in humidity chamber for 1200 h is shown in Figure 7.

The given fatigue curves (1 and 3, see Figure 6) demonstrate that application of HFMP technology as a method of SPD of the metal of joints near the areas of fatigue damage accumulation essentially improves fatigue resistance characteristics of tee welded joints without corrosion damage. Cyclic fatigue life of joints rises more than 20 times, and limited endurance limit on the base of $2 \cdot 10^6$ cycles is increased by approximately 47 % (from 180 to 265 MPa). Soaking of tee welded joint specimens in the chamber at higher humidity and temperature for 1200 h leads to lowering of limited endurance limits on the base of $2 \cdot 10^6$ cycles of unstrengthened welded joints by approximately 14 % (from 180 to 155 MPa), and in those strengthened by HFMP — by approximately 13 % (from 265 to 230 MPa). Results obtained on welded joints after corrosive impact (curves 2 and 4) show that prior strengthening by HFMP increases the limited endurance limit of such joints by approximately 48 % (from 155 to 230 MPa), while cyclic fatigue life rises by 6–8 times. Fracture of HFMP-strengthened welded joints,

tested both before and after soaking in G4 humidity chamber, ran mainly at a distance from the weld and HAZ.

Thus, experimental results are indicative of high effectiveness of HFMP technology application to improve fatigue resistance characteristics of tee welded joints in metal structures, operating under moderate climatic conditions under the impact of alternating loading (curves 2 and 4, see Figure 6). Here, it should be noted that protection of HFMP-strengthened surface metal layer from direct impact of atmospheric conditions, i.e. from corrosion damage (for instance, due to application of lacquer-paint coatings), allows achieving maximum characteristics of fatigue resistance of such joints (see curve 1).

Conclusions

1. Metallographic investigations were performed of surface layers of metal of weld and HAZ in as-welded (unstrengthened) and HFMP-strengthened states before and after corrosive medium impact. Proceeding from calculations of the extent and depth, as well as total size of projection of the area of damage by corrosion spots and cavities in surface layers of metal of fillet welds and HAZ of tee welded joints, it was established that strengthening by HFMP technology

improves joint resistance to the impact of higher humidity and temperature.

2. It was confirmed that strengthening by HFMP essentially improves the fatigue resistance characteristics of low-alloy steel welded joints in air. Cyclic fatigue life of tee welded joints of 15KhSND steel after strengthening rises by more than 20 times, and limited endurance limit on the base of $2 \cdot 10^6$ cycles increases by 47 %.

3. High effectiveness of HFMP application to improve fatigue resistance characteristics of welded joints of metal structures, operating under moderate climatic conditions, was established. Strengthening of tee welded joints of 15KhSND steel before soaking in higher humidity and temperature chamber for 1200 h leads to 6–8 times increase of cyclic fatigue life, depending on levels of applied stresses, and 48 % increase of limited endurance limit on the base of $2 \cdot 10^6$ cycles.

1. Kulekci, M.K., Esmé, U. (2014) Critical analysis of processes and apparatus for industrial surface peening technologies. *Int. J. Advanced Manufact. Techn.*, **74**(9), 1551–1565.
2. Pokhmursky, V.I., Khoma, M.S. (2008) *Corrosion fatigue of metals and alloys*. Lviv: SPOLOM.
3. Kolomijtsev, E.V., Serenko, A.N. (1990) Effect of ultrasonic and laser treatment on fatigue resistance of butt welded joints in air and corrosion media. *Avtomatich. Svarka*, **11**, 13–15.
4. Nasilowska, B., Bogdanowicz, Z., Wojucki, M. (2015) Shot peening effect on 904L welds corrosion resistance. *J. Constr. Steel Res.*, Vol. 115, 276–282.
5. Ahmed, A.A., Mhaede, M., Wollmann, M. et al. (2014) Effect of surface and bulk plastic deformations on the corrosion resistance and corrosion fatigue performance of AISI 316L steel. *Surface & Coating Techn.*, Vol. 259, 448–455.
6. Lee Hang-sang, Kim Doo-soo, Jung June-sung et al. (2009) Influence of peening on the corrosion properties of AISI 304 stainless steel. *Corrosion Sci.*, Vol. 51, 2826–2830.
7. Knysh, V.V., Valteris, I.I., Kuzmenko, A.Z. et al. (2008) Corrosion fatigue resistance of welded joints strengthened by high-frequency mechanical peening. *The Paton Welding J.*, **4**, 2–4.
8. Kolomijtsev, E.V. (2012) Corrosion-fatigue strength of 12Kh18N10T steel T-joints and methods of its improvement. *Ibid.*, **12**, 36–38.
9. Mordiyuk, B.N., Prokopenko, G.I., Vasylyev, M.A. et al. (2007) Effect of structure evolution induced by ultrasonic peening on the corrosion behavior of AISI-321 stainless steel. *Mater. Sci. and Eng. A*, Vol. 458, 253–261.
10. Hashemi, B., Rezaee Yazdi, M., Azar, V. (2011) The wear and corrosion resistance of shot-peened nitrided 316L austenitic stainless steel. *Materials and Design*, **32**, 3287–3292.
11. Daavary, M., Sadough Vanini, S.A. (2015) Corrosion fatigue enhancement of welded steel pipes by ultrasonic impact treatment. *Mater. Lett.*, Vol. 139, 462–466.
12. Prokopenko, G.I., Mordiyuk, B.N., Knysh, V.V. et al. (2014) Improvement of fatigue and corrosion resistance of welded joints by ultrasonic impact treatment and electrical-discharge alloying. *Tekhn. Diagnostika i Nerazrush. Kontrol*, **3**, 34–40.

Received 02.02.2016

PECULIARITIES OF FORMATION OF STRUCTURE OF WELDED JOINTS IN ARC SURFACING WITH PULSE FEED OF ELECTRODE WIRE

V. A. LEBEDEV¹, I.V. LENDEL¹, A.V. YAROVITSYN¹, E.I. LOS¹ and S.V. DRAGAN²

¹E.O. Paton Electric Welding Institute, NASU

11 Kazimir Malevich Str., 03680, Kiev, Ukraine. E-mail: office@paton.kiev.ua

²National Shipbuilding University

19 Geroev Staliningrada Ave., 54025, Nikolaev, Ukraine

It is shown that process of CO₂ arc surfacing with pulse feed of electrode wire in contrast to its continuous feed is characterized by increased stability, lower loss of electrode metal for spattering and improved characteristics of wear resistance of 30KhGSA deposited metal. Determined was an optimum range of parameters of electrode wire pulse feed, namely frequency 10–30 Hz and relative pulse duration 3–5 units. It is shown that reduction of penetration depth of base metal is achieved due to current decrease at stage of droplet growth in elementary cycle of electrode metal transfer. Comparative examination of microstructure of deposited metal and HAZ was carried out employing scanning electron microscopy at continuous and pulse feed of electrode wire at $\times(500\text{--}2000)$ magnifications. 18 Ref., 2 Tables, 10 Figures.

Keywords: arc welding, surfacing, pulse algorithms, feed system, electrode wire, welded joint, microstructure

Mechanized and automatic methods of arc welding and surfacing, including in shielding gases, have gained wide acceptance and being continuously improved. Many of published works represent sufficiently important results on indicated processes, but frequently these are not finished researches.

Some delay in investigations of process efficiency of consumable electrode welding and surfacing using wire feed pulse mode system and arc movements along process line was earlier related with their technical imperfection. Currently a series of developments were carried out in this field employing current computerized electric drives based on AC electric motor of special design. In particular, it allowed realizing virtually any algorithm of electrode wire movement, including reverse motion with regulation of all constituents, namely frequency, pitch, pulse amplitude as well as relative pulse duration. At that, frequency range exceeding 50 Hz is achieved. Expanded process characteristics of new electrode wire feed systems provided the possibility for significant advance in control of geometry characteristics of welded joint, optimizing power consumption and loss of electrode metal.

Results received in works [1–3] allows stating that pulse functioning algorithms of the electrode wire feed systems can be one of the most efficient methods of improvement of mechanized and automatic methods of consumable electrode arc welding and surfacing.

It should be noted that research work on use of current regulated pulse feed systems is carried out with solution of very important problem, i.e. control (in that or another level) of weld metal structure. Importance and ways for solution of mentioned problem are indicated in series of works, for example [4, 5], however, as far as we know, at present time no system researches in considered direction using current methods of metallographic investigations are done.

Aim of the present work is a statement of results of carried investigations on process stability, transfer of alloying elements in deposited metal, wear resistance of beads, microstructure of welded joint employing undisturbed and pulse electrode wire feed for process of automatic CO₂ surfacing with description and interpretation of obtained results applicable to indices of deposited bead service characteristics.

Figure 1 represents a unit for surfacing of standard plates. Comparative evaluation of stability of process of CO₂ arc surfacing at continuous (CFEW) and pulse feed of electric wire (PFEW) were carried out by statistical analysis of recorded oscillograms of welding current and voltage on known procedures [6, 7]. Modes of bead deposition at CFEW and PFEW are the following: $I \approx 230\text{--}250$ A, $U = 27$ V and average rate of electrode wire feed $v_{\text{av.w.f}} = 0.1$ m/s. PFEW frequency made 25 Hz, relative pulse duration was 3 units.

Analysis of values of such statistical parameters, as dispersion, mean-square deviation and coefficients

Table 1. Parameters of surfacing process stability at CFEW and PFEW

Stability parameter	Surfacing modes			
	I_a	U_a	t_a	$t_{sh.c}$
CFEW				
$\bar{\chi}_{av}$	230.53	29.43	0.031	0.006
$\sigma^2(x)$	148.49	0.77	$0.75 \cdot 10^{-4}$	$0.1 \cdot 10^{-5}$
$\sigma(x)$	12.19	0.88	0.0087	0.001
$k_v(x)$	5.29	2.99	28.06	16.67
PFEW				
$\bar{\chi}_{av}$	175.54	30.05	0.036	0.004
$\sigma^2(x)$	71.17	0.0625	$0.4 \cdot 10^{-5}$	$0.17 \cdot 10^{-6}$
$\sigma(x)$	8.44	0.25	0.002	$0.41 \cdot 10^{-3}$
$k_v(x)$	4.81	0.83	5.56	10.25

$\bar{\chi}$ — process parameter of surfacing.

of current variation I_a and voltage U_a in a region of droplet growth, duration of this region t_a and time of short circuit $t_{sh.c}$ (Table 1) shows that at PFEW there is a reduction of the coefficients of voltage variation in region of droplet growth and 3.5 and 5 times decrease of duration of this region, respectively. It is known fact [6–8] that spattering of electrode metal and quality of deposited bead formation are tightly related with the indices of stability of burning of reverse polarity arc in consumable electrode. Therefore, significant increase of stability of surfacing process under effect of inertia, applied to electrode wire edge, can be an explanation of dramatic decrease of the value of electrode metal loss at PFEW [1–4]. The result of complex investigations on evaluation of effect of PFEW parameters on geometry of deposited metal and loss of electrode metal allowed determining a range of pulse frequency change for 1.2 mm electrode wire, which is mostly suitable for surfacing tasks (on criteria of minimum portion of the base metal), namely frequency $f = 10–30$ Hz and relative pulse duration $S = 3–5$ units.

Regardless the fact that volume of droplet of electrode metal and duration of its growth at PFEW are somewhat increased in comparison with CFEW (Figure 2, see Table 1), there are not conditions for

Table 2. Comparative results of emission spectral analysis of deposited metal of 30KhGSA type at CFEW and PFEW of 1.2 mm diameter in CO₂ surfacing

Specimen	Content of elements, wt.%				
	C	Si	Mn	Cr	Ni
1 layer (CFEW)	0.17	0.87	1.10	0.63	<0.10
1 layer (PFEW)	0.17	0.80	1.06	0.55	<0.10
5 layer (CFEW)	0.20	0.70	0.84	0.90	<0.10
5 layer (PFEW)	0.21	0.78	0.81	0.98	<0.10

Note. Surfacing was carried out on 09G2S steel plate (GOST 19281–89) using Np-30KhGSA wire (GOST 10534–98); data were taken from polished area of longitudinal bead surface (unit DFS-36).



Figure 1. IZRM-5 unit with PFEW mechanism

significant reduction of transfer of alloying elements in the deposited metal (Table 2). Calculated estimation of droplet temperature using its total heat, based on data of high-speed filming and oscillograms of welding current and voltage, showed its reduction by approximately 25 % at $f = 10–25$ Hz and $S = 3–5$ for PFEW.

Investigations of effect of parameters of PFEW on service properties of the deposited layer showed (Figure 3) that this method, applying $f = 15–20$ Hz and $S = 3–5$, allows acquiring wear resistance properties, similar to five-layer surfacing with CFEW, already in the first layer of the deposited metal. Comparison of wear resistance of five-layer deposited metal showed that PFEW also promotes for 1.2–1.4 times improvement of wear resistance (see Figure 3).

Increase of wear resistance characteristics of 30KhGSA deposited metal is provoked, first of all, by significant decrease of base metal penetration depth and, respectively, reduction of its portion in the deposited bead. This effect mainly appears due to 20–30 % limitation of heat amount being emitted at PFEW (Figure 4). This, in turn, based on comparative analysis of oscillograms at CFEW and PFEW, in the latter case is caused by drop of welding current value in the

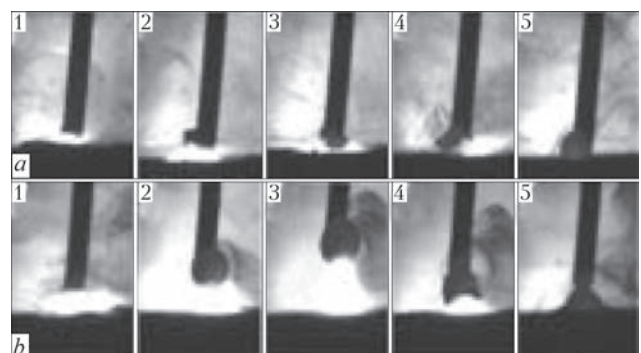


Figure 2. Shots of high-speed filming of electrode metal transfer cycle in CO₂ surfacing: a — CFEW; b — PFEW

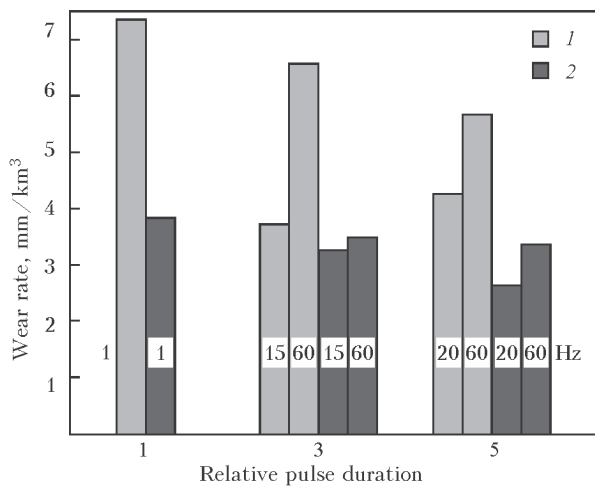


Figure 3. Histogram of evaluation of wear rate of specimens of 30KhGSA deposited metal in wiping of craters using shaft–plane scheme without additional lubrication in friction zone depending on frequency, relative pulse duration and amount of deposited layers $n = 1$ (1) and 5 (2) at $I_{av} = 220$ A and $U = 26$ V

stage of droplet growth due to periodic elongation of arc and reduction of its pressure force on molten weld pool metal.

Comparative experimental investigations of a base–deposited metal welded joint were carried out in order to explain the reasons of increase of wear resistance of 30KhGSA deposited metal at multi-layer surfacing, when effect of mixing of base and deposited metal is virtually eliminated. The microstructure of deposited metal and HAZ in the base metal was examined using optical $\times(50-500)$ and back-scattered SEM methods $\times(500-2000)$ on microsections of single-layer deposits etched in 4 % solution of HNO_3 . View of observed phases, formed as a result of decomposition of primary austenite grain (ferrite, bainite, pearlite), was specified by means of Vickers’s hardness measurement using LECO M400 hardness gauge at 100 g loading.

It is determined that structure of 30KhGSA deposits consists of acicular ferrite crystal grains [9, 10] ($HV0.1-2360-2540$ MPa), divided by ferrite layers of up to 2.5 μm thickness (Figure 5). Comparative anal-

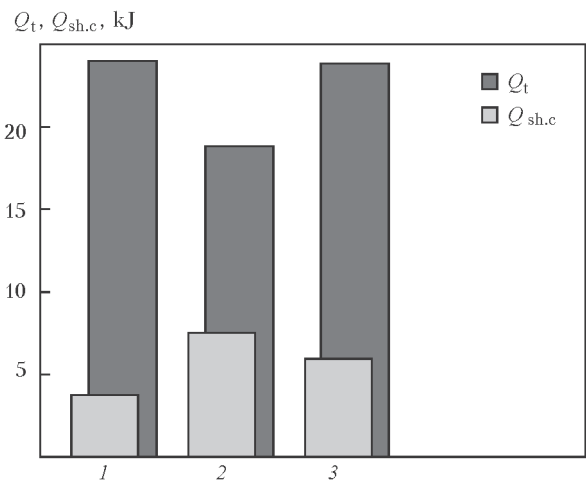


Figure 4. Histogram of evaluation of total heat power Q_t and power in short circuit area $Q_{sh,c}$ (portion of Q_t) at CFEW and PFEW during 5 s: 1 — CFEW; 2 — PFEW at 25 Hz; 3 — PFEW at 60 Hz

ysis of shape and size of crystal grains in the central part of the deposited metal showed that at PFEW they have somewhat smaller width and shape coefficient. Thus, in CO_2 surfacing the width of crystal grains at CFEW equals 97.5 and at PFEW it is 70 μm ; coefficient of shape of crystal grains at CFEW equals 6.8 and it makes 4.56 at PFEW. PFEW also promotes a tendency to limitation of length of crystal grains, significant part of which does not exceed 210 μm versus 640–700 μm at CFEW.

Metallographic analysis of the deposited metal at larger magnification $\times(1000-2000)$ showed that crystal grain boundary of more favorable shape (Figure 6) is observed at PFEW. In other words, thickness of layers of polygonal ferrite [9, 10], which is supposed to be the most dangerous structure from point of view of brittle fracture [11, 12], is mainly reduced in 1.5–2 times; lamellar (Widmanstatten) ferrite [9, 10] is absent on crystal grains periphery; precipitation of microparticles of acicular ferrite changes their shape mainly for polyhedrous.

It is known that the structure of acicular ferrite in the weld metal provides for optimum combination of

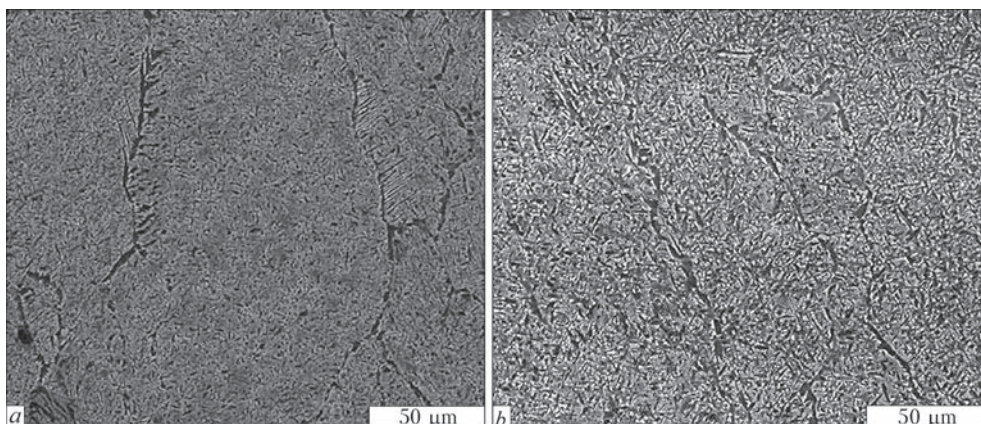


Figure 5. Microstructure of deposited metal of 30KhGSA type: *a* — CFEW; *b* — PFEW

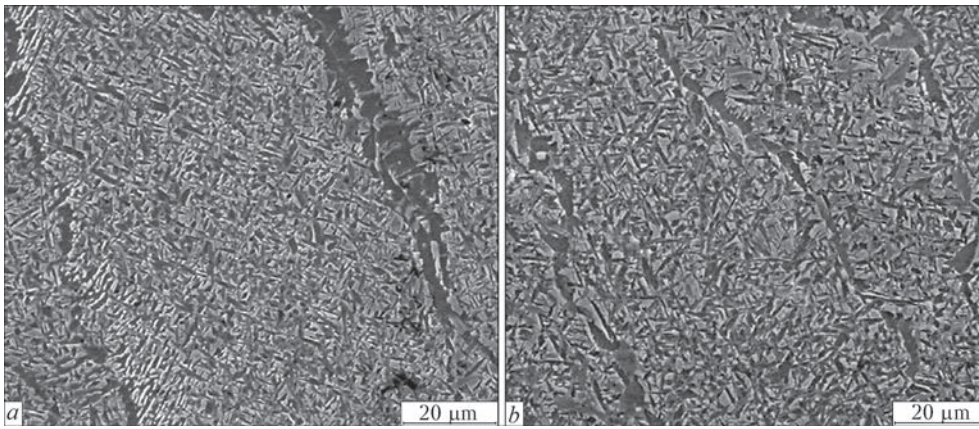


Figure 6. Microstructure of deposited metal of 30KhGSA type: *a* — CFEW; *b* — PFEW

characteristics of its strength and ductility [11–13] as well as, together with acicular troostite [14], differs by increased wear-resistance in comparison with ferrite-pearlite one (Figure 7). The latter fact is caused by refining the structure of microprecipitates of acicular ferrite to approximately 0.5 μm size under the effect of subsurface cold work [15]. The effect of increased wear resistance of acicular ferrite can also be related with presence in it of MAC-microcomplexes (MAC-phase [9, 16, 17]) (Figure 8), distributed inside the crystal grains and along polygonal ferrite layers.

Thus, 20–40 % improvement of wear resistance at five-layer surfacing with PFEW in comparison with CFEW (see Figure 3), under conditions of almost complete elimination of factor of mixing of the base and deposited metals, can be explained by enhancement of acicular ferrite structure, namely more favorable shape of crystal grains, reduction of volume fraction of polygonal and lamellar ferrite on their periphery, and, probably, optimization of morphology and distribution of MAC-phase in acicular ferrite content.

At CFEW the crystal grains of 20–40 μm width with ferrite fringes of 2.0–2.5 μm (Figure 9, *a*) are present in the deposited metal close to fusion line. It means significant increase of volume fraction of the fringes of polygonal and lamellar ferrite ($HV_{0.1}$ -2210–2280 MPa) on the periphery of crystal grains. Such a structure, based on data of work [13], promotes

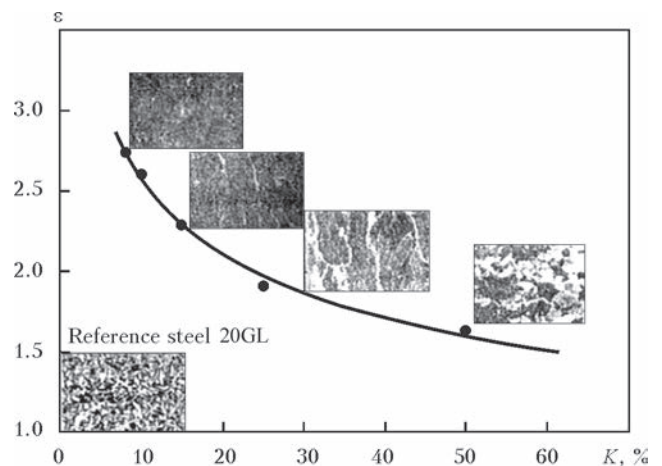


Figure 7. Relative wear resistance of deposited metal ϵ versus volume fraction of polygonal ferrite *K* [15]

for increase of weld susceptibility to brittle fracture. Presence of disoriented structure virtually without polygonal ferrite fringes (Figure 9, *b*) is observed at PFEW in the deposited metal close to fusion line.

The next structural constituents are observed (Figure 10) in HAZ in 09G2S base metal: lower bainite ($HV_{0.1}$ -3000–3500), upper bainite ($HV_{0.1}$ -2600–2660) and lamellar ferrite ($HV_{0.1}$ -2210–2280 MPa). More uniform microstructure, consisting of upper and lower bainite with somewhat reduced content of lamellar ferrite (Figure 10, *b*) is present at PFEW in HAZ metal in the coarse grain region. Also a tendency

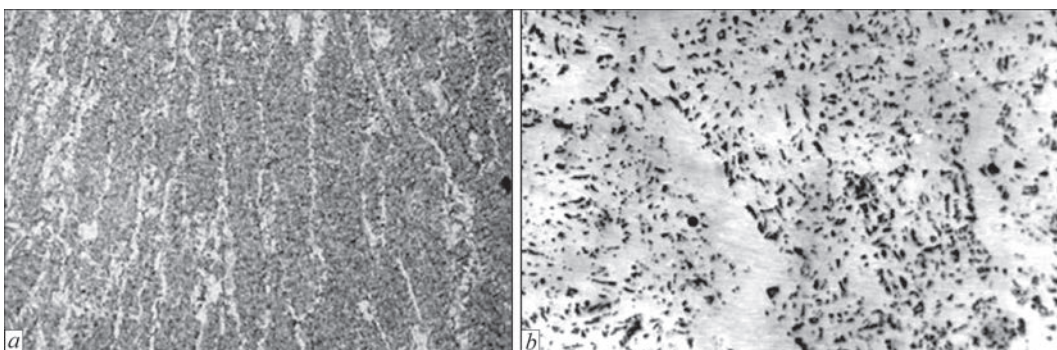


Figure 8. Microstructure of weld metal in 10G2FB steel obtained with Mn–Ni–Mo wire and flux AN60: *a* — etching in nital (×100); *b* — in sodium picrate (×800) [13]

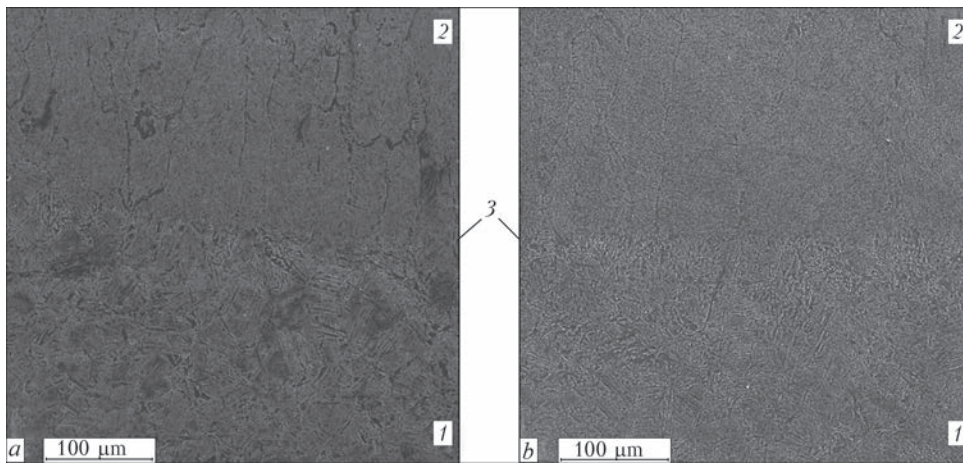


Figure 9. Microstructure in area of fusion line at CFEW (a) and PFEW (b): 1 — 09G2S base metal; 2 — 30KhGSA deposited metal; 3 — fusion line

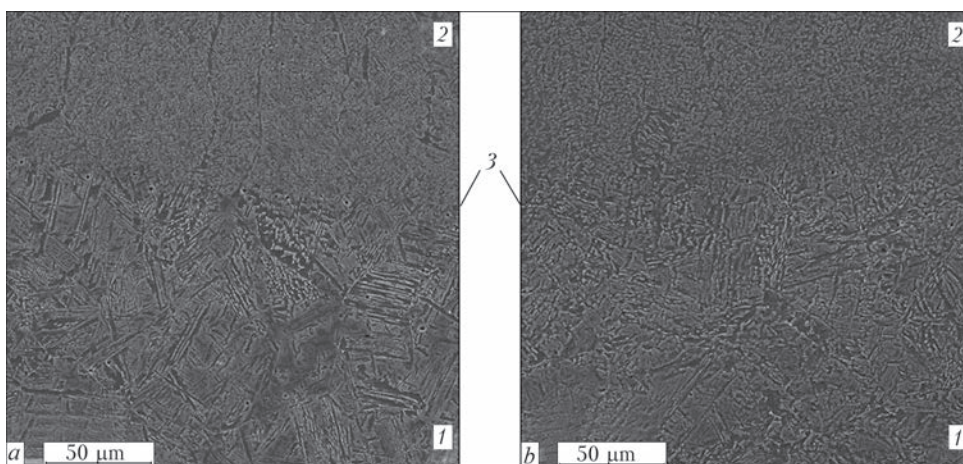


Figure 10. Microstructure in area of fusion line at CFEW (a) and PFEW (b): 1 — 09G2S base metal; 2 — 30KhGSA deposited metal; 3 — fusion line

to transfer of upper and lower bainite microstructure from acicular to grain morphology (see Figure 10, b) is noted in HAZ metal at PFEW. Based on data of work [18], such a structure is the most favorable from point of view of weldability of the base metal and service reliability of its HAZ, in particular, under conditions of low temperatures.

There is a significant drop of microhardness in fine grain region of HAZ of 09G2S base metal. It made $HV0.1$ -2160–2280 at CFEW and $HV0.1$ -2060–2130 MPa at PFEW. Ferrite regions were present in incomplete solidification area, and microhardness, respectively, approached to the values typical for base metal: $HV0.1$ -1700–1810 at CFEW and $HV0.1$ -1870–2060 MPa at PFEW. Banded ferrite-pearlite structure was present in the depth of 09G2S base metal; its microhardness made $HV0.1$ -1470–1600 MPa.

Conclusions

1. It is shown that process of CO_2 arc surfacing with PFEW is characterized by increased stability and

smaller loss of electrode metal for spattering in comparison with CFEW.

2. Optimum range of PFEW parameters is determined, namely $f = 10\text{--}30$ Hz and $S = 3\text{--}5$. It is shown that limitation of penetration depth is achieved due to current reduction at stage of droplet growth in elementary cycle of electrode metal transfer, and, respectively, heat inputs, common for this cycle.

3. It is determined that 30KhGSA metal deposited in optimum range of PFEW parameters has increased wear resistance in comparison with CFEW. This effect is reached due to reduction of portion of base metal in the deposited one and microlevel improvement of structure in the body and on the boundary of acicular ferrite crystal grains (magnification more than $\times 500$).

4. It is shown that at PFEW the microstructure of deposited metal in area of fusion line and HAZ of the base metal is the most favorable from point of view of weldability and service reliability of the welded joint.

1. Lobanov, L.M., Lebedev, V.A., Maksimov, S.Yu. et al. (2012) New capabilities of mechanized arc spot welding using pulse effects. *The Paton Welding J.*, 5, 12–16.

2. Lebedev, V.A., Lendel, I.V. (2013) Control of pulse movement of electrode wire in mechanized welding due to change of feed pitch. *Zagotovit. Proizv. v Mashinostroenii*, **3**, 10–14.
3. Paton, B.E., Lebedev, V.A., Poloskov, S.I. et al. (2013) Application of mechanical pulses for control of processes of automatic and mechanized consumable electrode welding. *Svarka i Diagnostika*, **6**, 16–20.
4. Lebedev, V.A., Lendel, I.V. (2015) Investigation of technological possibilities of arc welding and surfacing with pulsed feed of electrode wire. *Nauk. Tekhn. v Mashinostroenii*, **9**, 20–27.
5. Lebedev, V.A. (2007) Specifics of welding of steels with pulsed feed of electrode wire. *Svarochn. Proizvodstvo*, **8**, 30–35.
6. (1990) *Metallurgy of arc welding. Processes in arc and melting of electrodes*. Ed. by I.K. Pokhodnya. Kiev: Naukova Dumka.
7. Lankin, Yu.N. (2011) Indicators of stability of GMAW process. *The Paton Welding J.*, **1**, 6–13.
8. Potapievsky, A.G., Saraev, Yu.N., Chinakhov, D.A. (2012) *Gas metal arc welding of steels. Engineering and technology of future*. Tomsk: TomskPU.
9. Abson, D.I., Dolby, R.E., Hart, P.M. (1978) The role of non-metallic inclusions in ferrite nucleation in carbon steel weld metals. In: *Trends in steel and consumables for welding: TWI Conf. Proc.* London: TWI.
10. Hee Jin Kim, Bong Yong Kang (2000) Microstructural characteristics of steel weld metal. *J. KWS*, **18(5)**, 565–572.
11. Curry, D.C., Knott, J.F. (1978) Effects of microstructure on cleavage fracture stress in steel. *Metal Sci.*, Vol. 12, 511.
12. Kostin, V.A. (2008) Complex assessment of manganese and titanium effect on structure and properties of low-alloy steel welds. *Visnyk PryazovDTU*, **18**, 198–202.
13. Rybakov, A.A., Kostin, V.A., Filipchuk, T.N. et al. (2013) Peculiarities of microstructure formation of weld metal of gas-and-oil pipelines in welding of micro-alloy steels. *Visnyk ChernigDTU*, **63(1)**, 125–131.
14. Frumin, I.I. (1961) *Automatic electric arc surfacing*. Khar'kov: Metallurgizdat.
15. Abramenko, D.N. (2008) *Improvement of wear resistance of freight car parts by arc surfacing of steel layer with acicular ferrite structure*: Syn. of Thesis for Cand. of Techn. Sci. Degree. Moscow: TsNIITMASH.
16. Yurioka, N. (1995) TMPC steel and their welding. *Welding in the World*, **35(6)**, 375–390.
17. Hrivnak, I., Matsuda, F. (1994) Metallographic examinations of martensite-austenite component (MAC) of HAZ metal of high-strength low-alloy steels. *Avtomatich. Svarka*, **3**, 22–30.
18. Ivanajsky, A.A. (2006) *Analysis of structure, phase composition, properties of granular bainite and technology of its formation in welded joints and rolled metal for welded structures*: Syn. of Thesis for Cand. of Techn. Sci. Degree. Barnaul: AltajGTU.

Received 03.12.2015

CALCULATION-EXPERIMENTAL METHOD FOR DETERMINATION OF SPECTRUM COMPONENTS OF NON-STATIONARY LOADING OF CARBON STEEL WELDED JOINT

A.A. LUKASHEVICH

G.S. Pisarenko Institute for Problems of Strength, NASU
2 Timiryazevskaya Str., 01014, Kiev, Ukraine. E-mail: ips@ipp.kiev.ua

The time parameters of the spectrum components of non-stationary loading of welded joints of carbon steel were determined, having a dominant influence on the intensity of fatigue fracture of the structural elements of railway locomotives. A new method was offered for analysis of the results of strain gauge measuring of the evolution of deformation heterogeneity in the welded joint HAZ in the process of fatigue crack development. It was established that in each unit of loads at certain frequencies, the deformations exist which are dominant at fatigue fracture. 12 Ref., 5 Figures.

Keywords: non-stationary loads, fillet welded joint, carbon steel, fatigue crack growth, strain gauge null-indicator method, time-frequency analysis

The parts and elements of structure of transport vehicles are subjected to non-stationary load during service, which is caused by many operational factors [1] (Figure 1).

The oscillation frequency of elements of mechanical structures of carriage parts of railway rolling stock is in the range from 1.5 to 110 Hz [2]. The complex character of force influence of the roadway on the carriage parts is determined by the fact that the frames of carriages, frames of bodies, carrying bodies represent

the oscillating systems with many degrees of freedom and their excitation factors bear a random character. The long-time service is accompanied by the occurring of fatigue fractures such as cracks, in particular, in welded joint, that makes the metal of this zone the most vulnerable to the fracture [3].

The aim of this work is the creation of discrete method for determination of spectrum of the oscillation frequencies, which are correlated with the maximum amplitudes of deformations of the surface areas of the investigated structural element or specimen being under control at their non-stationary loading.

Object and testing procedure. The work presents the testing results on cantilever bending in the mode of non-stationary loading of laboratory specimens of carbon steel St3sp (killed) [4] with fillet welded joints. The specimens of corset type of $3 \times 60 \times 165$ mm size are manufactured according to the requirements of standard document [5], with fillet welded joint [6] and concentrator (Figure 2).

The sizes of mechanical concentrator, being experimentally determined (view *A* in Figure 2) are as follows: $a' = 570.4^{+141.6}_{-190.4}$ μm , $b' = 309.4^{+251.6}_{-104.4}$ μm . Here P_1 — direction of force action on the specimen; and *S* — switch. Specimen *I* with load 3 was installed on bracket 2 (Figure 2).

On modernized vibration stand VEDS-400A [7], fatigue crack was grown to 3–7 mm size in the specimens near the concentrator at nominal stresses of 88–98 MPa of cantilever bending.

The spectrum of specimen loading, which corresponds to the typical spectrum of cycle frequencies

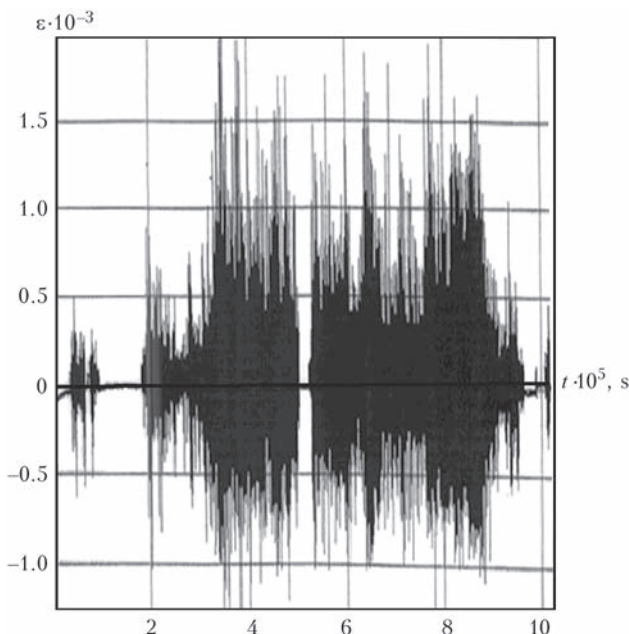


Figure 1. Spectrum of relative amplitudes of deformations of locomotive DS3 structural element during its service

in the range of 20–50 Hz (see Figure 1), is divided into three units according to the program, each having different duration. The loading is created by periodical movement of the vibrating table with amplitude of ± 8 mm in a certain frequency range.

The amplitude of deformations of the specimen surface was registered by strain gauges T1 and T2. In order to extend the dynamic range of sensitivity of the measuring system one of resistors T2 is located by its lattice towards the top of stress concentrator (see view A in Figure 2). The growth of fatigue crack in welded joint was registered using strain gauge null-indicator method by measuring the difference of deformation amplitudes using strain gauges T1 and T2 [8]. To increase sensitivity the signal amplifier up to $U_{\max} = 1500$ mV is installed in the system. The processing of measurement results was carried out using PC connected to device BVK-6 [9].

The deformation measurement results were stored on the flash-memory card of SD format. The information obtained as the separate files is recorded using the special program created on the basis of LabVIEW [10]. The number of units of the obtained information is defined by the volume of computer operative memory. After entering the experimental data into computer, the program displays the oscillograms of dependences of amplitudes deformation on time on the screen. The program runs with the information recognition frequency of 4096 points per second. On the computer monitor the oscillograms of oscillations and values of deformation amplitudes of the specimen with sampling frequency of 2048 p/s were displayed. The number of units where information is contained relatively to the deformation values measured in discrete points of the specimen surface is calculated by formula

$$N_u = N_{\text{inf}} / (N_p / 2), \quad (1)$$

where N_u is the number of units in the given volume of information; N_{inf} is the amount of recorded information of complete sampling; N_p is the number of amplitudes of maximum deformation (determined by the number of points in one information unit).

Analysis of the obtained results. The difference of amplitudes ΔU of the signals received by means of strain gauges T1 and T2, is calculated by formula

$$\Delta U = U_{T2} - U_{T1}, \quad (2)$$

where U_{T2} , U_{T1} is the drop of electric voltage at T2 and T1.

The difference of relative deformations amounted to

$$\Delta \varepsilon = \Delta U M_\varepsilon, \quad (3)$$

where $M_\varepsilon = 10^{-6} \text{ mV}^{-1}$ is the scale factor.

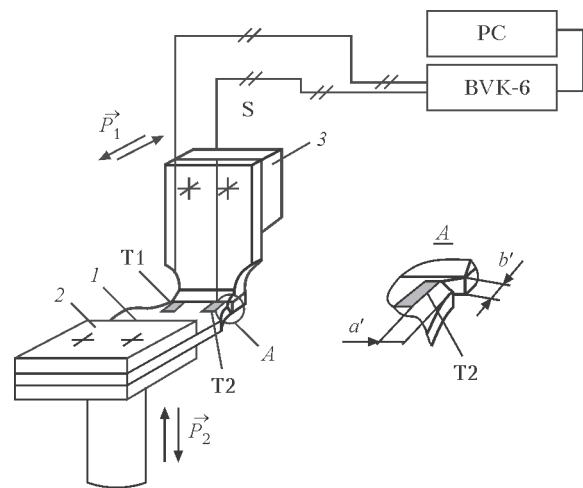


Figure 2. Scheme of loading the specimen on vibrating stand (designations see in the text)

The spectral analysis of units of relative deformation differences was realized using the method of wavelet transformation [11].

The wavelet transformation of $\Delta \varepsilon(t)$ signal has the following form [11]:

$$[W_\Psi \Delta \varepsilon](\tau, s) = \int_{-\infty}^{\infty} \Delta \varepsilon(t) \psi_{\tau, s}^*(t) dt, \quad (4)$$

where τ is the time shift; s is the scale; $\psi_{\tau, s}^*(t)$ is the Gauss mother wavelet [12]. Accepted that $\tau = 250$ ms and $s = 0-150 \text{ Hz}^{-1}$.

The mother wavelet is a function being the prototype of signal of all the scales s generated during wavelet transformation $[W_\Psi \Delta \varepsilon](\tau, s)$ and which is selected by the operator separately for each phase of temporary shift of oscillation period, matching the greatest similarity of signal of the selected maternal function with the scale and temporary factors. The most widespread mother wavelets are built basing on the derivatives of Gauss function [12]:

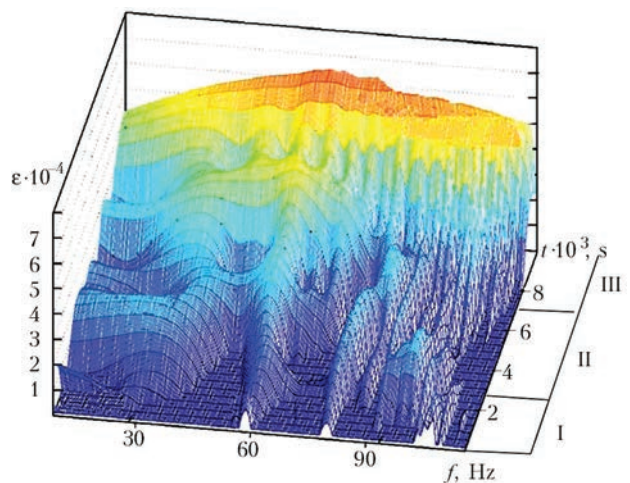


Figure 3. Volumetric wavelet-spectrum in 20–150 Hz frequency range of forced oscillations of fillet specimen of steel St3sp: I, II, III — time intervals corresponding to specific units of deformations

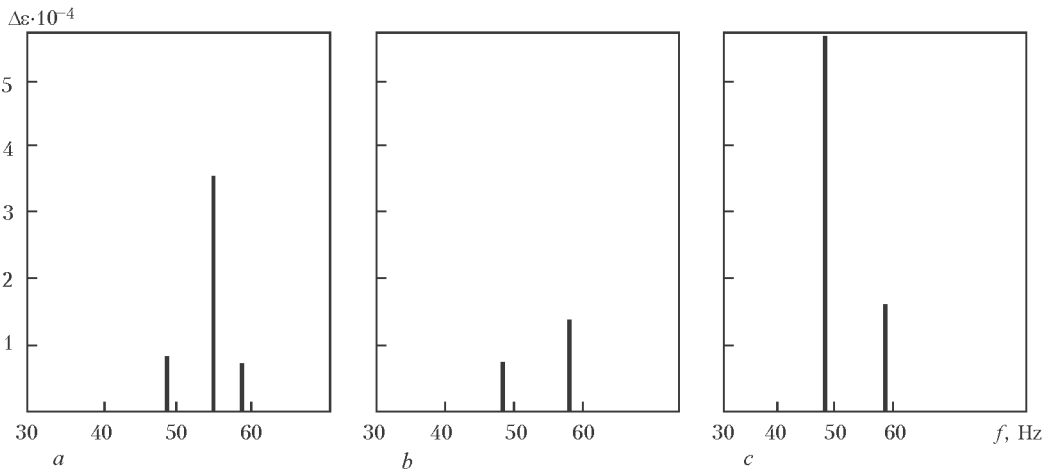


Figure 4. Difference of deformation amplitude versus frequency of specimen loading in units I (a), II (b) and III (c)

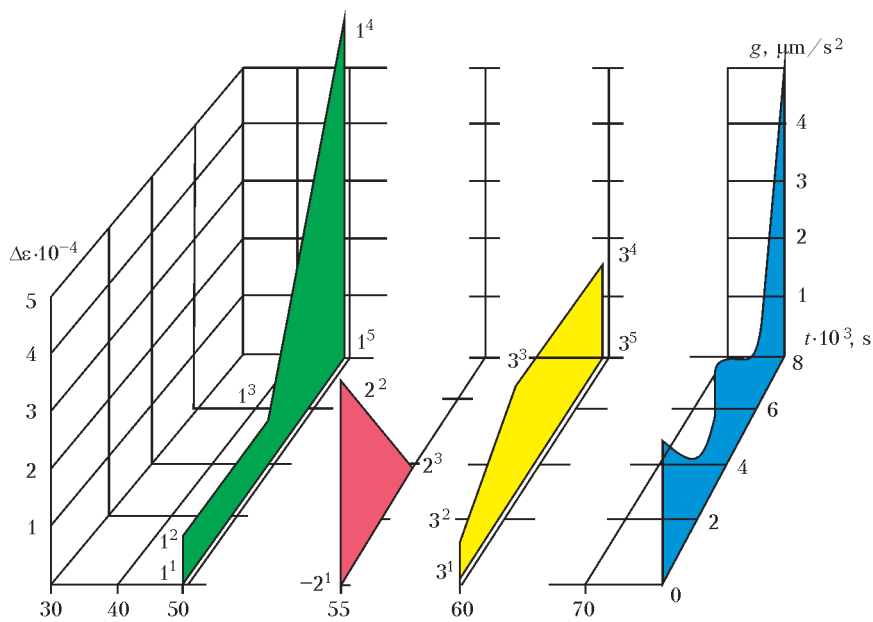


Figure 5. Distribution in time in different units of time-frequency analysis of dominant oscillation amplitudes of the specimen

$$\psi_{\tau, s}^*(t) = \exp(-t/2). \tag{5}$$

Plotting the diagram of distribution of frequencies of amplitude spectrum of deformations in time was performed using the appropriate software [10] (Figure 3).

Figure 4 shows the dependence of differences of amplitudes of deformations $\Delta\epsilon$ of the specimen surface on loads frequency f , which influence the fatigue fracture.

The distribution of signal frequencies, at which the differences in deformation amplitudes of the specimen surface were registered, amounted to 48, 55 and 58 Hz. The crack growth occurs at frequencies of 48, 55 and 58 Hz at deformation unit I, and at 48 and 58 Hz at units II and III, respectively. It was revealed that for each unit the frequencies exist, for which the amplitude of the specimen deformation as a splash (wavelet) is dominant in the process of fatigue fracture.

In Figure 5 in three-coordinate measurements the distribution of deformation cycles in time with specific frequencies is given. In particular, for unit I — 55 (plane $2^1-2^2-2^3$), for unit II — 58 (plane $3^1-3^2-3^3-3^4$), for unit III — 48 Hz (plane $1^3-1^4-1^5$). 3D distribution of oscillation frequencies of the specimen in time for the units of frequency-phase analysis of deformation differences $\Delta\epsilon$ are correlated with the distribution of accelerations g .

The representation of signal in three-coordinate form characterizes the duration of non-stationary loading process in time according to the action of deformation amplitudes of resonant splashes with specific frequencies and accelerations.

Conclusions

1. On the model of the welded structure element the correlation between the maximum amplitudes of frequency spectrum and damaging splashes of differenc-

es of deformations amplitude of the fillet specimen surface was determined.

2. The calculation experimental approach was offered for determination of dominant deformations based on the analysis of spectrum of frequencies of non-stationary loads, that creates new opportunities for improvement of methods of calculation of life of welded structural elements of transport vehicles.

1. Harris, W.J., Zakharov, S.M., Landgren, J. et al. (2002) *General conclusions of advanced experience of heavy-loaded traffic: Problems of interaction between wheel and rail*. 1st ed. Moscow: In-tekst.
2. Basov, G.G., Falaleev, N.I., Yatsko, S.I. (2004) Modern methods of design of locomotive servicing parts. *Zalozn. Transport Ukrainy*, **4**, 39–45.
3. Makhnenko, V.I. (2006) *Resource of safe operation of welded joints and units of modern structures*. Kiev: Naukova Dumka.
4. *DSTU 2651–94*: Ordinary carbon steel. Valid 01.01.96. Kyiv: Derzhstandart Ukrainy.
5. *GOST 25.502–79*: Calculations and strength tests in machine-building. Methods of mechanical tests of metals. Methods of strength tests. Valid 01.01.81. Moscow: Standart.
6. *GOST 5264–80*: Manual arc welding. Welded joints. Main types, structural elements and sizes. Valid 01.07.81. Moscow: Standartinform.
7. Troshchenko, V.T., Tsibanev, G.V., Gryaznov, B.A. et al. (2009) *Fatigue of metals. Influence of surface state and contact interaction*. Vol. 2. Kiev: IPP.
8. Leonets, V.A., Lukashevych, A.O., Degtyarev, V.O. et al. (2012) Assessment of the null-indicator method for the detection of fatigue cracks in structural elements. *Strength of Materials*, **44**(3), 325–332.
9. Tokarev, O.D., Leonets, V.A., Leonets, A.A. et al. (2002) System of dynamic-strength tests of load-carrying structures of rolling stock and track structure at higher speeds of traffic. *ZhD Transport Mira*, **9**, 73–76.
10. Travis, J., Kring, J. (2008) *LabVIEW for all*. Moscow: DMK Press.
11. Astafieva, N.M. (1996) Wavelet-analysis: Bases of theory and examples of application. *Uspekhi Fizich. Nauk*, **11**, 1145–1170.
12. Diakov, V.P. (2002) *Wavelet. From theory to practice*. Moscow: Solon.

Received 20.01.2016

IMPROVEMENT OF THE TECHNOLOGY OF WELDING HIGH-TEMPERATURE DIAPHRAGMS IN STEAM TURBINE FLOW SECTION*

A.K. TSARYUK¹, V.Yu. SKULSKY¹, M.A. NIMKO¹, A.N. GUBSKY², A.V. VAVILOV² and A.G. KANTOR²

¹E.O. Paton Electric Welding Institute, NASU

11 Kazimir Malevich Str., 03680, Kiev, Ukraine. E-mail: office@paton.kiev.ua

²Company «Turboatom»

199 Moskovsky Ave., 61037, Kharkov, Ukraine. E-mail: office@turboatom.com.ua

Special features and causes for operational damage in welded components of high-temperature diaphragms are considered. Comparative testing was performed of welding-technological properties of some commercially available coated electrode grades for welding heat-resistant steels of Cr–Mo and Cr–Mo–V compositions. Implant procedure and welding of Tekken technological samples were used to assess the delayed fracture susceptibility of 15Kh12VNMF + 15Kh1M1FL steel welded joints at application of selected electrodes. It is established that to ensure a high cold cracking resistance of these steel welded joints, it is necessary to apply preheating at 200–250 °C. Proceeding from the data of measurement of metal hardness in welds and HAZ of welded joints and weld metal impact toughness, an optimum mode of heat treatment of 15Kh12VNMF + 15Kh1M1FL steel welded joints was determined. It is shown that a softening zone of lower hardness forms in the HAZ metal structure of 15Kh12VNMF steel, in which the samples fail at testing for static tension at working temperature of 570 °C. 8 Ref., 4 Tables, 10 Figures.

Keywords: arc welding, heat-resistant steels, dissimilar steel welded joints, cold cracks, heat treatment

Characteristic features of components making up the turbine flow section are the impact of dynamic and vibrational forces on them in operation and high requirements to manufacturing accuracy. Combination of various steel grades in one component is extensively applied in these structures. At present, flow section structures in the welded form have become widely accepted in turbine construction practices.

Heat-resistant steels of pearlitic class of 15Kh1M1F type are the usually applied materials for diaphragm body and rim in manufacture of high-temperature

welded diaphragms for high (HPC) and medium pressure cylinders (MPC).

The vanes are made of high-temperature chromium steels of 15Kh11MF, 15Kh12VNMF (EI-802) or 18Kh11MFB type. Stainless chromium steel 12Kh13 is the most extensively applied for shrouds (shroud strip). In manufacture of high-temperature diaphragms these steels should be welded to each other in different combinations. Considering that, the above steels belong to different structural classes, their welding involves certain difficulties in terms of ensuring the required physical-mechanical and service properties of welded joints, as well as their reliable operation under creep conditions at working temperatures from 480 to 600 °C. Therefore, the purpose of this work was optimization of the technology of welding parts from dissimilar steels in manufacture of high-temperature diaphragms to increase the reliability and life of steam turbine flow section.

The diaphragms pertain to the most mass welded components of turbine units. Stationary steam turbines can contain a considerable number of stages (up to 20) and the same number of diaphragms of different type size, respectively. The diaphragms are used to



Figure 1. Control assembly of diaphragms in MPC body

*Based on materials of the work performed under purpose-oriented integrated program of the NAS of Ukraine «Problems of residual life and safe operation of structures, constructions and machines» (2013–2015).

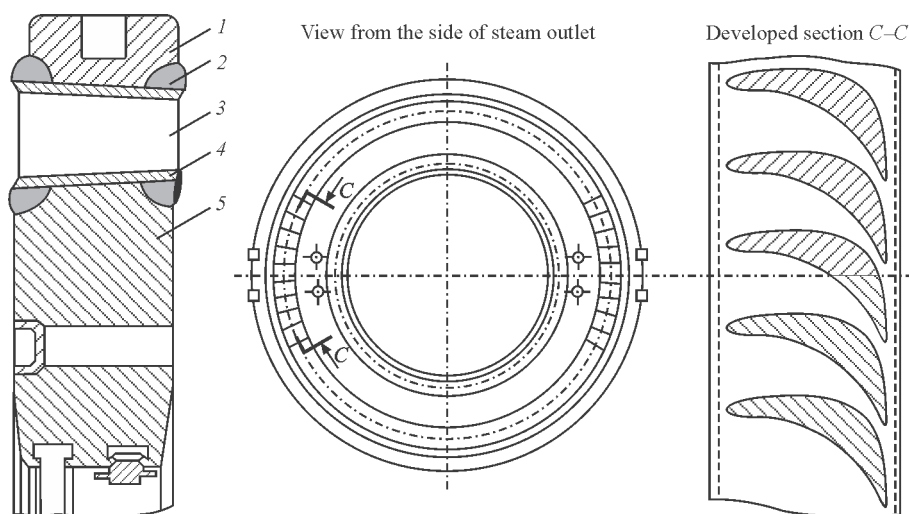


Figure 2. Typical structure of steam turbine welded diaphragm: 1 — rim; 2 — upper shroud strip; 3 — guide vanes; 4 — lower shroud strip; 5 — body

divide turbine cylinder into individual compartments. In the guide-vane assembly of the diaphragms the steam flow potential energy turns into kinetic energy. Moreover, flow direction is established. The guide-vane assembly consists of guide vane grid, forming the nozzle channels.

Diaphragm is one of the most critical parts of the turbine. It has a horizontal joint and consists of two halves. One half is fixed in the lower, and the other —

in the upper half of cylinder body (Figure 1). The diaphragms are inserted directly into the body bores or into special yokes, fixed on the body [1, 2].

Typical structure of steam turbine welded diaphragm (Figure 2) consists of the body, rim and guide-vane grid, including the inner and outer shroud strips with punched holes, into which the vanes are inserted. The shroud strips curved along a cylindri-

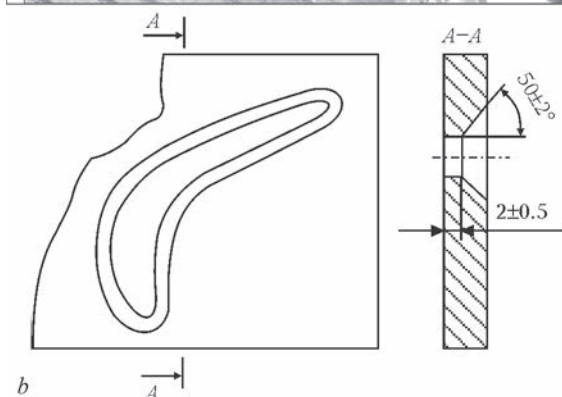


Figure 3. Welding of guide vane end faces to shroud strips by technological weld: *a* — appearance of the grid after welding; *b* — groove shape for vane welding around the contour of profile holes in shroud strip

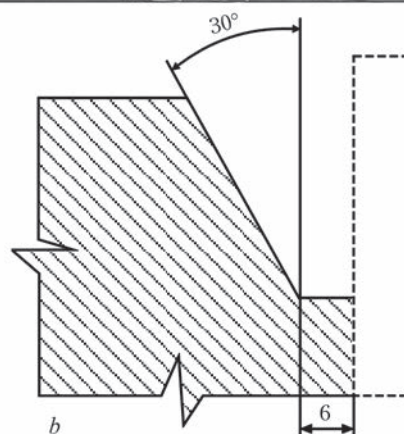


Figure 4. Assembly of diaphragm half for welding of load-carrying welds: *a* — appearance of assembled diaphragm; *b* — typical groove shape in the body (rim) for manual arc welding of load-carrying welds

cal surface are usually made of 4–10 mm thick strip. When assembling the grid, the vanes are mounted in the shroud strip slots, inserting them for 2–3 mm. To ensure a reliable connection of the vanes to the body and the shroud, their end faces are welded around the hole contour by a technological weld, flush with the shroud strip (Figure 3). Then, the vane grid, together with shroud, is welded by the main load-carrying welds to the diaphragm body and the rim (Figure 4). Typical groove shape for welding the main welds of the diaphragm is shown in Figure 4, *b*. These welds are the most stressed areas of welded diaphragms, as they join the shroud strips and vanes to the body and rim, and forces, applied to the vanes due to working medium pressure, are transmitted through them to diaphragm rim. Usually, the height of welds, connecting the grid with the body and rim, is equal to 0.2–0.3 of profile width. Further increase of weld height is not rational, as it leads to excess deformation of the structure in welding.

As shown by calculations [3] and experimental results [4], stresses in the diaphragms are non-uniformly distributed and are the highest in the vanes and welds adjacent to the joint. These stresses decrease markedly at greater distance from the joint. Diaphragm testing to fracture [5] confirms that fracture usually starts from welds of near-the-joint vanes at the body, i.e. in the location that is the most stressed one, according to calculation. Requirements made to accu-

racy of diaphragm manufacture, specify the need to maintain the basic dimensions of the flow section with very close tolerances. Measures ensuring the required accuracy of structure geometry should be specially envisaged to meet the requirements made at all the stages of the technological process of manufacturing the diaphragms. These measures include assembly and welding of diaphragm components in special devices, providing the required accuracy of mounting the inserted parts, allowing for welding deformations when punching slots in shroud strips and application of additional ruggedness in welding, which reduces structure distortion.

Welding deformations are the main reason, causing deviation of diaphragm dimensions from the specified ones. Slot piercing in shroud strips and item machining are performed with sufficient accuracy and tolerances for these operations performance completely fit within the general tolerances for diaphragms. At the same time, welding deformations, as a rule, exceed the admissible ones by the structure operating conditions.

At long-term operation of steam turbines in TPP, emergency situations can develop in the flow section of HPC and MPC, associated with fracture of high-temperature diaphragms. Figure 5 shows the damage of such diaphragms and blades.

The main damage during long-term operation is found in welded joints of guide vanes with diaphragm

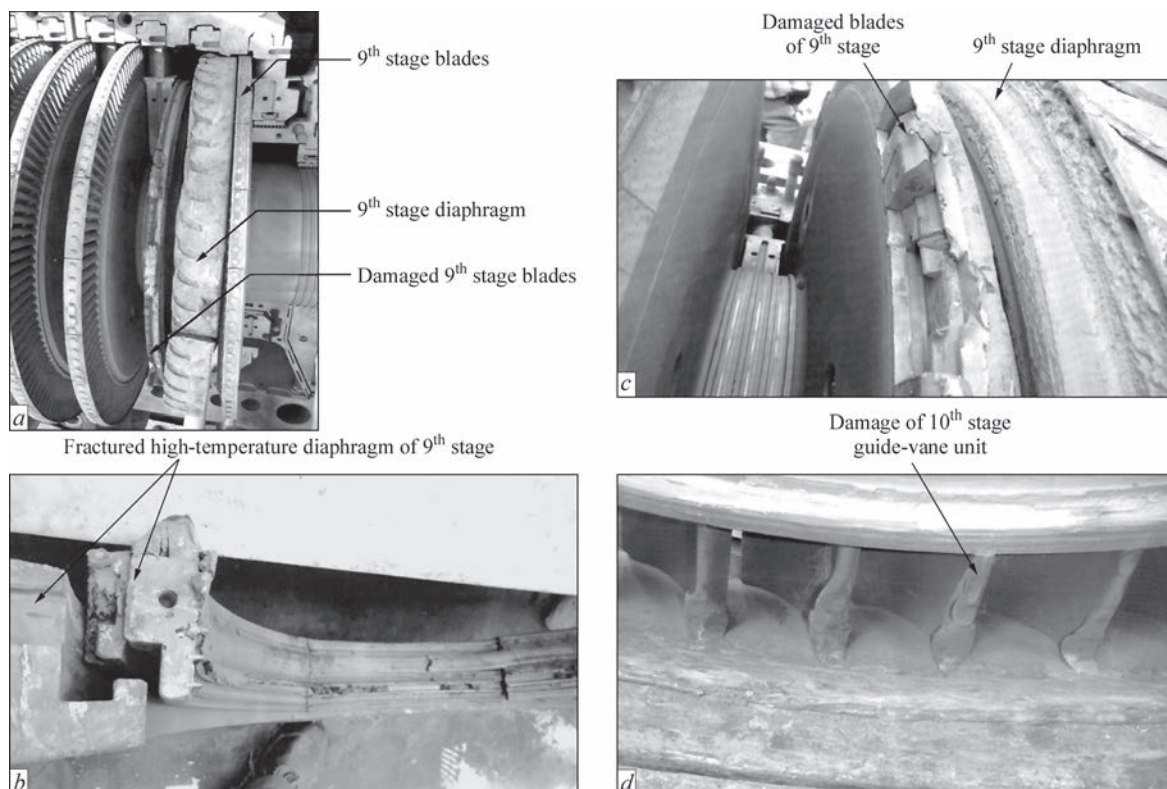


Figure 5. Damage of diaphragms and blades of K-160-130 turbine: *a* — HPC; *b* — HPC; *c* — appearance of damage in HPC flow section; *d* — cracking of guide-vane unit of HPC

Table 1. Composition of metal deposited with coated electrodes for welding high-temperature diaphragms

Electrode grade	Mass fraction of elements, %							
	C	Mn	Si	Mo	Cr	V	S	P
TML-3U	0.06–0.12	0.50–0.90	0.15–0.40	0.40–0.70	0.80–1.25	0.15–0.30	≤0.025	≤0.030
TsL-20	0.06–0.12	0.60–0.90	0.18–0.40	0.40–0.70	0.80–1.25	0.12–0.30	≤0.025	≤0.030

body and rim. Fracture runs in the fusion zone of guide vane end face with weld metal. This zone is the most high-loaded and vulnerable portion of the diaphragm, and determines the serviceability of the diaphragm as a whole. The cause for damage and failure of guide-vane assemblies, apparently, is the influence of technological factors in diaphragm manufacture, as well as formation of stress-strain state in diaphragm structural components under working conditions of turbine operation.

To clarify the possible influence of technological factors in manufacture of welded high-temperature diaphragms, it is of interest to perform analysis of the process of diaphragm assembly, welding and heat treatment at Company «Turboatom» (Kharkov) [6].

Technological instructions on manufacture of welded diaphragms envisage performance of all regulated operations in strict compliance with the requirements of OST 108.021.04–78 [2], RTM 108.020.35–81 [7], as well as design documentation of «Turboatom» DB.

The following welding consumables are applied for welded high-temperature diaphragm components:

- EA-395/9 coated electrodes — for welding the guide vanes from 15Kh12VNMF (EI-802) or 15Kh11MFA steel to shroud strip from 12Kh13 steel;
- TML-3U coated electrodes — for welding the grid to diaphragm body and rim.

Fixing the guide vanes in shroud strip slots during assembly is performed with tack welds of 10–15 mm length. Vane welding around the contour is done in one pass. Welding is conducted simultaneously along the outer and inner shrouds, starting from the segment middle, 2–3 blades at a time, then from the joint side, etc. Grid welding is performed only in its horizontal position.

Application of EA-395/9 electrodes for assembly and welding of chromium steels in grid manufacture enables elimination of preheating and performance of postweld heat treatment (high tempering at 690 °C). Assembly and welding are performed without preheating at reverse polarity direct current. Welding current was 60–80 A for 3.0 mm electrode.

Uphill welding is performed by a short arc with narrow beads. Vane weld sections located vertically or inclined at not more than 15° angle to the vertical can be welded in downhill direction.

Assembly of the diaphragm (grid joining to diaphragm body and rim) is performed in a special de-

vice with TML-3U or TsL-20 electrodes using tack welds of 80 to 120 mm length with local preheating of tack location to 250–300 °C.

Composition of metal deposited with these electrodes is given in Table 1.

Assembled diaphragm is sent on for welding. Diaphragm welding is performed with the same electrodes with preheating and concurrent heating to not lower than 300 °C.

When welding the grid to diaphragm body and rim, groove filling should be started from the side of steam inlet. During welding, periodical tilting of the diaphragm through 180 °C should be performed. The number of tilting operations is determined by the technology of welding this diaphragm.

During welding of circular welds, their peening should be performed. Peening of the first and last layer is not applied. Figure 6 shows the sequence of groove filling. Groove filling is performed in sections of 250–350 mm length in the direction from the middle to the edges. Taking into account the diaphragm tilting, first a layer from the body side, then one from the rim side are welded and so on, continuously alternating layer bead deposition in welds joining the grid to the body and rim.

After welding the diaphragm, not letting it cool below 300 °C, it is placed into the furnace, and tempering is performed at 710–720 °C. Heating to tempering temperature should be conducted at the rate of 50–60 °C/h. A pause between welding and heat treatment of up to 72 h is allowed under the condition of

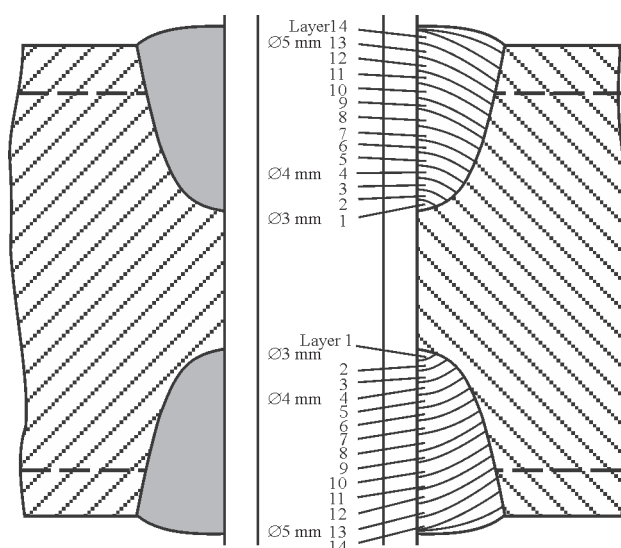
**Figure 6.** Sequence of filling the grooves of load-carrying welds

Table 2. Composition of metal deposited with MTS-4 and Kupfer 3KC electrodes

Electrode grade	Composition, wt. %													
	C	Si	Mn	Cr	Ni	W	V	Mo	Nb	Cu	P	S	[N ₂]	[O ₂]
MTS-4	0.16	0.20	0.53	10.5	0.51	0.47	0.21	0.87	0.046	<0.1	0.017	0.007	0.03	0.052
Kupfer 3KC	0.12	0.35	0.91	1.38	0.07	–	0.25	1.0	–	<0.1	0.021	0.012	0.03	0.048

weldment soaking after welding for 5 h at preheating temperature and delayed cooling. Soaking at specified temperature is performed for 6–12 h. Cooling is conducted at not more than 50 °C/h rate to the temperature of 150 °C.

Performed analysis of the causes for damage of high-temperature diaphragms (see Figure 5), as well as studying the currently applied technology of welding the guide-vane assembly and the load-carrying welds of the diaphragm shows that one of the determinant factors of fracture is the low level of load-carrying weld metal service properties (ultimate strength and yield limit). Coated electrodes of TML-3U or TsL-20 type, applied for manual welding of load-carrying welds, cannot ensure the required service properties of welded joints of guide vanes from 15Kh11MFA steel with body and rim of diaphragm from 15Kh1M1FL steel. As to long-term strength values, the metal of weld, made with the above electrodes, is significantly inferior even to cast steel 15Kh1M1FL of the body and rim. This is indicative of the need to improve the currently available technology of welding the diaphragm joints. In view of the above, selection of advanced welding consumables and improvement of the technology of welding high-temperature diaphragms is an extremely important problem. The urgency of its solution rises in connection with the need to create new generation turbogenerators with high steam parameters (up to 600 °C temperature and 300 bar pressure).

A marketing search was first conducted to find coated electrodes for welding heat-resistant steels of Cr–Mo and Cr–Mo–V composition, providing guaranteed long-term strength (σ_{lt}) of weld metal at 570 °C during 100,000 h at the level of 140–150 MPa (σ_{lt} of 15Kh1M1FL steel at 570 °C for 100,000 h is equal to 100 MPa). Local electrodes, as well as electrodes of Bohler (Germany), ECAB (Sweden) and other foreign manufacturers were considered. Based on marketing search results, preference was given to the following electrodes manufactured by Bohler:

- Thermanit MTS-4 (basic coated chromium electrodes (up to 11 % Cr) for welding steels, operating at up to 580 °C temperatures);
- Phoenix SH Kupfer 3KC (basic coated Cr–Mo–V electrodes for welding components operating at up to 600 °C temperatures).

Comparative studies of the above electrodes demonstrated somewhat better welding-technological properties at application of Phoenix SH Kupfer 3KC electrodes.

Main element content and gas content in the metal deposited with the above electrodes is given in Table 2.

Content of diffusible hydrogen in the deposited metal was studied using alcohol sample [8]. Investigation results showed that diffusible hydrogen content in the deposited metal in welding with MTS-4 electrodes is at the level of $[H]_{dif} = 2.1\text{--}2.3$, and in welding with Kupfer 3KC electrodes $[H]_{dif} = 1.8\text{--}2.0$ cm³/100 g. In keeping with the data of [8], diffusible hydrogen level in the deposited metal should be lower than 5.0 cm³/100 g, that corresponds to the requirements made of both the coated electrode grades.

Thus, the conducted comparative testing of welding-technological properties of coated electrodes for welding combined joints of heat-resistant steels of Cr–Mo–V composition and chromium steel with 11–12 % Cr showed that tested electrode grades MTS-4 and Kupfer 3KC are, in principle, suitable for making load-carrying welds of high-temperature diaphragms.

Delayed cracking susceptibility of welded joints of 15Kh12VNMFA steel was assessed by testing by Implant procedure and by welding technological samples of Tekken type (GOST 26388–84) with application of selected electrodes. The criterion of delayed fracture resistance by Implant method is critical stress, above which test joints fail. Stress in the joint is calculated as the ratio of loading force to sample cross-section.

Results of testing by Implant method are given in Figure 7. It is seen that compared to welding without preheating, a significant increase of critical stresses is in place at preheating above 150 °C. Maximum level of stresses in 15Kh12VNMFA steel joint is maintained at $T_{pr} \sim 250$ °C. The highest cracking resistance corresponds to this condition. Preheating to higher temperature under these experimental conditions did not give any advantage. Cracking resistance remained at approximately the same level, as in joints welded with $T_{pr} = 250$ °C.

Results of Implant testing of 15Kh12VNMFA steel joints, made with Kupfer 3KC electrodes, are given in Figure 7, *b*. The curve, separating the regions of crack presence and absence, consists of tentative values of critical stresses.

Preheating up to 100 °C practically does not affect crack resistance — critical stresses remain on the same level as in welding without preheating. At preheating above 100 °C, crack resistance rises markedly, that is indicative of the rationality of application of preheating at these temperatures. At application of $T_{pr} = 200\text{--}250$ °C delayed cracking resistance rises more intensively than at preheating in the range of 150–200 °C. This is confirmed by a steeper rise of the curve in 200–250 °C section than in that for 150–200 °C (or greater angle α_2 of inclination of the tangent to the curve in 200–250 °C section than angle α_1 in 150–200 °C section).

Derived testing results confirm that preheating in the range of 200–250 °C should be used to ensure a high delayed cracking resistance of 15Kh12VMFA steel welded joints at application of Kupfer 3KC electrodes. Investigation of macrosections showed that the main type of deposited metal structure is high-tempered bainite, formed without pre-deformation (from cast metal) with coagulated carbides.

Thus, investigations showed the high cold cracking resistance of the deposited metal under the condition of welding 15Kh12VMFA steel joint with preheating and concurrent heating up to the temperature of 250 °C.

Additional testing for crack resistance with application of rigid joint of Tekken type was used to refine the thermal mode of welding. Tekken technological samples were welded with Thermanit MTS-4 and Kupfer 3KC electrodes without preheating and with preheating at 150, 200 and 250 °C. After welding the butt joints were subjected to thermal relaxation — soaking in a furnace with 200 °C temperature. After relaxation, the joints were cooled in still air to room temperature and were stored for 48 h.

Such soaking is required to enable development of delayed fracture in joints susceptible to cracking, and check the guaranteed resistance of welded joint to this kind of fracture. This was followed by examination of the metal of weld and HAZ with a magnifier with three-fold increase and in MBS microscope.

It was found that in welding of technological samples without preheating cold cracks formed in all the cases.

Table 3 gives the results of assessment of technological strength in sample welding with preheating to 150, 200 and 250 °C.

Obtained results confirm the need to apply preheating to 200–250 °C to provide high cold cracking resistance of 15Kh12VMFA steel welded joints. Here, the necessary condition to ensure the required thermal mode of welding is achieving cooling rate $\omega_{5/3}$ of HAZ metal at the level, not higher than 9 °C/s.

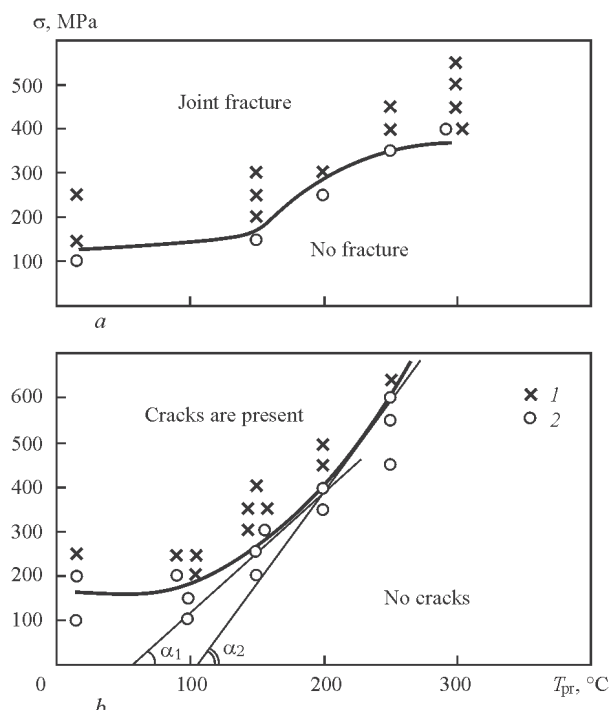


Figure 7. Influence of 15Kh12VMFA steel preheating temperature on delayed cracking susceptibility by Implant method testing: *a* — critical breaking stresses in welding with electrodes MTS-4; *b* — Kupfer 3KC electrodes; 1 — test conditions, in which delayed fracture was absent; 2 — conditions, leading to fracture

Investigations showed that at preheating temperature of 150 °C, the weld metal can form cracks. In HAZ metal cracks are absent. At temperature increase to 200 °C, cracks are absent in all the zones of welded joint. Considering the need to ensure a margin of technological strength at development of steel MAW technology, temperature of preheating and concurrent heating was set at the level of 250 °C.

Thus, proceeding from obtained results, the following approach to welding joints of 15Kh12VMFA and 15Kh1M1FL steel can be recommended:

- welding with preheating to 200–250 °C at mandatory temperature monitoring, to prevent its lowering below 200 °C;
- relaxation after welding at 200 °C during the time, determined from the ratio of 10 min/1 mm of weld thickness (determined experimentally from the condition of ensuring cold cracking resistance in a technological sample with about 5 mm thick weld at soaking at the above temperature for 20 min);
- joint cooling to the temperature of approximately 150 °C (for completion of residual austenite decomposition);

Table 3. Influence of preheating temperature on cooling rate of HAZ metal and delayed cracking resistance of Tekken butt samples on 15Kh12VMFA steel

T_{pr} , °C	150	200	250
$\omega_{5/3}$, °C/s	9.7	6.3	4.2
Cracks	Present	None	None

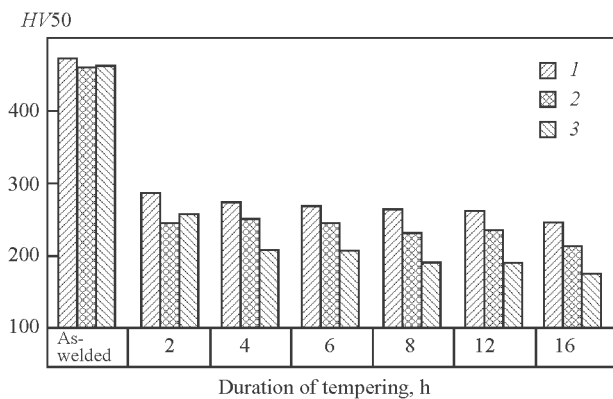


Figure 8. Influence of duration of tempering of combined welded joints on hardness of weld metal and HAZ sections at 0.2–0.5 mm distance from the fusion line: 1 — 15Kh12VNMF steel; 2 — MTS-4 weld; 3 — 15Kh1M1F steel

• performance of high tempering.

Selection of optimum heat treatment mode is based on the results of measurement of welded joint hardness (in the metal of weld and HAZ) and impact bend testing of weld metal after various tempering modes.

Results of hardness measurement in as-welded and tempered states are given in Figure 8. It is seen that after an abrupt hardness decrease during tempering for 2 h, further soaking leads to gradual lowering of hardness values for all the joint zones. Hardness starts decreasing more abruptly after more than 12 h soaking. Here, after tempering for 16 h hardness of HAZ metal in 15Kh1M1F steel reaches *HV* 173 (that corresponds to about *HB* 163), in steel with 12 % Cr — *HV* 246 (or about *HB* 235). In all the tempering modes, weld hardness takes up an intermediate position. After 16 h tempering, the weld has *HV* 215 (*HB* 204).

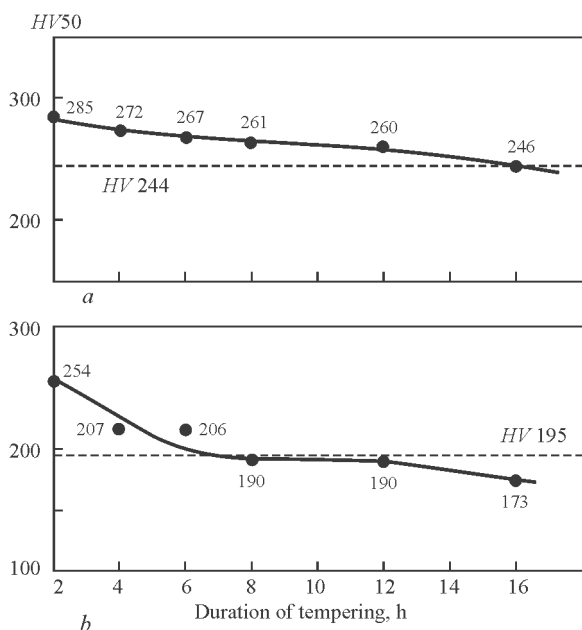


Figure 9. HAZ metal hardness at welded joint tempering at 720 °C, compared with initial hardness of steel: a — 15Kh12VNMF steel HAZ; b — 15Kh1M1F

During heat treatment, it is important to prevent deterioration of mechanical properties of base metal and metal in welded joint zone. In this case, such a characteristic can be strength, proportional to hardness value. As is seen from Figure 9, a, hardness of HAZ metal in 15Kh12VNMF steel drops below that of steel in the initial state (dashed line on the level of *HV* 244) after tempering at 720 °C of more than 16 h duration. HAZ metal hardness from the side of 15Kh1M1F steel (Figure 9, b) drops below that of initial steel after soaking for 8–12 h.

Therefore, tempering for more than 8 h leads to softening of welded joints (both HAZ and, probably, base metal) in the region of 15Kh1M1F steel. In 15Kh12VNMF steel such softening occurs at tempering for more than 16 h.

Results of hardness measurement lead to the conclusion that tempering duration should be not more than 8 h.

Results of checking the influence of tempering mode on impact toughness *KCV* of weld metal are given in Figure 10. The above data shows that the welds had quite high *KCV* values after all soaking at 720 °C. Thus, the following mode can be recommended for tempering the studied combined joints: temperature of 720 °C, duration of 8 h.

Testing for static tension was performed on transverse samples from the welded joint and longitudinal samples of weld metal. Impact bend testing was performed using transverse samples with a sharp notch in the weld (type IX, GOST 6996–66). Testing was conducted at room (20 °C) and at working (570 °C) temperatures. Samples of type II were used for static tension tests at 20 °C, and samples of type IV to GOST 6996–66 were applied at 570 °C.

Test results are given in Table 4.

In all the cases, at static tension tests of transverse samples fracture proceeded through HAZ metal of one of the steels being welded, depending on testing temperature. At $T_{test} = 20$ °C, fracture ran through 15Kh1M1F steel, at 570 °C it ran through 15Kh12VNMF steel.

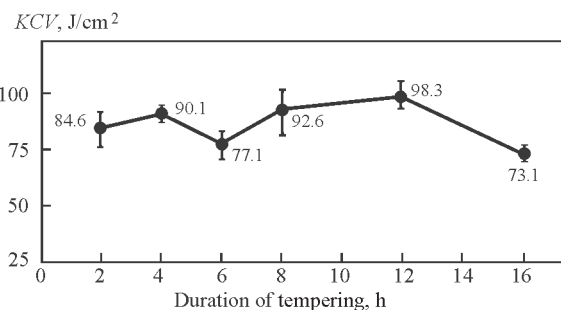


Figure 10. Influence of long-term tempering at 720 °C on *KCV* of weld metal in joints of 15Kh1M1F and 15Kh12VNMF steel welded with Thermanit MTS-4 electrodes

Table 4. Mechanical properties of joints of 15Kh1M1F + 15Kh12VNMF type welded with Thermanit MTS-4 electrodes (tempering at 720 °C, 8 h) with fracture through HAZ

$T_{\text{test}}, ^\circ\text{C}$	$\sigma_{0.2}, \text{MPa}$	σ_p, MPa	$\delta, \%$	$\psi, \%$	$KCV, \text{J/cm}^2$	σ_p, MPa	$\psi, \%$
	Weld metal					Welded joint	
20	553.8–557.7	690.7–717.7	22.75*	55.0–57.9	93	554.2–569.1	48.6–57.6
570	317.6–321.7	381.6–395.0	29.2–30.3	80.7–84.3	184.3–195.5	371.6–379.7	67.0–68.8

*Fracture beyond the base.

Microstructural features in as-welded condition and after earlier established optimum tempering at 720 °C for 8 h were studied. Revealing the microstructure on polished sections was performed by two-stage etching:

- chemical, in 3% alcohol solution of nitric acid;
- electrochemical, in chromic acid at voltage of 8 V for 20 s.

First etching was used to identify the structure in low-alloyed steel, the second one — in the weld and high-alloyed steel.

The following structural features of base metal and welded joints were revealed.

First of all, it should be noted that microstructures of welded joint, particularly, HAZ metal, are characterized by non-uniform structure. Microinhomogeneity is more pronounced in the HAZ metal of 15Kh1M1F steel. Here, microregions of different etching intensity and different colouring form, because of the possibility of formation of a number of austenite transformation products and their partial modification under the impact of thermodeformational cycles in multipass welding.

A feature of HAZ metal structure in 15Kh1M1F steel after high tempering is appearance of α -ferrite regions located along the boundary with the weld. Regions in the form of interlayers, consisting just of ferrite, and regions of mixed structure in the form of ferrite grains and products of tempering of initial acicular quenching structure are observed. Ferrite interlayer has different width at different levels of the joint cross-section, varying approximately from 0.7 to 1.4 mm. A carbide interlayer (ridge) formed in the weld along the weld–HAZ interface, which acquired a dark colour after etching.

Development of structural inhomogeneity along the HAZ–weld boundary is the consequence of diffusion redistribution of carbon, caused by the difference in the content of carbide-forming elements in the base metal and weld. In this joint, the difference in chromium alloying of low-alloyed steel and high-alloyed weld had a decisive influence on development of non-uniform carbon distribution. Carbon tends to accumulate in the region of greater chromium content. In this case, depletion of carbon in the regions adjacent to the weld led to appearance of α -ferrite,

and its accumulation in the weld — to increased carbide concentration. Such structural inhomogeneity is characteristic for combined joints and can form both in welding and in tempering. On the whole, it does not seem possible to prevent its appearance without changing weld alloying or welding technology.

HAZ metal structure of chromium high-alloyed steel after tempering of initial martensite is a ferrite-carbide mixture, formed as a result of carbide precipitation along the boundaries of primary austenite grains and along the sub-boundaries inside the grains. In addition to martensite tempering products, individual grains of δ -ferrite, initially present in the base metal, are observed in the HAZ metal structure.

It is found that the studied steel HAZ has a region of lower hardness. It can be assumed that fracture of tensile samples at testing at 570 °C ran exactly through this softening zone.

Metallographic examination of metal microstructure in the fracture zone was additionally performed. The metal failed at development of plastic flow, that was seen in the arrangement of rows of disperse intragranular precipitates along the deformation directions. In the locations, where tempered martensite structure contained δ -ferrite, fracture ran along δ -ferrite–martensite interphases; no fractures were found in the ferrite phase.

Thus, it can be assumed that lowering of HAZ metal strength in 15Kh12VNMF steel can be related to fine structural changes and to additional tempering, due to the impact of welding heating.

Structure of weld of Thermanit MTS-4 type with high chromium content, similar to 15Kh12VNMF steel, after initial martensite tempering, is a uniform finely dispersed ferrite-carbide mixture. Weld hardness varies approximately from HV 250 near the low-alloyed steel edge to HV 290 at high-chromium steel.

Proceeding from the conducted investigations, the main principles of basic technology of welding and heat treatment of combined joints of 15Kh1M1FL steel with 15Kh12VNMF steel were developed.

To finalize selection of electrode grades for welding the load-carrying welds, samples of welded joints of 15Kh1M1FL steel with 15Kh12VNMF steel, made with Thermanit MTS-4 and Phoenix SH Kupfer

3KC electrodes, were prepared for long-term strength and creep testing at 570 °C. These test results will be used to take an engineering decision on selection and application of electrodes for welding standard items.

Conclusions

1. Diaphragm is one of the most critical components of steam turbine flow section, responsible for ensuring the reliability and performance of the turbine unit and TPP power unit as a whole.

2. Currently available technology of welding the high-temperature diaphragms of HPC and MPC does not provide operational reliability of the flow section of powerful steam turbines, contributes to shortening of operating life and leads to emergency situations at TPP.

3. Features of operational damage in high-temperature diaphragm welded components were studied. It is shown that the main damage in long-term operation forms in welded joints of guide vanes with the diaphragm body and rim. Fracture runs through the zone of fusion of guide vane end face with weld metal.

4. To increase the operational efficiency and reliability of high-temperature diaphragms, new consumables were selected for welding load-carrying welds, and main principles of basic technology of welding and heat treatment were developed, providing high quality and required performance of combined joints.

1. Shlyakhin, P.N. (1974) *Steam and gas turbines*. Moscow: Energiya.
2. *OST 108.021.04–78*: Stationary steam turbines. Welded diaphragms, guide apparatuses. General specifications. Introd. 01.01.79.
3. Mellerovich, G.M., Pelipenko, E.N., Pokrassa, M.I. et al. (1969) Study of stress state of steam turbine casings and diaphragms. *Problemy Prochnosti*, **4**, 19–22.
4. (1978) *Stresses and strains in steam turbine parts*. Kiev: Naukova Dumka.
5. Kulagina, G.F. (1960) Experimental study of stresses and deflections of diaphragms. In: *Study of steam and gas turbines and axial compressors*, 333–346. Moscow: Mashgiz.
6. *TI-656–2007*: Welded diaphragms, preparation for welding, welding, heat treatment and quality control. Kharkov: Turboatom.
7. *RTM 108.020.35–81*: Stationary steam turbines. Welding and heat treatment of diaphragms and guide apparatuses. Fundamentals.
8. Kozlov, R.A. (1986) *Welding of heat-resistant steels*. Leningrad: Mashinostroenie.

Received 22.12.2015

EXTENSION OF SERVICE LIFE OF WELDED TANKS OF STAINLESS STEEL BY INCREASING PITTING RESISTANCE

V.M. KULIK, S.A. OSADCHUK, L.I. NYRKOVA, V.P. ELAGIN and S.L. MELNICHUK

E.O. Paton Electric Welding Institute, NASU

11 Kazimir Malevich Str., 03680, Kiev, Ukraine. E-mail: office@paton.kiev.ua

During long service of the tanks, manufactured of stainless steel, the pits are formed on the surface contacting with periodically preheated aggressive liquid, mainly in welded joints, and the danger of through fracture of wall arises. The aim of the work was to increase the reliability and longevity of tanks for storage of aggressive liquid, first of all, by increasing the resistance of welded joints against pitting formation. The specimens, being untreated and mechanically treated in different ways with penetration of the untreated surface and polished sheet steel 12Kh18N10T were subjected to accelerated tests for resistance against pitting corrosion at room temperature and preheatings of FeCl_3 solution similar to the technological ones. The resistance against pitting corrosion of welded joints is significantly increased after abrasive treatments, surface peening to a lesser extent and is independent of the surface roughness. The pitting resistance is also increased by replacing the indirect preheating of solution through the specimen to its direct preheating by the immersed heater. The results of the work are advisable for using in manufacture, repair and service of chemical, petrochemical, food and other equipment. 9 Ref., 2 Tables, 5 Figures.

Keywords: tank, stainless steel, welded joint, pitting corrosion, abrasive treatment, peening, preheating, surface roughness

In the production of abrasives the formalin is used supplied from vertical welded tank of 3.2 m diameter and 7.2 m height manufactured of corrosion-resistant two-layer steel 12Kh18N10T. In the process of long service of the tank, formalin preheated for technological purposes, mainly in cold season, causes the formation and development of corrosion pits on clad layer, mostly in welded joints and bottom. When the pits reach the base layer, the corrosion process is intensified resulting in through corrosion fracture of the wall in short time and environmental pollution with combustible toxic substances. At the E.O. Paton Electric Welding Institute the monitoring procedure was developed [1], which allows establishing the moment of violation of clad sealing by the pitting. For rewelding the local corrosion fractures a long break in tank service is required, which leads to material and labor expenses.

The aim of the work is the increase of service reliability and longevity of tanks for storage of aggressive liquids by increasing their resistance, first of all welded joints of stainless steel, against pitting formation.

The analysis of pits distribution in the tank evidences of a noticeable influence of temperature, method of formalin preheating, spatial position and duration of wall contact with formalin, thermal effects on metal during welding and the possible influence of surface metal condition on their formation. A partial confirmation to this fact is a higher tendency of stainless steel to pitting corrosion established by us at its

horizontal arrangement unlike the vertical one, that was taken into account during corrosion tests.

It is known that corrosion-resistant steels are prone to pitting corrosion [2] due to the formation of galvanic couple between the passivated surface and its separate areas unpassivated for different reasons. The development of pits inside depth occurs at rate exceeding the rate of uniform corrosion by ten thousand times.

The tendency of stainless steel to pitting corrosion increases usually with increase in temperature of aggressive solution and depends on the type and temperature of heat treatment and the subsequent heating [3, 4]. The resistance to pitting corrosion of austenitic steel 12Kh18N10T increases by tensile deformation with the formation of martensitic α' -phase [5]. The increase in resistance against stress corrosion and corrosion fatigue failure are positively affected by rollers running, shot blasting, scratching by metallic brush, reduction of roughness of stainless steel surface and its welded joints, as well as high-frequency machining treatment of welded joints of low-alloyed steels [6–8].

To clarify the influence of state of the metal and surface of welded joint of stainless steel as well as the method of preheating the aggressive solution contacting with it on pitting formation, the plane specimens of 50×70 mm sheet steel 12Kh18N10T of 8 mm thickness in as-delivered state, and 7 mm thickness



Figure 1. Penetration of high-alloyed steel of 8 mm thickness using tungsten electrode in argon

after finishing grinding with emulsion cooling were manufactured to remove the possible surface defects.

The specimens were subjected to partial penetration using tungsten-electrode argon-arc welding without filler metal (TIG) applying welding machine ARK-1 with power source VDUCh-315. Observing $I_w = 150$ A, $U_a = 11$ V and $v_w = 5.5$ m/h, the depth, width and reinforcement (excess of base metal surface) of penetration amounted to 3, 11–13 and about 0.5 mm, respectively (Figure 1), that is acceptable for rewelding the local fractures of inner surface of the tank. The weld metal (of penetration) is produced almost with the same chemical composition as the base metal, and the columnar crystallites of the upper part of weld are oriented generally normally to the surface.

A part of the specimens of welded joints was subjected to the following surface machining: using abrasive disc on grinding machine-tool also with the subsequent manual abrasive treatment using skin with the formation of clearly visible scratches, using vulcanite disc on grinding machine-tool until getting a mirror shine (polishing), using edge friction with and without elastic shocks by hardened steel rod using a hand drill with the formation of poorly-visible scratches, using manual and high-frequency mechanical peening with the formation of dents.

The untreated weld is characterized by rippled surface in the form of isotherms of weld pool solidification. They are eliminated by abrasive treatments, friction with the formation of plurality of scratches of different depth, frequency of distribution and peening with surface plastic deformation of metal without

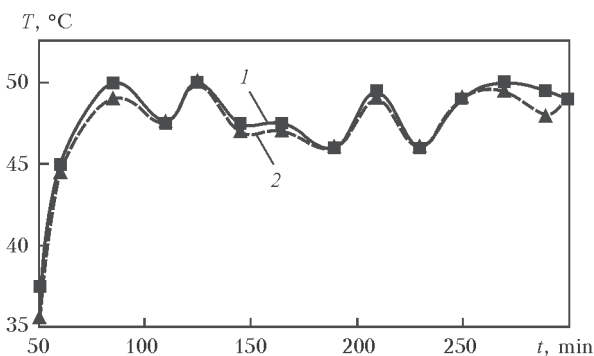


Figure 2. Change of temperature of water FeCl_3 solution heated on electric plate at distance of 5 (1) and 45 (2) mm from the surface of specimen

the formation of scratches. After these treatments the weld surface is determined only by its reinforcement above the base metal.

The corrosion tests for revealing the tendency to pitting corrosion of horizontally arranged welded specimens were carried out in 10 % water solution of FeCl_3 at room temperature of 25–27 °C during 5, 24, 48 and 72 h in the process of preheating during 5 h according to GOST 9.912–89. The preheating of the solution column of 90 mm height in cylindrical cell of 40 mm diameter, installed vertically on the specimen surface, was carried out on electric plate through the specimen and using the electric heater immersed into the solution to depth of 45 mm during cooling the specimen by running tap water of 18–20 °C from the reverse side. The temperature of the solution at different levels was controlled by the submerged mercury thermometer and regulated by operation changes of the supplied voltage of the laboratory autotransformer and also by forced cooling of test tube with cold water submerged from the top.

In the process of preheating the water solution on electric plate the temperature rises to 45 °C during 1 h and is stabilized at 46–50 °C after expiration of 75–80 min (Figure 2). At the same, time due to convection a small difference of temperatures of the solution of 0–1.5 °C is established in the range of 5–45 mm from the specimen. Under the conditions of convective heat exchange the temperature of the specimen surface is slightly higher than the temperature of preheating solution.

During preheating using the immersed electric heater the temperature of solution near the surface of the specimen increases longer and to the lower values than it does near the heater, and is stabilized at 28.0–28.5 and 51–56 °C at distance of 5 and 45 mm from the surface of specimen after 110 min of preheating (Table 1). Taking into account the gradient of temperatures along height of 0.55–0.60 °C/mm, the temperature of solution at the very surface of specimen should be 25–26 °C. The absence of convection causes decreased intensity of heat exchange and preheating of the specimen, that in combination with its

Table 1. Change of temperature of FeCl_3 water solution in height preheated by immersed heater and cooled beneath

Preheating duration, min	Temperature of solution (°C) in height (mm)				
	5	15	25	33	45
0	22	22	24	24	24
50–58	25	29	31	41	52
75–80	27	31	–	44	52
110–120	28	34	40	48	51
163–171	28.5	–	41	–	56
197–240	28.5	34	–	48	53



Figure 3. Surface of welded joint of sheet steel 12Kh18N10T tested for pitting corrosion during 5 h in as-welded state (*a*) and after abrasive treatment (*b*)

forced cooling from the reverse side (as a wall of the tank in the cold season) determines the establishment of temperature on its surface being lower than it does during preheating on electric plate, being at least 20–25 °C and lower than room temperature.

Under the influence of FeCl_3 solution at room temperature the untreated welded joint of stainless steel in as-delivery state is prone to pitting formation: the

relatively large ones on the weld and smaller different ones at distance of 3–8 mm from the weld and more (Figure 3, *a*; Table 2).

A high tendency to pitting formation of the joint can be explained by the appearance of tensile stresses in the surface layer [7], enrichment of border areas of the columnar crystallite cells near the surface of weld metal with sulfur and other impurities, and the

Table 2. Pitting formation in welded joints of steel 12Kh18N10T depending on treatment

Steel	Treatment method. Roughness of surface R_a , μm		Test duration, h	Number of pits, pcs*	
	Joint			Penetration	HAZ
Without treatment. 0.2–1.6	Without treatment		5	26	60
	Weld	HAZ			
Same	Using abrasive disc		5	2	5
	40–60	40–60			
»	Using abrasive disc and skin		5	1	2
	20–40	20–40			
Grinding. 0.2–0.8	Without treatment		5	20	1
			24	20	1
	After welding	0.2–0.8	48	20	1
			72	20	1
Same	Manual peening		5	14	1
			24	14	1
	After peening		48	14	1
			72	14	1
»	High-frequency mechanical peening		5	14	1
			24	14	1
	After peening		48	14	1
			72	14	1
»	Polishing		5	N/D	N/D
			24	N/D	N/D
	0.2–1.6	0.2–1.6	48	N/D	N/D
			72	N/D	N/D
»	Using edge friction		5	11	4
			24	21	15
	5–10	5–10	48	21	15
			72	21	15
»	Using edge friction with shocks		5	20	4
			24	27	20
	5–10	5–10	48	27	20
			72	27	20

*For 40 mm length of welded joint.

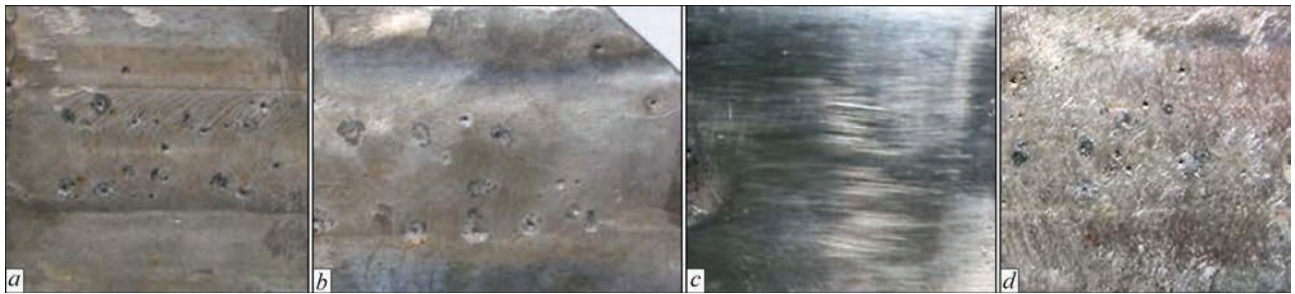


Figure 4. Surface of welded joints of grinded stainless steel tested for pitting corrosion after welding (*a*), pinning (*b*), polishing (*c*) and edge friction (*d*)

presence of surface defects in the sheet rolled metal in combination with unfavorable heating temperatures during welding. The abrasive treatments on grinding machine-tool using disc and those using skin removing the near-surface layers with defects and weld ripples significantly reduce (to single cases) the tendency to pitting formation in welded joints, despite the increase in roughness of the surface (formation of scratches), which remains almost unchanged in the process of corrosion tests (Figure 3, *b*; Table 2).

A significant decrease in number of pits formed in the HAZ metal is achieved by grinding (without visible scratches) of specimen before welding as compared to preservation of their large number in the untreated weld (Figure 4, *a*; Table 2). The tendency to pitting corrosion of the weld is reduced as a result of surface manual and high-frequency mechanical peening (Figure 4, *b*; Table 2), after which the tensile stresses are reduced and the compressive stresses arise in the metal of subsurface layer [9]. The practical elimination of welded joint tendency to pitting formation is carried out by polishing using vulcanite disc until getting a mirror shine, combining the removal of the subsurface layer defects with decreasing the surface roughness (Figure 4, *c*; Table 2). The joints treated with mechanical friction, especially with elas-

tic shocks, are more prone to pitting formation (Figure 4, *d*; Table 2), the cause of which can be arising of tensile stresses in the subsurface layer. The pits are formed mainly during the first 5 h of tests, after which their number does not increase significantly.

Preheating of welded specimen of untreated steel and water solution on the electric plate in the process of corrosion tests during 5 h causes increase in number and sizes of pits formed on the surface of welded joint, especially in the HAZ area at distance of 3–5 mm from the joint (Figures 3, *a* and 5, *a*). During its test with preheating of solution using the immersed electric heater and forced cooling of the specimen from the reverse side the shallow pits are formed detectable with magnifying glass, mainly on the weld surface (Figures 3, *a* and 5, *b*) inferior by number and sizes to the pits formed at room temperature. The reduction in tendency to pitting formation of welded joint occurs due to the combined reduction in its surface temperature and solution in the area of their contact, which is also possible by dispersion of heat through the metal.

Performing the abrasive treatments, particularly polishing, of welded joints and rewelding corrosion-resistant steel and replacing the indirect preheating of aggressive liquid through the wall of tank to direct preheating using the immersed heater from the

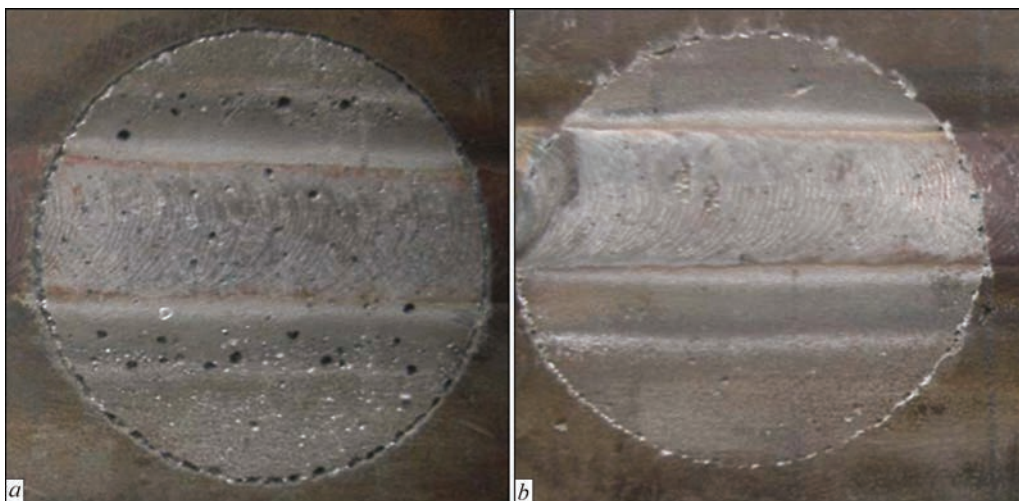


Figure 5. Surface of welded joints of mechanically untreated steel after tests on pitting corrosion with preheating on electric plate (*a*) and using the immersed electric heater (*b*)

inside, helps to increase the reliability and service life of the tank. During outside preheating this is also possible due to dispersion of the supplied heat, when the density of heat flux, the temperature of inner wall and boundary layer of liquid are decreased. It was established that a little increase in pitting resistance of welded joint is achieved by surface peening.

Conclusions

1. The weld and HAZ of the joints of steel 12Kh18N10T with the same chemical composition of metal, for example, after TIG welding without special treatment are prone to pitting corrosion in formalin.

2. A significant increase in resistance to pitting formation, first of all, in the welded joints of stainless steel is provided by abrasive treatments, especially by polishing, removing the subsurface layers with increased number of defects of different types. At the same time, the roughness (cleanness of treatment) of the surface does not determine the tendency to pitting corrosion. Increasing the resistance against pitting formation is also possible by surface peening, but it is less effective. These treatments are appropriate for application in manufacture and repair of tanks of corrosion-resistant steel.

3. The reliability and service life of tank can be increased by replacing the technological outside preheating through the wall of tank to the preheating of

aggressive liquid by the heater immersed from the inside or by dispersion of heat supplied at indirect outside preheating.

1. Nyrkova, L.I., Osadchuk, S.O., Rybakov, A.O. et al. (2015) Monitoring of corrosion state of bimetal tank for products of oil processing and its repair. In: *Problems of life and service safety of structures, constructions and machines*: Transact., 531–537. Kyiv: PWI.
2. Idelchik, B.M., Lyashchenko, A.E. (1984) *Corrosion protection of compressor machines*. Leningrad: Mashinostroenie.
3. Tomashev, N.D. (1986) *Theory of corrosion and corrosion-resistant structural alloys*. Moscow: Metallurgiya.
4. Shabudeeva, L.I., Revyakina, O.K., Makarchuk, T.B. et al. (1996) Effect of heating on corrosion resistance of stainless steel 12Kh18N10T. *Fizika Poverkhnosti i Zashchita Materialov*, 32(2), 24–30.
5. Yarovchuk, A.V., Voronina, T.A., Tivanova, O.V. (2007) Influence of deformation martensite on resistance to pitting corrosion of stainless steel 12Kh18N10T. *Polzunovsky Almanakh*, 1/2, 190–196.
6. Pachurin, G.V. (2011) Optimization of modes of surface plastic treatment for increase service life of metal products. *Uspekhi Sovr. Estestvoznaniya*, 2, 91–95.
7. Knysh, V.V., Valteris, I.I., Kuzmenko, A.Z. et al. (2008) Corrosion fatigue resistance of welded joints strengthened by high-frequency mechanical peening. *The Paton Welding J.*, 4, 2–4.
8. Klimenko, A.V., Solovej, S.A., Kovalenko, S.Yu. (2013) Increase in resistance of pipe steel welded joints to stress-corrosion fracture. *Visnyk SkhUkr. NU*, 202(13), 178–183.
9. Kyrian, V.I., Knysh, V.V. (2008) High-frequency mechanical peening of welded joints of metal structures. *Avtomatich. Svarka*, 11, 36–41.

Received 02.02.2016

DEVELOPMENT OF TECHNOLOGY OF MECHANIZED ARC WELDING IN REPAIR OF PRESSURIZED MAIN GAS PIPELINE*

O.I. OLEJNIK, S.Yu. MAKSIMOV, A.P. PALTSEVICH and E.I. GONCHARENKO

E.O. Paton Electric Welding Institute, NASU

11 Kazimir Malevich Str., 03680, Kiev, Ukraine. E-mail: office@paton.kiev.ua

Complex of investigations was carried out on development of a technology of mechanized gas-shielded arc welding applicable to repair of main gas pipelines by reinforcing structures. Determined are the conditions for prevention of pore formation in welded joints due to break of gas shield under effect of wild blast. The tests were made with weld metal of the butt and lap-butt joints, welded using modern flux-cored wires and solid wire Sv-08G2S. Effect of butt joint welding practice on mechanical properties and impact toughness of the weld metal is shown. Influence of factors, determining a risk of cold crack formation in welded joints from X70 strength class low-alloy steel, is investigated. It is determined that Sv-08G2S, E71T-1 and DW-A55 welding wires correspond to the requirements on providing a necessary level of mechanical characteristics and impact toughness of weld metal, content of diffusion hydrogen in deposited metal and can be recommended for further technology approval under conditions of field repair of in-service pipelines. Main recommendations on the welding practice of butt and lap-butt welded joints and approximate modes of welding in different spatial positions are stated. 19 Ref., 6 Tables, 7 Figures.

Keywords: main gas pipeline, arc welding, welded joints, flux-cored wire, cold cracks, pre-heating, diffusion hydrogen

It is known fact that mechanized gas-shielded arc welding results in a rise of efficiency of welding works in comparison with manual welding. Systems for mechanized arc welding over pipelines, developed by leading world companies (ESAB, Lincoln Electric, CRC) have been already used at least for 40 years. However, all these developments are related to the conditions of welding during main gas pipelines (MGP) construction. Experience of mechanization of repair welding works on pressurized main pipelines under field conditions is extremely limited.

Technologies providing for application of manual arc welding are currently used in Ukraine during repair of pressurized MGP. On the one hand, it is related with welding process simplicity, its accessibility under field repair conditions, wide spectrum of available welding consumables and equipment. At the same time, manual method of welding is regulated by different reference documents which are used for work performance on MGP, including one under pressure. The main disadvantage is a relatively low speed of welding, that effects repair process duration. For example, it can be mentioned that welding of only one circumferential joint on 1420 mm diameter pipeline takes more than 5 h for two welders. Taking into account that this sort of repair requires decrease

of pressure in the main pipeline, such a possibility, on different reasons under conditions of gas transit by the territory of Ukraine, can appear only at nighttime, when gas consumption volumes being reduced. Therefore, a risk of defects in welded joints due to insufficient visibility increases.

Thus, it is a need to intensify the welding-repair works with simultaneous rise of their quality and safety. One of ways out from such a situation is application of technology of mechanized gas-shielded arc welding using novel welding consumables.

Selection of welding consumables for mechanized arc welding. Currently, solid wires and flux-cored wires, which correspond to the requirements [1–5], are provided for application with mechanized gas-shielded arc welding at MGP construction and repair.

The following welding consumables, namely solid wire Sv-08G2S (Ukraine) and flux-cored wires DW-50, DW-A55 (Kobelco, Japan), E71T-1 (Baoding lanyu welding material, PRC) and PPs-TMB7 (TM. WELTEC, Ukraine), were selected for working out a technology of mechanized gas-shielded arc welding in all spatial positions (overhead, vertical, horizontal on vertical surface, flat). Such a choice is based on the need to compare welding-technological

*Based on materials of the work performed under purpose-oriented integrated program of the NAS of Ukraine «Problems of residual life and safe operation of structures, constructions and machines» (2013–2015).

characteristics of new, modern high-quality flux-cored wires with experience of wide industrial application of well-known cheaper wire Sv-08G2S. It is done for determination of possibility of their further application under conditions of repair of pressurized MGP. All the wires were of the same diameter 1.2 mm.

Effect of wind speed on quality of butt welds formation. In welding performance one of the factors, effecting welded joint quality, is reliability of shield of a weld metal molten by arc from air. This factor becomes critical for mechanized arc welding under field conditions, due to expected detrimental effect of wild gusts on arc gas shield. Therefore, there is a necessity in experimental determination of effect of wind speed on efficiency of shielding of welding zone, and, respectively, quality of butt joints formation depending on shielding gas consumption. Welding wires Sv-08G2S and E71T-1, and shielding gas CO₂ were used for investigations.

Limit values of shielding gas consumption Q_g , which allows prevention of pores at set air movement speed, were experimentally received at the first stage. It is determined that solid wire Sv-08G2S eliminates appearance of pores at wind speed up to $v_{wind} = 2$ m/s in CO₂ welding under field conditions, as well as it is shown that application of flux-cored wire increases allowable wind speed to 2.6 m/s due to presence of gas-slag shield from core components. Such a result is achieved at rise of gas consumption from 10–15 ($v_{wind} = 0–0.25$ m/s) to 30 l/min.

It is known fact that nitrogen and oxygen are impurities in low-alloy steels [6, 7]. Therefore, the second stage was dedicated to the experiments on determination of effect of wind speed on content of these elements in the weld metal. Specimens Mi99 for gas analysis were manufactured from metal deposited at different v_{wind} values. The investigations were carried out using gas analyzer LECO TC 436. The results are given in Table 1.

It can be seen that consumption of shielding gas in the amount necessary for maximum allowable v_{wind} values provides for insignificant rise of nitrogen and oxygen content in the weld metal. According to absolute value received nitrogen content is 3–3.5 times less than maximum recommended (0.02 %) one for mechanized CO₂ welding. Total content of oxygen in the weld, made by solid wire, is less of that was received for Sv-08G2S earlier (0.0573 %) in work [8]. As for flux-cored wire it should be noted that some rise of oxygen in the weld metal is related with its presence in the core, but in absolute determination the oxygen content is on the level of reference values for wires with rutile type core ([O] = 0.060–0.085 %) [9].

Table 1. Content of nitrogen and oxygen in deposited metal for different welding consumables

Wire	Q_g , l/min	[N], %	[O], %	v_{wind} , m/s
Sv-08G2S	10	0.0065	0.045	0.0
	27	0.0068	0.045	2.0
E71T-1	10	0.0054	0.056	0.0
	30	0.0058	0.062	2.5

Mechanical properties of metal of butt and lap-butt welds. Bandages and pipe sleeves of different structure are used in repair of MGP damages sections. They provide for strengthening of pipe wall as well as preserve working efficiency of the main pipe at integrity damage of the wall in place of the defect under sleeve. Longitudinal butt and circumferential lap-butt welds are used for joining separate cylinder elements between themselves as well as with pipeline.

Reference documents [10] require that the welding consumables used for MGP with outer diameter to 1420 mm, made from steels of strength class up to K60 included and operating under working pressure up to 8.3 MPa, correspond to the following requirements:

1) ultimate tensile strength at static tension testing should be not lower than reference value of that of the pipe base metal;

2) weld metal hardness should be not more than HV10-280, HAZ — not more than HV10-300 for pipes of strength class up to K55 included, and not more than HV10-325 for pipes of strength class more than K55 till K60 included;

3) Charpy impact toughness of weld metal should be not less than 34 J/cm² at temperature 20 °C lower than minimum temperature of wall of in-service gas pipeline (in Ukraine such a temperature for buried gas pipelines should be 0 °C).

Butt joints of 16 mm thickness with groove preparation of total angle 60° were welded for determination of welded joint mechanical properties. Each layer

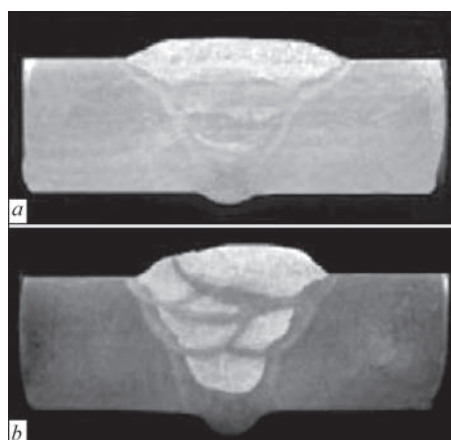


Figure 1. Macrosection of butt welded joint: *a* — welding «one layer per one pass»; *b* — welding by stringer bead

Table 2. Mechanical characteristics of weld metal

Wire, shielding gas	σ_y , MPa	σ_t , MPa	δ_5 , %	ψ , %	KVC, J/cm ² , at T, °C		
					0	-20	-40
Sv-08G2S, CO ₂	423	552	27.4	72.1	(168–138)/153	(91–88)/89	(71–62)/67
Sv-08G2S, Ar + CO ₂	430	561	30.9	75.1	(177–154)/165	(98–93)/95	(75–71)/72
E7IT-1, Ar + CO ₂	444	557	29.0	71.6	(151–107)/128	(55–53)/53	(63–32)/46
DW-A55, Ar + CO ₂	484	589	27.3	71.0	(176–152)/164	(147–128)/136	(49–45)/46
DW-50, CO ₂	468	567	29.1	72.8	(44–40)/41	(23–22)/22	(14–13)/13
PPs-TMV7, CO ₂	476	570	29.0	71.6	(172–170)/170	(125–110)/117	(86–80)/83

Table 3. Average hardness HV10 of weld metal and HAZ

Area of examination	Wire, shielding gas					
	Sv-08G2S, CO ₂	Sv-08G2S, Ar + CO ₂	E7IT-1, Ar + CO ₂	DW-A55, Ar + CO ₂	DW-50, CO ₂	PPs-TMV7, CO ₂
Weld metal	149	148	148	153	149	148
HAZ	162	160	154	158	165	155

was made per one pass (Figure 1, a). The material was pipe steel X70 with $\sigma_y > 480$ MPa, $\sigma_t > 560$ MPa, $\delta_5 > 18$ %, which was used in Ukraine in 1980s during construction of gas pipeline «Urengoj–Pomary–Uzhgorod».

Welding was carried out using combined technology [10], i.e. root weld of butt joint was performed manually using stick electrode UONI 13/45 of 3 mm diameter, the groove was filled by wires. CO₂ and mixture of Ar + 18 % CO₂ were applied as shielding gases. There were following modes of welding: for Sv-08G2S wire — $I_w = 140–150$ A, $U = 20–21$ V; for flux-cored wires — $I_w = 200–220$ A, $U = 25–27$ V. Welding speed $v_w = 0.2–0.25$ m/min, $Q_g = 15$ l/min. Specimens for determination of weld metal mechanical characteristics Mi12 type 2 and impact toughness Mi50 type 11 were cut out according to the requirements of [3, 5]. The results of tests are given in Table 2.

Analysis of received data and their comparison showed that from point of view of fulfillment of the first condition wires E7IT-1, DW-50, PPs-TMV76 and Sv-08G2S can be used in welding of steel of K55 strength class, and flux-cored wire DW-A55 for pipes of K60 (X70) strength class. Measurement of metal hardness in the weld center and HAZ showed that

all wire grades correspond to the second requirement (Table 3).

In regard to impact toughness indices (KVC) it was determined that flux-cored wire DW-50 doesn't correspond to the third requirement for -20 and -40 °C testing temperatures (see Table 2). It is suggested that one of the reasons of low KVC indices is related with welding practice, namely weaving technique with high specific heat input indices [11] was used for groove filling.

Therefore, it is decided to change a scheme of groove filling and use, one in which butt welding is carried out by stringer beads without weaving (Figure 1, b) with moderate heat input. CO₂ was used as shielding gas. Test results of specimens of weld metal being welded using new scheme showed significant rise of mechanical characteristics and impact toughness: $\sigma_y = 540$ MPa; $\sigma_t = 612$ MPa; $\delta_5 = 27$ %; $\psi = 71.5$ %; $KCV_0 = (217–172)/197$, $KCV_{-20} = (160–101)/125$, $KCV_{-40} = (87–51)/70$ J/cm².

Comparison of these results with preliminary received ones show that increase of mechanical characteristics and impact toughness of welded joint metal requires change of the preliminary selected practice of butt welding for one providing groove filling by stringer beads without oscillations. Such a conclusion was verified in evaluation of impact toughness of the

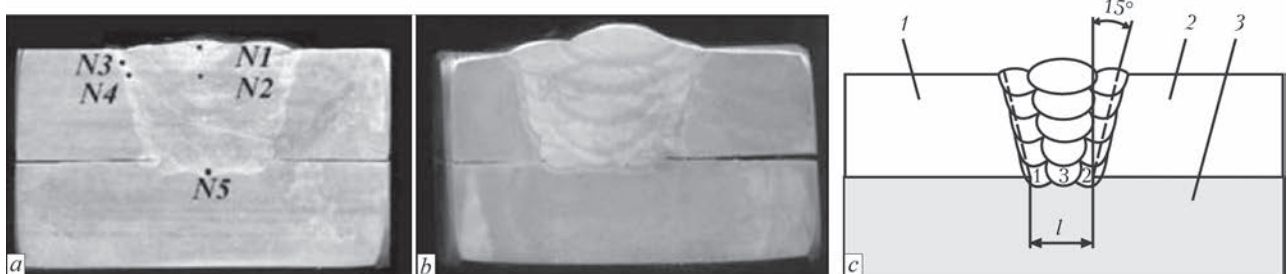


Figure 2. Macrosection of lap-butt welded joint made with wire Sv-08G2S (a) and PPs-TMV7 (b), and scheme of groove preparation and welding (c): 1 — sleeve; 2 — technological ring; 3 — gas pipeline wall; l — gap between pipe sleeve elements

Table 4. Impact toughness of metal of lap-butt welds

Wire, shielding gas	KVC, J/cm ² , at T, °C		
	0	-20	-40
Sv-08G2S, CO ₂	(164–148)/155	(171–125)/142	(100–65)/81
PPs-TMV7, CO ₂	(176–153)/165	(160–127)/140	(127–105)/118

lap-butt joints, in which every layer was carried out by inside separate beads 1, 2 on every edge, after what bead 3 was deposited (Figure 2, c). Wires PPs-TMV7 and Sv-08G2S were used for welding.

Table 4 provides for the results of Mi50 specimen testing. Analysis of data showed that high impact toughness level, which significantly exceeds minimum necessary level of this index — not less than 34 J/cm², is preserved for all range of testing temperature.

The following sections were taken for metallographic examinations: *N1* — weld metal of the last layer; *N2* — HAZ in the weld metal; *N3* — zone of coarse grain of the last layer; *N4* — zone of coarse grain with structural changes after performance of the following layer; *N5* — zone of coarse grain in weld root (Figure 2, a).

Examination of joint specimens showed that parts *N1* and *N2* have ferrite-pearlite structure at dominance of ferrite phase. Hardness makes HV1-1650–1750 MPa. Metal structure in *N2* as a result of heat effect is fine ferrite-pearlite with mesh 10 grain. In HAZ metal (*N3* and *N4*) the structure is ferrite-pearlite with 1970–2130 MPa hardness. Increase of hardness up to 2360–2640 MPa is observed in *N5* part due to accelerated cooling. It is determine that welding by separate beads allows receiving fine, virtually uniform on joint height ferrite-pearlite structure, and this promotes for solution of a problem of acquiring increased values of impact toughness in welds in comparison with minimum necessary one.

Evaluation of welded joint resistance to cold crack formation. One of the factors in risk of cold crack appearance is a stress-strain state of the welded joint [12, 13]. «Patch-sleeve» or «patch-sleeve with soil» structures [14] are used in repair of pipes with local corrosion defects. The peculiarity of these structures is presence of circumferential lap-butt weld which joins 100–120 mm diameter pitch with sleeve and pipe along the contour. High level of stresses as a result of metal shrinkage and rigid fixing is observed in a multi-layer weld at such technical solution. There is a risk of appearance of cold cracks in combination with other factors (diffusion hydrogen, microstructure).

Tests using Marine sample [15, 16] were carried out for determination of the conditions effecting re-

sistance to cold cracks formation in «patch-sleeve» lap-butt joint. Such a technological sample (Figure 3) simulates a real weld in full measure, and corresponding relationship of disk diameter to plate width can develop a level of stresses close to steel yield strength.

Parts of two samples were manufactured from 1420 mm diameter pipe segments. CO₂ welding using flux-cored wire PPs-TMV7 was carried out according to indicated scheme. Welding mode was $I_w = 190\text{--}200$ A, $U_a = 26\text{--}27$ V, $v_{w.f} = 9.1$ m/min. Two micro-sections from each quadrant were cut out for crack visual detection. It was expected that the largest level of stresses would be developed in quadrant *IV*, where, respectively, the crack being expected [17].

Examination of sample microsection, which was not subjected to pre-heating, showed that deposition of the next bead after cooling of the previous one to 20 °C resulted in formation of cold crack in quadrant *IV* (Figure 4, a). Preliminary and concurrent heating to 160–180 °C allowed eliminating its appearance (Figure 4, b).

It is determined that in the first case the crack appeared in the root part at fusion line from circumferential weld face. The crack is nucleated in a stress raiser, namely zone of transfer of surfaces of sample lap elements in the weld metal. Radial stresses from

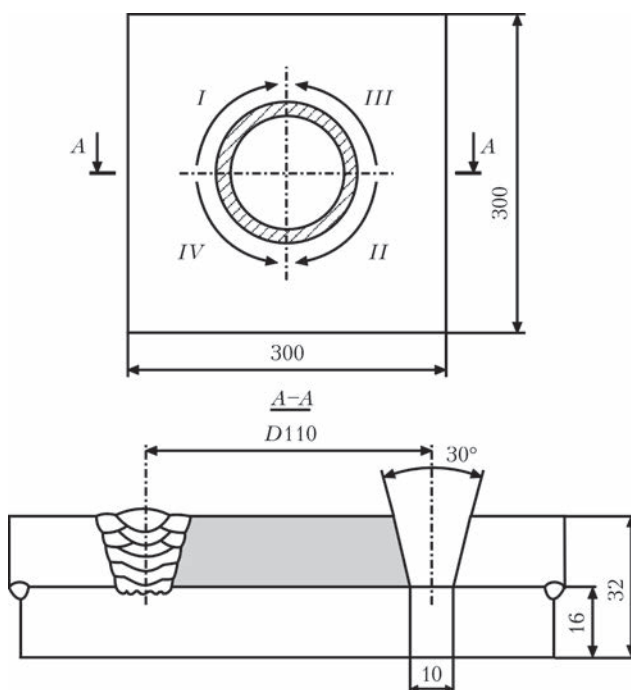


Figure 3. Scheme of Marine technological specimen with sequence of lap-butt weld

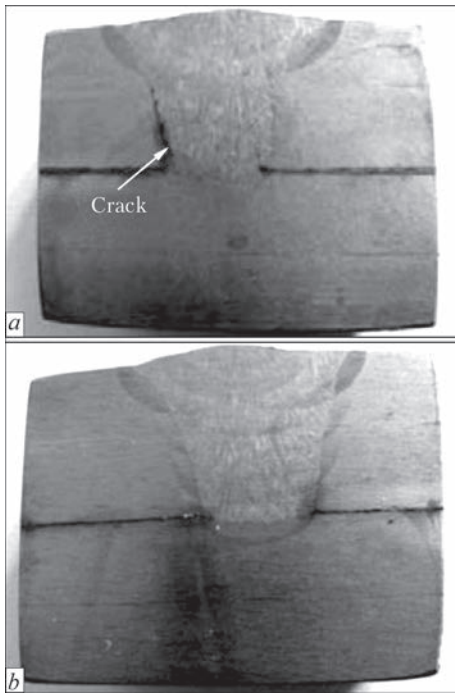


Figure 4. Macrosection of Marine specimen in mechanized welding: *a* — without pre-heating; *b* — with pre-heating and concurrent heating to 160–180 °C

metal shrinkage, being higher from the weld face than that acting from the inner side [18], are the reason of this defect. In this relation, pre-heating to 160–180 °C with keeping such a temperature before performance of each next pass is reasonable to be used for prevention of cold crack formation in the multi-layer welds, as well as quality welding consumables are to be applied having $\delta_5 > 20\%$ elasticity level at -20 °C and providing content of diffusion hydrogen in the deposited metal of not more than $10\text{ cm}^3/100\text{ g}$. Diameter of patch shall be additionally increased up to 200 mm for reduction of stress level.

Another factor, having significant effect on risk of cold crack appearance during mechanized arc weld-

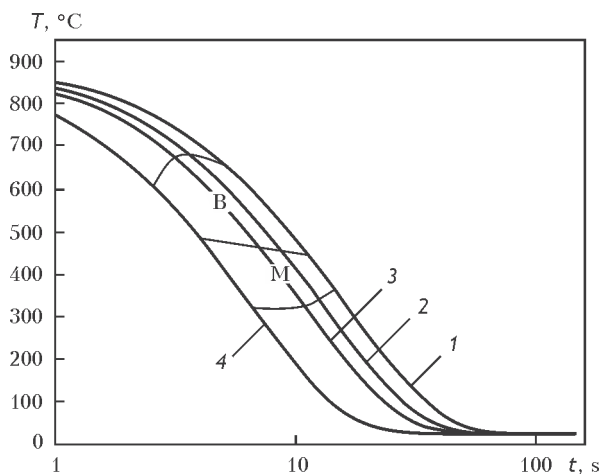


Figure 5. Austenite CCT diagram in HAZ metal of steel X70 at different cooling rates in 800–500 °C range: 1 — 40 (8.6 % M); 2 — 50 (20.4 % M); 3 — 60 (23 % M); 4 — 90 °C/s (67 % M)

ing on in-service MGP, is microstructure of HAZ metal. The information on time of weld and HAZ metal staying in 800–500 °C temperature interval at intensive heat sink was received in experimental-calculation way. It shows that cooling rate in welding without pre-heating makes 45–60 °C/s, and that at 150 °C pre-heating is 30–40 °C/s. Due to the fact that most pipe steel grades have tendency to formation of hardening structures under indicated conditions, the investigations were carried out on effect of metal cooling rate on structure of HAZ metal of X70 steel.

The investigations were carried out with the help of Gleeble 3800 complex. Special specimens were used for simulation of welding thermal cycles in HAZ metal overheating area, in which cooling rate for 800–500 °C temperature interval made 40, 50, 60 and 90 °C/s. Received austenite CCT diagram (Figure 5) and its analysis showed the following.

Amount of martensite phase increases from 8.6 to 23 % in steel X70 at cooling rate interval 40–60 °C/s and it is significantly less than 50 % value, at which it is assumed that this steel is subjected to cold crack formation. Increase of cooling rate to 90 °C/s, typical for conditions of wet underwater welding, rises amount of martensite in HAZ metal to 65–68 %, which is dangerous for welded joint working capacity.

Metallographic examinations of the specimens showed that integral hardness in HAZ metal lies in HV_{10} -270–300 range for 40–60 °C/s cooling rate. It does not exceed the limit HV_{10} -325 for steels of X70 strength class, and application of pre-heating to 150 °C has positive effect on morphology of HAZ metal microstructure. Reliable results, received with the help of Gleeble complex, allow making a conclusion on necessary continuation of investigations of long-term operated pipe steel of X52, X56, X60, X65 strength class applicable to MGP repair conditions.

It is known fact that diffusion hydrogen has significant effect on risk of cold crack appearance in welded joints, and one of its sources is electrode metal. Reference documents regulate application of welding consumables providing content of diffusion hydrogen in the deposited metal of not more than $10\text{ cm}^3/100\text{ g}$. In this connection examinations on determination of diffusion hydrogen in the deposited metal using chromatographic method [19] were carried out for all welding wires. Before experiments the flux-cored wires were dried in a furnace at 200–250 °C for not less than 3 h for moisture removal. Metal deposition on special specimens (three pieces for each wire grade) was carried out in $\text{Ar} + \text{CO}_2$ mixture using welding tractor TS-17 on modes providing heat input at 5.8–6.5 kJ/cm level. Average content of diffusion hydrogen in the deposited metal for each wire grade is the following: $[\text{H}]_{\text{dif.d.m.}} = 3.4\text{--}3.6$ for

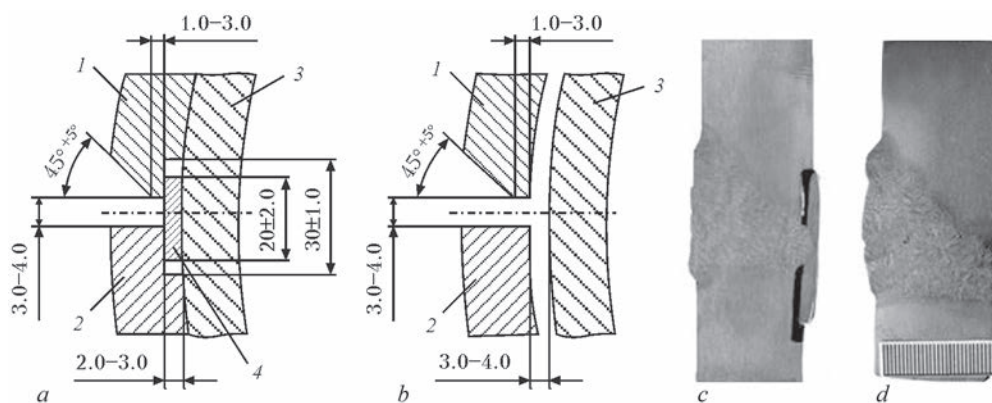


Figure 6. Longitudinal butt joints of strengthening structural elements: *a* — groove preparation for welding with backing; *b* — for welding without backing; *c* — macrosection of joint with backing plate (wire DW-A55); *d* — of joint made by Sv-08G2S wire without backing; 1, 2 — wall of upper and lower strengthening element, respectively; 3 — gas pipeline wall; 4 — backing plate

Table 5. Recommended modes of welding of butt joint with DW-A55 and Sv-08G2S* wire in mixture of Ar + 18 % CO₂

Parameter	Groove fill pass		
	Root	Filling	Facing
Wire feed rate, m/min	(9.0–9.2)/(3.6–3.8)	(9.0–9.2)/(4.0–4.1)	(7.4–7.7)/(3.6–3.8)
Welding current, A	(200–210)/(125–130)	(205–215)/(145–155)	(180–190)/(125–130)
Arc voltage, V	(26.0–26.3)/(18.0–18.5)	(26.5–27.0)/(19.0–20.0)	(25.0–26.0)/(18.0–18.5)
Wire extension, mm	(20–23)/(18–23)	(16–20)/(16–20)	(10–14)/(10–14)

*Nominator — for wire DW-A55, denominator — Sv-08G2S.

Sv-08G2S; 12.0–13.2 for DW-50; 7.6–8.5 for DW-A55; 9.7–10.0 for E71T-1; 10.1–11.8 cm³/100 g for PPs-TMV7 wire.

It can be seen that the lowest content of diffusion hydrogen in the deposited metal is observed in application of simple solid wire Sv-08G2S, and that corresponds to welding consumables providing its very low level up to 5 cm³/100 g. Flux-cored wires DW-A55 and E71T-1 correspond to welding consumables which provide for low level of diffusion hydrogen up to 10 cm³/100 g. Two more wires (DW-50 and PPs-TMV7) exceed allowable limit $[H]_{\text{dif.d.m.}} = 10 \text{ cm}^3/100 \text{ g}$ and currently can not be recommended for application for MGP repair conditions.

Development of technology for welding of reinforcing structural elements. The main attention in development of technology of mechanized gas-shielded arc welding of reinforcing elements was given to butt and lap-butt joints in different spatial positions. At that, it was an attempt to determine such welding modes, which, on the one hand, would provide quality formation of multilayer welds and, on the other hand, do not require significant correction in change of spatial position.

Welding of longitudinal butt joints in horizontal position over vertical plane (Figure 6, *a, b*) were carried out by DW-A55 and Sv-08G2S wires in Ar + CO₂ mixtures. The material is a segment of 1420 mm diameter X70 pipe with 16 mm pipe wall.

Flux-cored wire was used for welding variant with backing plate (Figure 6, *c*), and Sv-08G2S wire was

applied for welding without backing (Figure 6, *d*). Welding practice provided deposition of separate pass by stringer beads with small weaving. Root pass was made by backward inclined torch. The second and all other filling passes were carried out without transverse oscillations by stringer beads with forward inclined torch, correcting amount of passes in each layer depending on width of groove. Facing layer was carried out by separate passes with small transverse

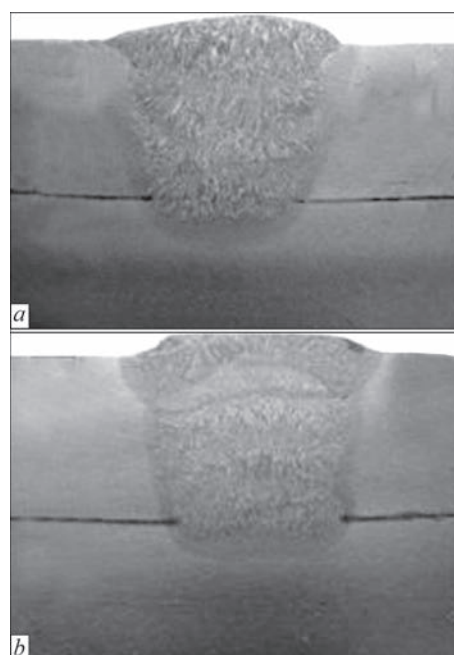


Figure 7. Macrosection of lap-butt joints of strengthening structural elements made with wire DW-A55 (*a*) and Sv-08G2S (*b*)

Table 6. Recommended modes of welding of lap-butt joint with DW-A55 and Sv-08G2S* wire in mixture of Ar +18 % CO₂

Parameter	Groove fill pass	
	Filling	Facing
Wire feed rate, m/min	(8.0–9.1)/(4.0–4.1)	(7.4–8.0)/(3.7–3.8)
Welding current, A	(190–220)/(135–140)	(180–200)/(125–130)
Arc voltage, V	(26.5–27.0)/(19.5–20.5)	(26.0–26.5)/(18.0–18.5)
Wire extension, mm	(12–23)/(12–23)	(10–16)/(10–16)

*Nominator — for wire DW-A55, denominator — Sv-08G2S

oscillations for providing smooth transfer to the base metal. Table 5 provides for modes of welding.

Technology of multilayer circumferential lap-butt joints provides for implementation of vertical upward welding process by sectors. All the layers are to be performed using «one layer per two passes» method at width of groove $l \geq 15$ mm (see Figure 2, c). This allows refinement of metal structure and additional increase of values of weld impact toughness. At $l > 15$ mm the first layer is performed using «one layer per one pass», and starting from the second «one layer per two passes» method is applied (Figure 7, a, b). Facing layer of the lap-butt joint should be made by «layer per pass» or «layer per two passes» depending on l value. Total number of layers in lap-butt joints is determined by wall thickness of reinforcing structural elements.

Overhead welding should be carried out with backward electrode position in order to guarantee fusion of edges with pipeline. Modes of welding are given in Table 6.

The equipment for mechanized gas-shielded arc welding should include professional power sources, which are designed for heavy work. The apparatuses should have protection class not less than IP23. The kitting should contain water-cooled four-rolls external feeding devices, which allow wire feed in the hoses of 6 m length. All the requirements to equipment, materials and shielding gases are stated in the developed technical documents.

In the conclusion it can be noted that application of mechanized gas-shielded arc welding using traditional (Sv-08G2S) and modern welding consumables (DW-A55 and E7IT-1) allow meeting the requirements made to service characteristics of repaired MGP sections. The result of carried work became development of reference documents on mechanized gas-shielded arc welding for MGP repair, agreed with Company «Ukrtransgaz».

The results of laboratory-research tests allowed making a decision on industrial approbation of the

developed technology at «Ukrtransgaz» enterprises for the purpose of its application in MGP repair under field conditions.

1. GOST 2246–70: Steel welding wire. Specifications. Introd. 01.01.1973. Moscow: Standartinform.
2. AWS A5.18: Carbon steel electrodes and rods for gas shielded arc welding. Miami: AWS.
3. AWS A5.28: Specification for low-alloy electrodes and rods for gas shielded arc welding. Ibid.
4. GOST 26271–84: Flux-cored wire for arc welding of carbon and low-alloy steels. General specifications. Introd. 01.01.1987. Moscow: Gosstandart SSSR.
5. AWS A5.36: Specification for carbon and low-alloy steel flux cored electrodes for flux cored arc welding and metal cored electrodes for gas metal arc welding. Miami: AWS.
6. Pidgaetsky, V.V. (1970) *Pores, inclusions and cracks in welds*. Kyiv: Tekhnika.
7. Pokhodnya, I.K., Yavdoshchin, I.R., Paltsevich, A.P. et al. (2004) *Metallurgy of arc welding. Interaction of metals with gases*. Kiev: Naukova Dumka.
8. Novozhilov, N.M. (1979) *Principles of metallurgy of gas arc welding*. Moscow: Mashinostroenie.
9. Pokhodnya, I.K., Suptel, A.M., Shlepkov, V.N. (1972) *Flux-cored wire welding*. Kiev: Naukova Dumka.
10. STO Gazprom 2-2.2-136–2007: Instruction on welding technologies in construction and repair of industrial and main gas pipelines. Pt 1: Welding technology in repair of industrial and main gas pipelines being in service. Introd. 22.09.2007.
11. ESAB Reference book on welding: All position flux-cored wires for non-alloy and low-alloy steels.
12. Makarov, E.L. (1981) *Cold cracks in welding of alloy steels*. Moscow: Mashinostroenie.
13. Makhnenko, V.I. (2006) *Safety service life of welded joints and assemblies of modern structures*. Kiev: Naukova Dumka.
14. GBN V.3.1-00013741-12:2011: Main pipelines. Repair by arc welding in service conditions. Valid from 06.09.2011. Kyiv: Ministry of Energy and Coal Industry of Ukraine.
15. (1967) *Testing of metals*: Transact. Moscow: Metallurgiya.
16. But, V.S., Maksimov, S.Yu., Olejnik, O.I. (2014) Cracking susceptibility of welded joints in repair structures on main gas pipelines. *The Paton Welding J.*, **11**, 15–23.
17. Bekker, M.V., But, V.S., Govdyak, R.M. et al. (2008) *Repair of main pipelines under pressure*. Kyiv: Kyj.
18. Nikolaev, G.A., Kurkin, S.A., Vinokurov, V.A. (1982) *Welded structures. Strength of welded joints and deformation of structures*. Moscow: Vysshaya Shkola.
19. GOST 23338–91: Welding of metals. Methods for analysis of diffusion hydrogen content in deposited and weld metal. Introd. 01.07.1992. Moscow: Gosstandart SSSR.

Received 02.02.2016

DEVELOPMENT OF ADHESION AND ADHESION-WELDING TECHNOLOGY FOR REPAIR OF BEARING SEATS FOR EXTENSION OF SERVICE LIFE OF CASING PARTS OF POWER EQUIPMENT*

Yu.S. VASILEV, N.I. OLEJNIK and L.S. PARSHUTINA

E.O. Paton Electric Welding Institute, NASU

11 Kazimir Malevich Str., 03680, Kiev, Ukraine. E-mail: office@paton.kiev.ua

The analysis of physical and mechanical factors determining the service life of bearing units was carried out. The adhesion and adhesion-welding technologies for restoration of bearing seats in the supports of heavily loaded gears were developed. The compositions of repair composite material based on adhesive «Koutex» and the optimal modes of stage-by-stage deposition of coupling, filling and finishing coating layers were selected. The limit values of rheological characteristics of the adhesive compositions for formation of adhesion-welding repair joint were established. 4 Ref., 7 Figures.

Keywords: *repair technology, bearing unit, adhesion-welding technology, repair adhesive compositions, reducer*

In Ukraine a large number of industrial equipment is operated, which has already worked out the service life specified by the manufacturer. The high degree of wear of geometrical parameters, the presence of fatigue and corrosion damages requires a large amount of repair works. The most common defect of casing parts wear is the wear of bearing seat surfaces. The restoration of mass casing parts is economically rational because it can significantly reduce the consumption of spare parts for repair and provide the necessary longevity of assembly units of the machines.

At the present time, a sufficient experience on repair of bearing units in the different-purpose structures was gained, which takes into account the operating modes and conditions of the equipment service, reliability and long life of bearings, convenience and easy maintenance during the operation process. The methods for restoration of worn-out surfaces on the basis of welding, spraying and surfacing using metal materials and powders have been widely used at the large specialized enterprises, where high-precision equipment for machining of bearing seats is applied to provide parallelism of axes and center-to-center distances. The application of welding and subsequent machining significantly increase the volume of accompanying works associated with disassembly and

subsequent assembly of equipment elements, including overhead costs for transportation of disassembled equipment to repair and production sites. Therefore, development of effective repair and restoration technology of worn-out and damaged units of industrial equipment directly under the operation conditions or at the repair site is an urgent problem.

The use of polymeric materials greatly simplifies the technology for restoration of seats and increases the service life of rolling bearings due to redistribution of external load between the rolling elements [1]. In repair works of industrial equipment the highly filled metal-polymeric adhesive compositions (multi-metals) have been widely applied, and the technology was called «cold molecular welding». These composite materials (as compared with pure polymers) possess a high rigidity, strength and vibration resistance, heat resistance, dimensional stability and decreased gas and water permeability. The combining of technological welding and adhesion processes while using the metal-polymer compositions can improve rigid and strength properties of metal structures without reduction in operational loads.

The aim the research work was to develop adhesion and adhesion-welding technologies for repair of bearing units of power equipment at the place of oper-

*Based on materials of the work performed under purpose-oriented integrated program of the NAS of Ukraine «Problems of residual life and safe operation of structures, constructions and machines» (2013–2015).

ation on the basis of domestic metal-adhesive compositions produced according to prescription modification of industrially produced polymeric matrices.

Basing upon the experience of design and service of metal rolling bearings the character of mating the bearing rings with the shaft and casings was determined, which depends on the type of their loading, i.e. circulating or local one [2]. The circulative-loaded rings should be joined with the mating part immovably. The presence of gap between the circulation loaded ring and the part coupled with it results in slipping of the ring relatively to the seat, that results in beading and wear of the shaft neck or casing, usually manufactured of softer metal than material of the bearing ring. On the contrary, a movable joining of locally loaded rings with the coupled parts provides the presence of gap or slight tightness between the ring and the seat, that under the action of shocks and vibrations allows the ring to slip slowly relatively to its seat, and in the operation instead of limited area the entire race of the ring is involved. Such a method of mounting the locally loaded rings greatly increases the service life of bearing, because otherwise wear of the ring race occurs at only one of its areas.

In accordance with the character of mating of bearings ring with the casing and taking into account the volume of wear of seat holes, the following repair methods of bearing units using the adhesive composite materials (ACM) were investigated:

1. Pasting-in the bearing rings into the seat with formation of fixed joint.
2. Formation of the seat holes of nominal size in the casing part with formation of minimum gap or small tightness.

It is recommended to perform pasting-in the bearings during wear of up to 0.25 mm using the fluid

anaerobic adhesive composites such as Anaterm and Unigerm (Russia), Loctite (US), Permabond (Great Britain) [1]. The principle of this method is that the process of restoration of the seat assembly is combined with bearing assembly operation, resulting in fixed joint of the bearing and the shaft (casing) which is many times superior as to its strength characteristics which in such cases is recommended for tight seating. It reliably protects bearing rings against slipping, eliminates fretting corrosion and provides a more reliable unit operation. At the same time, pasting-in unlike tight seating, does not result in arising stresses and deformations of bearing rings, that also contributes to a more reliable operation.

As an offer for substitution of imported foreign anaerobic materials we carried out the investigation on restoration of bearing units using the domestic adhesive compositions on epoxy and polyurethane polymer matrices. As the most technological and repairable adhesive composition «Koutex» was determined, which is the joint development of the *Institute of High-Molecular Compounds* (NASU) and Production Group «Diver». The composition represents a fluid two-package adhesive system (base + solidifier in ratio of 1:1) possessing a high adhesion to wetted and oily surfaces. The process of formation of repair joints consists in preliminary mechanical-chemical treatment of seats, deposition of thin layer of adhesive composition on the outer surface of the outer bearing ring and assembly of the bearing unit.

For repair of bearing units with wear of not more than 1 mm, thixotropic adhesive composition «Koutex» is used, and the desired accuracy of assembly is endured by means of devices for fixing the parts in specific position for the period of solidifying. Otherwise, under the action of gravity the adhesive is ex-

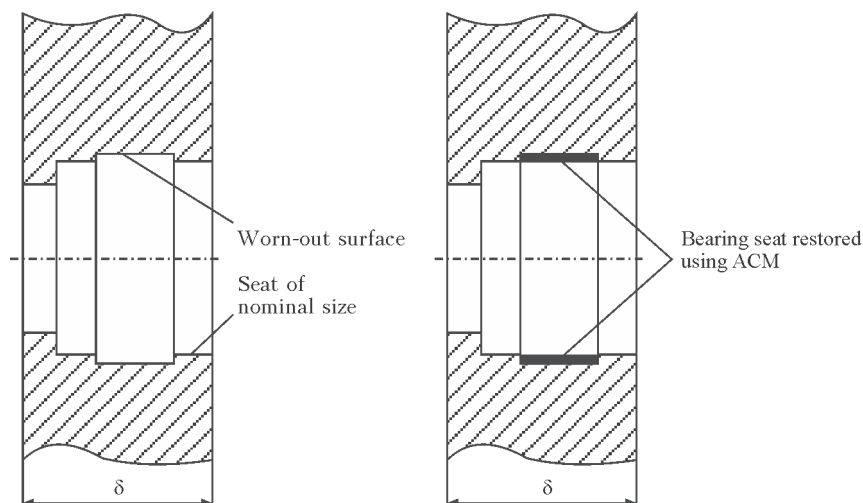


Figure 1. Restoration of bearing seats using ACM [3]

truded and the coaxiality of seat hole with bearing shaft is violated.

The repair of bearing units in the large-sized reducers of the power equipment consists in restoration of geometry of support bearing surfaces using ACM of different degrees of filling with inorganic particles. The pasty ACM is excessively applied on the place of wear and treated to the nominal size after solidification (Figure 1) [3]. The ACM interlayer between the outer bearing ring and the seating ring of the reducer casing is deformed under the action of external load, providing its rational distribution between the rotation bodies. In work [4] the optimal physical and mechanical characteristics of the polymer layer were determined depending on acting load and gap between the ring and the seat.

The necessary requirement to the applied ACM is providing the sufficient level of technological (initial) strength of adhesive-bonded joints in 30–60 min after deposition. This provides a significant reduction of labor intensity of the technological adhesion process due to possibility of carrying out the subsequent operations until the repair is fully completed. Within that period the adhesives with a long viability do not gain technological strength, that increases the repair period and duration of equipment downtime. Therefore, to develop the adhesion and adhesion-welding repair technologies of bearing units the investigations on improvement of adhesive compositions were carried out to develop the repair materials with the required level of rheological characteristics and viability.

In order to specify the chemical composition and quantitative content of components of the repair adhesive compositions (RAC) the analysis of investigations of materials of «Durmetall» (Switzerland) and «Chester Molecular» (USA), similar according to their purpose, was carried out. The results showed that the polymer base of the chosen materials is aromatic epoxy resin, which is confirmed by the presence of absorption peaks in the range of 2900 cm^{-1} (aromatic rings) and in the range of 830 cm^{-1} (epoxy groups). This conclusion is correlated also with the analysis of the mass-spectra having lines of molecular mass of 43 (epoxy group) and 94 (benzene ring). The solidifiers can be classified as anhydride (absorption bands of 1513 and 1718 cm^{-1}) or oxide ones with the following rearrangement into amine groups at the presence of catalyst PCl_5 . This is confirmed by the presence of HCN remnants with molecular mass of 27 according to mass-spectrum and the band of 812 cm^{-1} according to IR-spectrum. The mass spectroscopy of the acti-

vator of accelerated type shows the presence of line with molecular mass of 19 indicating that the catalyst is a complex of trifluoride boron with ether. The investigations carried out using the method of pyrolysis showed a high filling with inorganic particles ranging from 5 to $150\text{ }\mu\text{m}$.

The revealed materials science regularities for creation of dispersion strengthened polymer composite materials formed the basis for the development of RAC on the base of domestic adhesive polymer matrix «Koutex» and solidifying systems like UP-583, UP-0633M and L-19, which is also an active plasticizer possessing the properties of surface-active agents. The investigations of RAC filling processes were carried out with introduction of particles of Ti, Fe, Cr, Zn oxides, iron powders, quartz as well as particles of scaly form on the basis of basalt.

The interaction of the polymer matrix with amine solidifiers at the presence of the mentioned oxides was studied using the method of differential thermal analysis (DTA). It was established that all the used metal oxides influence the solidifying process of epoxy oligomer. At the same time, some shifting of temperature of the reaction beginning and the temperatures of maximum peak of DTA curve to the region of lower values is fixed as compared to the unfilled composition. Chromium oxide has the opposite effect. At the introduction of dispersed particles the exothermic effect is increased in the following order: $\text{Cr}_2\text{O}_3 \rightarrow$ pure composition $\rightarrow \text{Fe}_2\text{O}_3 > \text{ZnO} \rightarrow \text{TiO}_2$. At the introduction of oxides in epoxy composition the decrease in activation energy of the solidifying process is observed. The given data indicate the catalytic activity of Ti, Fe, Zn oxides and the inhibitory effect of Cr_2O_3 on the solidification process of epoxyamine compositions. In order to reduce the cost of consumables the quartz powder was used in form of particles of up to $200\text{ }\mu\text{m}$ size.

It is known that introduction of highly dispersed particles of less than $1\text{ }\mu\text{m}$ into polymer matrix leads to formation of chain structures, clusters and aggregates. In the process of multifraction filling the highly dispersed particles are filling the «free» volume between the larger fractions, increasing the degree of packing and strength values. The RAC strengthening was carried out by introducing ultra-dispersed powder (UDP) of silicon carbide (SiC) with the particle size of $0.03\text{--}0.2\text{ }\mu\text{m}$ and specific surface of about $20\text{ m}^2/\text{g}$. At the introduction of UDP with volumetric fraction of about $0.1\text{--}0.20$ the strengthening effect of the filler is revealed in increase of the surface energy of de-

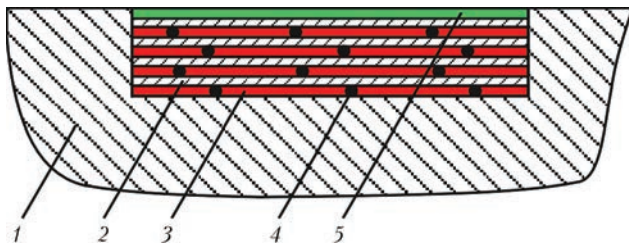


Figure 2. Adhesion-welding method for restoration of bearing seat in casing part: 1 — support; 2 — multilayer of sheet steel 05kp (rimmed); 3 — filler of interlayer space (anaerobic sealant); 4 — weld spot; 5 — finishing layer of composite



Figure 3. Casing of reducer RLKU-250M



Figure 4. Wear of bearings seats

struction and tensile strength. In the composition an infinite volumetric cluster of UDP particle chains appears connected with the coarse-dispersed particles through the film matrix interlayers, and forming the frame representing a spatial network. During loading such a frame is deformed and its cells are distorted either stretching or compressing depending on direction of the applied load.

We developed the adhesion technology for restoration of bearing seat surfaces in the reducer casing based on the formation of three-layer repair composite coating. The first layer is the finishing agent (primer) with high adhesive capacity to the restorable support surface (RAC-1). The second is filling one with the high strength and damping characteristics (RAC-2). The third is finishing one providing the maximum value of the actual contact (RAC-3).

To repair the heavily loaded bearing units and compensate the significant wear of bearing surfaces, we proposed the adhesion-welding design of repair rolling bearing seat in the casing of large-sized reducer in order to improve the bearing capacity and bending rigidity of so-called «filling layer» (Figure 2).

The repair structure represents multilayer, composed of set of thin-sheet metal plates of 0.1–0.5 mm thickness joined by weld spots and adhesive interlayers. The contact surface with bearing is formed of the elastic adhesive composite material (see Figure 2).

The practicing of technological methods for repair of power equipment using the experimental RAC was carried out at the enterprises of Donetsk Fuel-Energy Company DTEK. As an object of investigations the repair of large-sized cylindrical reducer RLKU-250M (Figure 3) was selected. As a result of inspection of

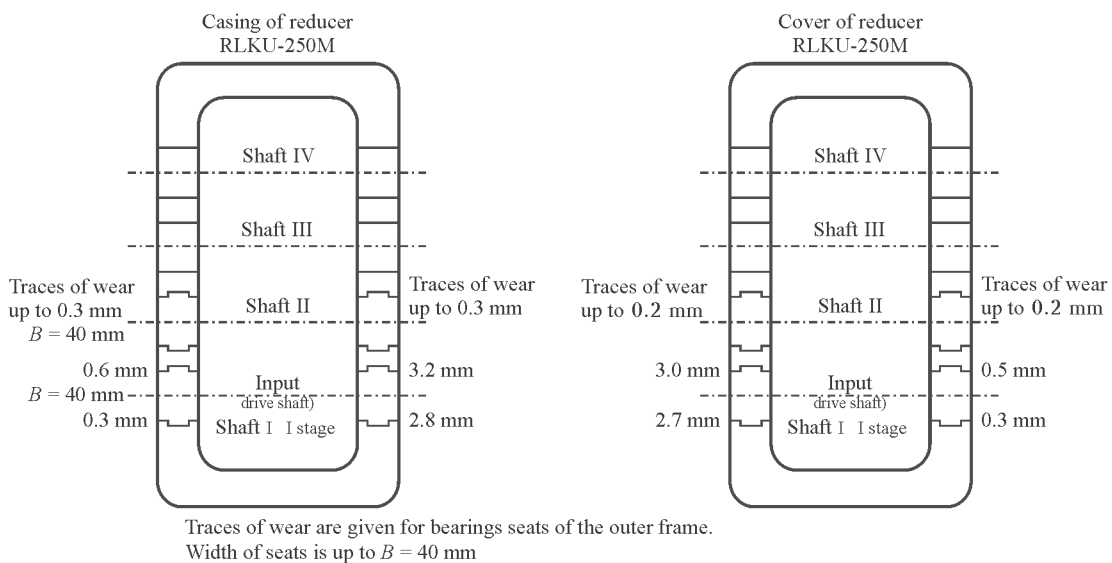


Figure 5. Map of location and sizes of defects subjected to repair using RAC



Figure 6. Installation of false shafts on bearing seats

the reducer, the places of wear were revealed and the sizes of defects were measured (Figures 4 and 5). The checking of ovality and conicity of seats, not subjected to wear, using the false shaft (Figure 6) demonstrated their compliance with the dimensions and tolerances specified in the working drawings. The restoration of seat bearings (shafts I and II) was performed according to the technological regulations of reducer repair.

The final inspection of the restored bearing seats was performed by painting method using the false shafts (Figure 7).



Figure 7. Control of accuracy of bearing seats restoration

After the industrial tests the repaired reducer is operated at the Pershotravnesky repair-mechanical plant since March 2014 until now.

1. Gryaznov, B.A., Bukhtiyarov, V.K., Kakuevitsky, V.A. et al. (2013) *Application and strength of polymer materials in manufacturing and repair of machines and equipment*. Kiev: IP3.
2. Perel, L.Ya. (1983) *Rolling bearings: Calculation, design and maintenance of supports*: Refer. book. Moscow: Mashinostroenie.
3. Goncharov, A.B., Tulinov, A.B., Odintsov, L.G. *Method of diameter size reconstruction of drying cylinder of papermaking equipment*. Pat. 2364487 UA. Publ. 20.08.2009.
4. Tulinov, A.B., Goncharov, A.B. (2003) New composite materials in repair production. *Remont. Vosstanovlenie. Moderniz.*, **11**, 46–49.

Received 22.12.2015

ON THE 100th ANNIVERSARY OF BORIS I. MEDOVAR



29 March 2016 marks the centenary of the birth of Ukrainian metallurgical scientist, pioneer of modern electroslag remelting, academician of the NASU Boris Izrailevich Medovar.

B.I. Medovar is one of the brightest representatives of Paton scientific school, faithful disciple and colleague of Evgeny O. Paton and Boris E. Paton. Throughout his life, except for two years on the Great Patriotic War frontlines, B. Medovar worked at the E.O. Paton Electric Welding Institute of the NASU. A man of his time, he grew and developed together with the Soviet Union, has experienced its heyday, fall and collapse, has worked in the independent Ukrainian state and obtained new scientific results, even in the last years of his life. In the Internet, encyclopedias of the Soviet era and independent Ukraine, the scientists' major achievements, awards and academic status are highlighted in details.

Here we'll try to remember a great personality and follow B. Medovar own estimates, which he has repeatedly expressed among students and colleagues, recall his life's journey and achievements, becoming a welder, metallographer and metallurgist.

B.I. Medovar started at the Electric Welding Institute as a researcher of welding processes. The war veteran-armor crewman, he was proud of the fact that forward welding and the relevant terms of the Regulations of armored troops on forming-up of machines in wedge formation and inverted wedge formation were introduced in welding technology with his filing. After the war, the scientist engaged in creation of equipment and technology of welding gas pipes of large diameter at Khartsyzsk Pipe Plant. In 1950, this work was marked by the Stalin Prize. Specialists-pipe makers are well aware that even today large-diameter pipe welding is carried out on the principles developed by B.I. Medovar in the middle of the last century.

A separate bright page of his creative life has been studies in the field of welding of austenitic steels and alloys. His monograph «Welding of heat-resistant austenitic steels and alloys» went through three editions, and according to many welders, especially those related to nuclear energy machine building, it served as a daily desktop tool. Very instructive and well-known in the circles of welders and metallurgists became a story about doctoral thesis defense by B. Medovar. In 1960, he defended the second edition of the mentioned book as his thesis. Suddenly, a wave of sharply negative reviews went in the Scientific Council, which alleged that the applicant should be deprived of the PhD degree leaving alone the doctorate... The current scientific degree seekers, usually defending the thesis without the «black» balls, it is difficult to imagine a defense when positive result decided by one vote, and nearly a third of the Council votes against. Anyway, after this defense none of welders or metallographers defended doctoral thesis in the form of a book.

Iron character of B. Medovar fully appeared at this time. Remembering that, the Academician repeatedly stressed that many colleagues helped him to survive, but above all — the support of his wife and the Director of the Institute — friend and teacher — Boris E. Paton.

And the transition from welding to metallurgy was not easy for him. For many years he continued his studies as a welder and as a metallurgist in parallel, creating a hitherto unknown metallurgical process — electroslag remelting. After all, the ability to create entirely new technology and equipment has won: step by step, the scientist has been reducing working on welding problems and increasingly focused own and his team efforts on creation and development of ESR. Today, it is hard to imagine, but the modern ESR was born in Kiev, exactly at the Electric Welding Institute. From Kiev ESR began its triumphal march around the world: in 1958, in Zaporozhie at electrometallurgical plant «Dneprospetsstal», and at Novo-Kramatorsk Machine-Building Works, the world's first ESR furnaces became operational, and in 1963, the license for using the ESR technology was sold to France. For many years, the Electric Welding Institute and Medovar's team have been leaders in this area of the world



At the Caucasian front (1942)

metallurgy. Licenses and ESR furnaces, created on the basis of their research appeared in the US, Sweden, Germany, Japan, and the Eastern European countries. According to the estimates by Boris Medovar, the peak in the ESR area for him and his team became a unique plant for 40-ton ESR slab ingots, built in Japan under the license of the PWI.

We'll notice that ESR has become the metallurgical basis for creating a powerful submarine fleet in the USSR. Nothing like this they had either in the US or in other countries. ESR found many other military applications at home and abroad, in particular, for production of tank guns. Interestingly, in 1991, an American journalist came to Kiev to photograph B.I. Medovar near T-34 tank in the yard of the first building of the Institute. This tank is a monument to the Paton Institute employees, who were creating tank production during the years of the Great Patriotic War. But the American in the short article stressed another thing — specifically that thanks to the license for the technology of ESR hollow ingots purchased in the USSR, American tanks did not concede to Russian...

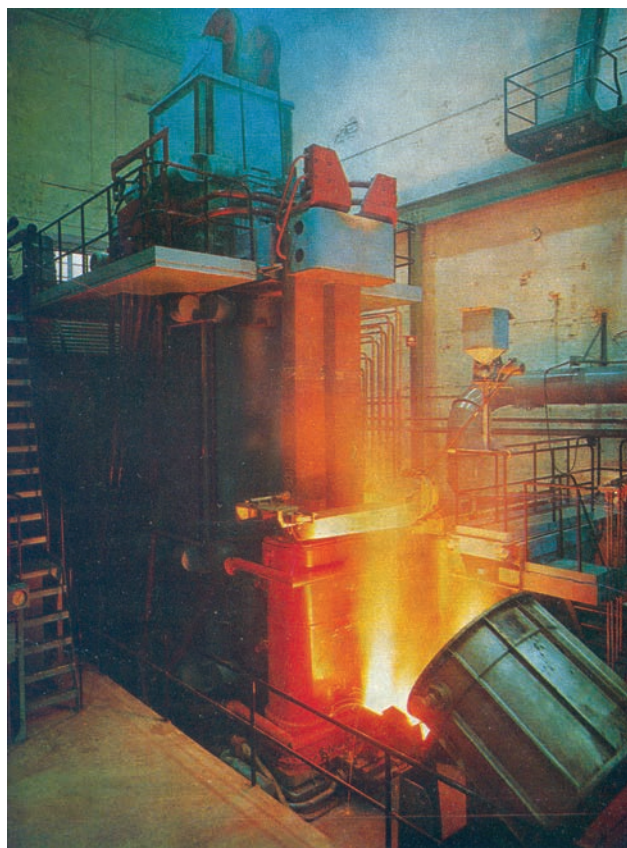
As the years passed, and as this happens, keeping the leadership failed — the arms race and increasing concentration of efforts led by Academician team on solving practical problems of military-industrial complex have slowed exploration work. As a result, in new Ukraine in the beginning of a new period of life and work, the scientist and his colleagues faced the fact that competitors have advanced far ahead, especially in the creation of new slags, modeling of ESR, creation of new structures of furnaces and power supplies. However, B.I. Medovar succeeded in this difficult period to create a range of new ESR technology with direct processing of liquid metal, to develop fundamentally new equipment and implement it in the industry.

Features of character Boris Medovar developed in communication, with both familiar and unfamiliar people, with subordinates and not depending on him people. He was an enthusiastic man, sometimes not careful with words, but always trying to support people. That's why he brought dozens of candidates and doctors of technical science. His desire and willing-

ness to help people specifically highlighted in those years when Medovar — deputy of the Supreme Council of Ukraine — continuously met with voters and tried to help people in their struggle against the bureaucracy of the Soviet state.

This fact also speaks a lot — while preparing for his first speech in the United States at a symposium on ESR (1967), he spent hours rehearsing its report and with the help of a tape recorder corrected English pronunciation learned by self-teaching guide. It's interesting that he was able to read and communicate with colleagues without interpreters not only in English-speaking countries, but also in Germany and in France, read in the original foreign scientific articles. Consistent and purposeful self-training was another characteristic feature throughout the life of the scientist. Already being recognized, Medovar did not hesitate to learn from the young, has never hidden if he did not know any thing...

Students and academic colleagues have been repeatedly struck by his intuition and ability that is called «the tip of the pen» to find solutions to complex problems. For example, in the last quarter of his life, at his desk, he created low-carbon steel armor, boldly dropping almost twice the carbon content in compar-



Furnace U-436M for production of slab ingots of up to 9 t mass (company «Avesta», Sweden, 1970)



B.I. Medovar (*third from the left*) with his followers and Japanese metallurgists of «Nippon Steel» company standing on the first in the world 40-ton ESR slab ingot (Yawata, Japan, 1974)

ison with the conventional level of 0.35–0.40 %, invented a new slag for rolling mill roll cladding and decided to go for considered impossible hardening and tempering low-carbon low-alloyed steel of 09G2S type. In all these cases, the practice proved brilliantly bold foresight and technical solutions of B. Medovar.

In conclusion, we'll notice that today a number of B.I. Medovar developments and his apprentices and followers have not surpassed by anyone in the world. This, above all, is the technology of ESR hollow ingots, providing the production of cast ESR metal with physical and mechanical properties at the level of forged metal. Today, the technology of ESR slab

ingots for rolling particularly thick sheet of high-strength steels has no peers. The business of one of the founders of our magazine is alive and continues to grow worldwide.

Despite the well understood difficulties of the present time in Ukraine and the PWI, the ESR studies are successfully continued. In particular, established during the life of Boris I. Medovar ESR bypass technology has been applied in the production of bimetals and making bars of heat-resistant alloys without freckle-type segregation, and decades later his long-standing idea of ESR rail steel is making its way into industrial production.

Editorial Board